UNIVERSIDAD AUTONOMA DE MADRID

Programa de Doctorado en Biociencias Moleculares

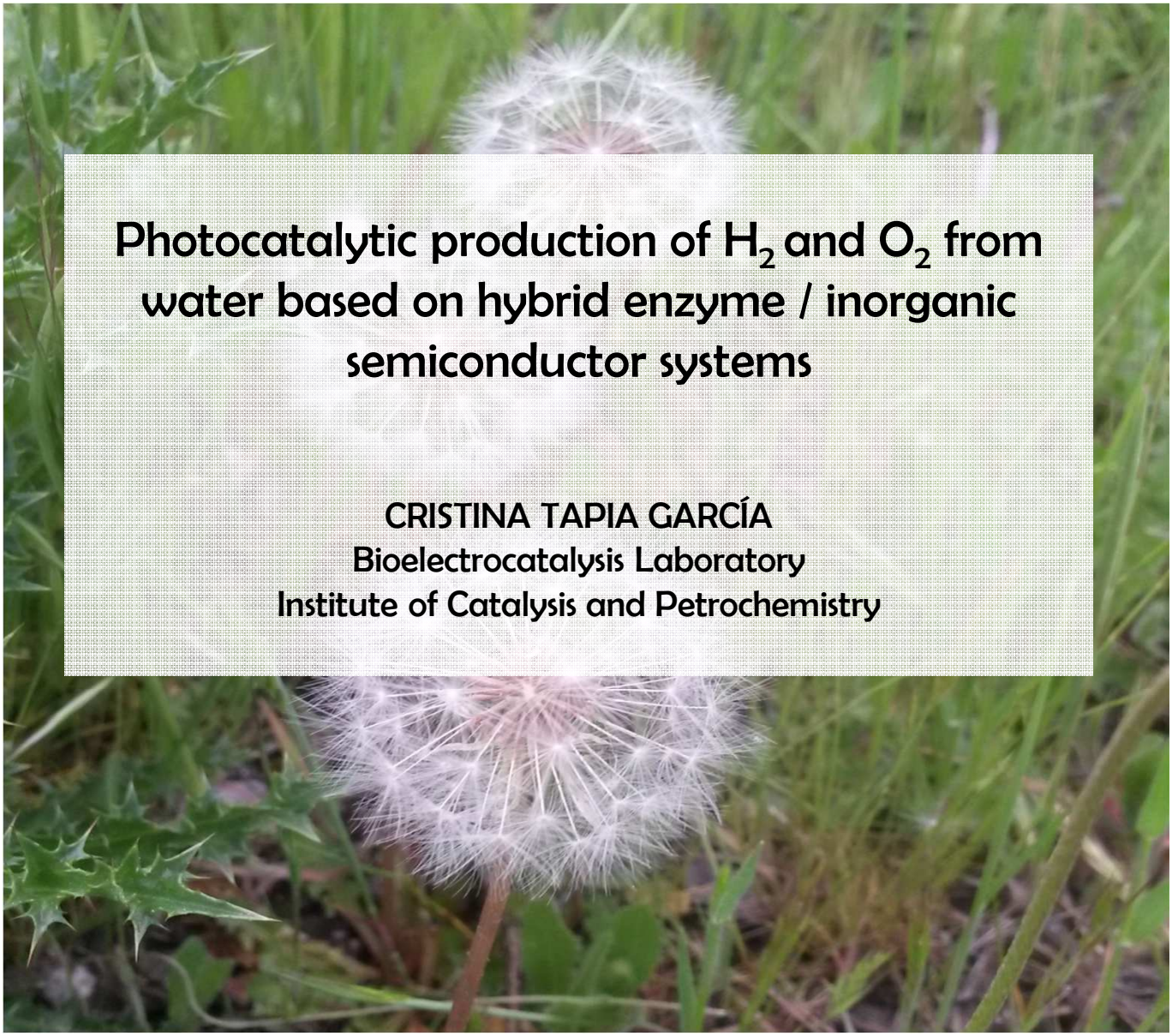

Photocatalytic production of H_2 and O_2 from water based on hybrid enzyme / inorganic semiconductor systems

CRISTINA TAPIA GARCÍA
Bioelectrocatalysis Laboratory
Institute of Catalysis and Petrochemistry

TESIS DOCTORAL
Madrid, 2017

UNIVERSIDAD AUTONOMA DE MADRID

Facultad de Ciencias

Departamento de Biología Molecular

Photocatalytic production of H_2 and O_2 from water based on hybrid enzyme / inorganic semiconductor systems

Cristina Tapia García

Tesis Doctoral

Madrid, 2017

UNIVERSIDAD AUTONOMA DE MADRID

Facultad de Ciencias

Departamento de Biología Molecular

Programa de Doctorado en Biociencias Moleculares

Photocatalytic production of H_2 and O_2 from water based on hybrid enzyme / inorganic semiconductor systems

Institute of Catalysis and Petrochemistry (ICP)

Spanish Council for Scientific Research (CSIC)

Cristina Tapia García

Director: Dr. Marcos Pita Martínez

Co-Director: Dr. Antonio López de Lacey

Tutora: María Fernández Lobato

Tesis Doctoral

Madrid, 2017

MARCOS PITA MARTÍNEZ Y ANTONIO LÓPEZ DE LACEY, DRS. EN CIENCIAS QUÍMICAS, CIENTÍFICO TITULAR E INVESTIGADOR CIENTÍFICO RESPECTIVAMENTE DEL C.S.I.C. EN EL INSTITUTO DE CATÁLISIS Y PETROLEOQUÍMICA

CERTIFICAN: Que el presente trabajo "Photocatalytic production of H_2 and O_2 from water based on hybrid enzyme/ inorganic semiconductor systems", que constituye la Memoria que presenta la Licenciada en Biotecnología por la Universitat Autònoma de Barcelona, Cristina Tapia García, ha sido realizado bajo su dirección en el Departamento de Biocatálisis del Instituto de Catálisis y Petroleoquímica del C.S.I.C., Campus de Excelencia Internacional UAM+CSIC, Madrid.

Para que conste, firman el presente certificado a 5 de Septiembre de 2017.

Dr. Marcos Pita Martínez

Director de la Tesis Doctoral

Dr. Antonio López de Lacey

Co-Director de la Tesis Doctoral

AGRADECIMIENTOS / ACKNOWLEDGEMENTS

En primer lugar, quisiera agradecer a mis directores de tesis, el Dr. Marcos Pita y el Dr. Antonio López de Lacey, el darme la oportunidad no sólo de trabajar en su grupo de investigación sino también de descubrir el mundo de la fotocatálisis.

Quisiera agradecer en especial al Dr. Sebastian Fiechter y al Dr. Lo Gorton su cálida acogida y supervisión durante mis estancias en Helmholtz Zentrum Berlin y en Lund University respectivamente. He adquirido conocimientos muy valiosos para mi carrera profesional, algunos vitales para que esta tesis saliera adelante con buenos resultados.

Doy las gracias también al Dr. José Carlos Conesa por su colaboración en el proyecto y su especial contribución dando a conocer los resultados obtenidos durante la tesis en varios congresos internacionales. También quisiera agradecer diversas colaboraciones fundamentales en el proyecto como la de la Dra. Inés A. Pereira, la Dra. Shelley Minteer y el Dr. Sergey Shleev.

Quisiera dar las gracias también a mis compañeros de laboratorio, tanto del ICP como en las diversas estancias, por el día a día, los viajes, los buenos ratos dentro y fuera de la ciencia, porque de todo se aprende. Gracias Chiara, Fernando, Asier, María, Alejandro, Óscar, Cristina, Sandro, Sonia, Lara, Sean, Carol, Galina, Elena, Sonia Zacarias, y muchos otros. Gracias también al personal del Servicio de Apoyo a la Investigación del ICP, a los chicos de mantenimiento y gases, en especial a José y Armando, y a Carmen y Pili.

En el terreno más personal, llegar hasta aquí no habría sido posible sin al apoyo constante, moral y económico, de mis padres y mi hermana. Quiero dar las gracias en especial a Raquel por estar siempre ahí, desde niñas, para lo bueno y para lo malo, sin duda mi mejor compañera de vida. A Dani por su paciencia y siempre sacarme una sonrisa. A mis amigos del pueblo por un sinfín de buenos momentos, y a Lore y Vero por nuestras estupendas quedadas atletas y perrunas semanales que siempre acaban con cerveza.

Y como no, a la mejor parte de mí, mi querido Yango.

Gracias a todos.

SUMMARY

Water splitting to form hydrogen (H_2) and oxygen (O_2) is considered a sustainable process for energy conversion. The integration of light-harvesting, multistep transfer of electrons and protons and chemical conversion processes, using water as an electron source and sunlight as an energy source, to synthesize biofuels is the principle of photosynthesis. The global aim of this thesis is the development of inorganic/biological hybrid systems for the artificial photosynthesis of H_2 and O_2 from water.

The first approach of this thesis for H_2 electrochemical photoproduction was to combine two biological catalysts, photosystem I (PSI) from spinach's thylakoids as light absorber able to donate high energy electrons, and the [NiFe] hydrogenase from *Desulfovibrio gigas,* with two hydrogels containing different inorganic redox complexes. This combined photocatalytic system was developed on a gold electrode, which allowed the electron transfer from the electrode to the PSI and then from the PSI to the Hase for H_2 evolution. At the same time, the photocurrents derived from the illumination of the system with visible light could be monitored.

The aim of the second approach for H_2 evolution was based on the combination of In_2S_3, an inorganic semiconductor able to absorb in the visible light spectral range, with the [NiFeSe] Hydrogenase from *Desulfovibrio vulgaris* Hildenborough for protons' reduction. In_2S_3 was synthesized and characterized for this purpose. This hybrid photocatalytic system was developed by mixing both components in solution and measuring the H_2 photoproduction by mass spectrometry.

The last approach of this thesis was the photoelectrochemical evolution of O_2 from water by a hybrid system combining the In_2S_3 semiconductor with the *Trametes hirsuta* Laccase, a biocatalyst able to oxidize water to O_2. In this case a Fluorine-doped tin oxide (FTO) coated glass was used as electrode substrate, which was drop-coated with In_2S_3, and the laccase was covalently bound to it. The O_2 photoproduction and faradaic yield were estimated according to the registered photocurrents on the electrode and the response of an O_2 microsensor placed near to the electrode.

RESUMEN

La descomposición del agua para formar los gases de hidrógeno (H_2) y oxígeno (O_2) está considerado un proceso sostenible de conversión energética. La combinación de materiales absorbentes de luz, sistemas de transferencia electrónica y de protones, y centros catalíticos, utilizando agua y luz solar para la síntesis de combustibles, es el principio en el que se basa el fenómeno de la fotosíntesis. El propósito de esta tesis es el desarrollo de sistemas híbridos inorgánicos/biológicos para la fotosíntesis artificial de H_2 y O_2 partiendo de H_2O.

La primera propuesta fue la construcción de un sistema para la fotoproducción electroquímica de H_2 basado en la combinación de dos catalizadores biológicos, el fotosistema I (PSI) extraído de los tilacoides de espinacas como componente absorbente de luz para producir de electrones de alta energía y la [NiFe] Hidrogenasa de *Desulfovibrio gigas*, para catalizar la reducción de protones, con polímeros que contienen complejos metálicos redox. Este sistema combinado se desarrolló sobre un electrodo de oro, permitiendo la transferencia electrónica del electrodo al PSI y del PSI a la hidrogenasa para la evolución de H_2. Se pudo monitorizar la reacción de producción de H_2 registrando las diferencias en la fotocorriente del electrodo cuando éste era iluminado con luz visible.

La segunda construcción desarrollada, también para la fotoproducción de H_2, se basó en la combinación de un material semiconductor inorgánico, el In_2S_3, que es capaz de absorber luz en el intervalo espectral del visible, con la [NiFeSe] Hidrogenasa de *Desulfovibrio vulgaris* Hildenborough como biocatalizador. El In_2S_3 se sintetizó y caracterizó para este fin. La fotoproducción de H_2 se midió para el sistema hibrido de In_2S_3 e hidrogenasa mezclados en disolución, monitorizado por espectrometría de masas.

La tercera y última construcción estudiada en esta tesis tenía por objetivo la fotoproducción electroquímica de O_2 mediante la combinación del In_2S_3, como absorbente de luz, y la lacasa de *Trametes hirsuta*, como biocatalizador para la reacción de oxidación de agua. En este caso se utilizó como sustrato electrodos de vidrio transparente con recubrimiento de Oxido de Estaño y Flúor (FTO), donde se depositó el semiconductor y posteriormente la lacasa unida covalentemente a éste. La fotoproducción de O_2 y el rendimiento faradaico se estimaron por las fotocorrientes registradas en el electrodo y mediante la señal de un microsensor de O_2 situado próximo al electrodo.

CONTENTS

ACRONYMS

- **PSI:** Photosystem I
- **PSII:** Photosystem II
- **FNR:** Ferredoxin $NADP^+$ reductase
- **Hase:** Hydrogenase
- **TOF:** Turnover frequency
- ***Dg*[NiFe] Hase:** *Desulfovibrio gigas* [NiFe] hydrogenase
- ***Dv*[NiFe] Hase:** *Desulfovibrio vulgaris* [NiFeSe] hydrogenase
- **FTIR:** Fourier transform infrared spectroscopy
- **IET:** Intramolecular electron transfer
- **DET:** Direct electron transfer
- ***Th*Lc:** *Trametes hirsuta* Laccase
- **VB:** Valence band
- **CB:** Conduction band
- **ET:** Electron transfer
- **WE:** Working electrode
- **RE:** Reference electrode
- **SHE:** Standard hydrogen electrode
- **Ag/AgCl:** Silver/ silver chloride electrode
- **SCE:** Calomel electrode
- **CE:** Counter electrode
- **PEC:** Photoelectrochemical cell
- **MET:** Mediated electron transfer
- **SAM:** Self-assembled monolayer
- **MV:** methyl viologen
- **$MV^{+\cdot}$:** reduced methyl viologen
- **Cc-monomer:** bis(cyclopentadienyl)cobalt (III) hexafluorophosphate
- **DMSO:** dimethyl sulfoxide
- **PEGDE:** poly(ethylene glycol)diglycidyl ether
- **TRIS:** TRIS (hydroxymethyl)-aminomethane
- **HEPES:** 2-[4-(2-hydroxyethyl) piperazin-1-yl] ethanesulfonic acid
- **4-ATP:** 4-aminothiophenol

· **ABTS:** 2,2'-Azino-bis (3-ethylbenzothiazoline-6-sulfonic acid) diammonium salt

· **MES:** 2-(N-Morpholino) ethanesulfonic acid hydrate, 4-Morpholineethanesulfonic acid

· **4-Dz:** 4-nitrophenyldiazonium perchlorate

· **EDC:** N-(3-dimethylaminopropyl)-N'-ethylcarbodiimide hydrochloride

· **HRP:** Type I horseradish peroxidase 147 $U \cdot mg^{-1}$

· **NHS:** N-hydroxysuccinimide

· **FTO:** fluorine-doped tin oxide coated glass

· **LDG:** low density graphite

· **ITQB:** Instituto de Tecnologia Química e Biológica, Universidade Nova de Lisboa.

· **ICP:** Instituto de Catálisis y Petroleoquímica, CSIC.

· **Os-PVI:** Osmium polymer / ($[Os(2,2'\text{-bipyridine})_2(\text{polyvinylimidazole})Cl]^{+}$)

· **MV-LPEI:** viologen-pendant linear poly(ethylenimine) redox polymer

· **Cc-BPEI:** cobaltocene redox polymer

· **CV:** Cyclic voltammetry

· **XRD:** X-Ray Diffraction

· **SEM:** scanning electron microscopy

· **TEM:** transmission electron microscopy

· **ICP-OES:** inductively coupled plasma optical emission spectrometry

· **BET:** Brunauer-Emmett-Teller

· **EIS:** electrochemical impedance spectroscopy

· **CO:** Carbon monoxide

1. INTRODUCTION

1. INTRODUCTION

The development of renewable energy technologies appears as the main solution to supply the world's energy demands while preventing the greenhouse gas emissions. These technologies include energy storage and energy efficiency for wind, geothermal, biomass and solar resources.

1.1 ARTIFICIAL PHOTOSYNTHESIS

Several decades of development in solar photovoltaic cells have decreased significantly their cost while increasing the lifetime even longer than 25 years. However, the solar input is intermittent and the storage of this energy is still one of the main concerns in research, society and technological applications. Water splitting into hydrogen (H_2) and oxygen (O_2) is considered a sustainable process for energy conversion. This reaction is a thermodynamically unfavorable reaction ($\Delta G° = 237$ kJ·mol^{-1} = 2.46 eV per molecule).[1,2] In this process both half-reactions, O_2 evolution by water oxidation and H_2 evolution by protons' reduction, are critical steps due to the overpotential needed.

$$H_2O \rightarrow H_2 + ½\ O_2$$

In nature, the solar energy is converted to chemical energy by the process of photosynthesis, producing energy essential for the survival of life on earth. This process takes place in the thylakoid membranes of plants, algae and cyanobacteria. Two photosystems are implicated: Photosystem I (PSI) and Photosystem II (PSII). When PSI gets photo-excited electrons are transferred to a series of electron acceptors, and PSI is oxidized. The oxidized PSI captures electrons from PSII, which are transferred through several redox molecules. The PSII then oxidizes water resulting in evolution of O_2. Schematic representation of this process is shown in **Figure 1.1**.

The energy-storage problem can be solved by constructing artificial photosynthetic systems that mimic natural photochemical conversion. Solar fuel production based on both natural and artificial photosynthetic systems has received significant attention in recent years.[3-6] However, an effective system has not been developed.

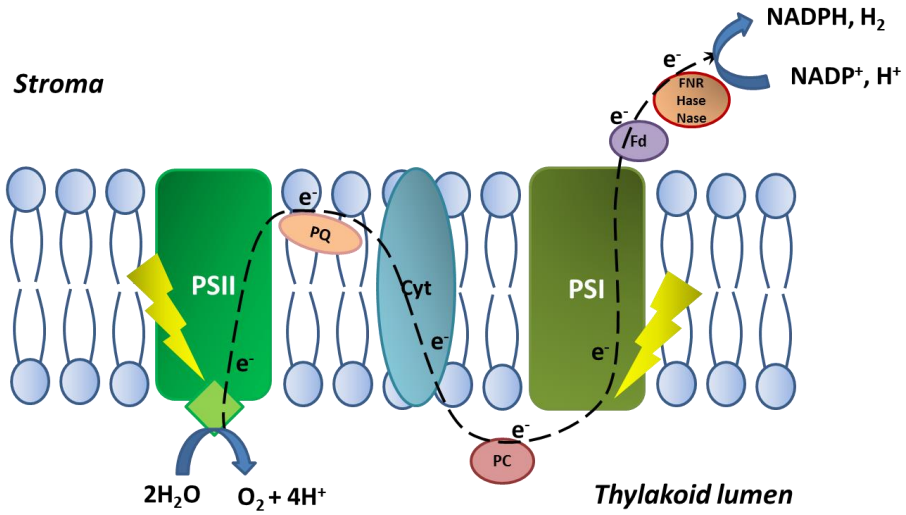

Figure 1.1 ***Schematic process of photosynthesis involving PSI and PSII.*** *When PSI is illuminated the excited electrons are transferred to ferredoxin and are used by ferredoxin NADP$^+$ reductase (FNR) for NADPH production. Also, the electrons transferred to the ferredoxin can be used by hydrogenase (Hase) or nitrogenase (Nase) for H$^+$ reduction. When PSII is illuminated the exited electrons are transferred to Plastoquinone and then to the Plastocyanin through cytochrome b_6f. The oxidized PSI accepts the electrons from the reduced Plastocyanin. The PSII then oxidizes water in O_2.*

The first published studies in photolysis of water are from Honda-Fujishima on 1972 using TiO_2 photoelectrode,[1,2] which is the best-known photocatalyst and photoelectrode. It is stable, affordable and highly photoactive, however its large bandgap (E_g= 3.0-3.2 eV) limits absorption to UV light, disregarding ≥ 95% of the solar spectrum. Efficient photocatalytic production of H_2 and O_2 from water can be achieved by the formation of a hybrid photocatalyst that combines an inorganic semiconductor, able to absorb in the visible light spectral range, with a catalyst for reducing protons to H_2 or water oxidation.[6-9] Hydrogenases (Hases) have shown to be good catalysts for photocatalytic H_2 production when adsorbed on TiO_2,[10] CdS,[11] CdTe,[12] or carbon nitride[13] semiconductors. Other metal-free catalysts, such as organic semiconductors, have also been studied for H_2 photoelectroproduction.[14] A part from semiconductors, other molecular entities or polymers have been proposed and reviewed[3,6,15-17] as photocatalysts. For efficient H_2O oxidation to O_2, other enzymes like *i.e.* PSII have been studied in several works for their immobilization on electrodes, either within a conductive polymer or in presence of a redox mediator in the electrolyte in order to transfer the electrons from the catalytic site of PSII to the electrode surface. [18-20]

The components of artificial photosynthetic systems that mimic natural photochemical conversion for energy storage will be described in the next subsections. There will be detailed the properties of the biological components, the enzymes, and the inorganic semiconductor materials for light –harvesting. The fundaments of electron transfer and connections between light absorber and catalyst will also be described.

1.2 THE ENZYMES

A catalyst is defined as a molecule or material that increases the rate of a chemical reaction because it decreases the activation energy (**Figure 1.2**). When this molecule is a protein it is called enzyme. They are responsible for thousands of chemical reactions in life. The most important properties of the enzymes are their high selectivity and specificity for the substrate due to complementary molecular fitting at the active site. [21]

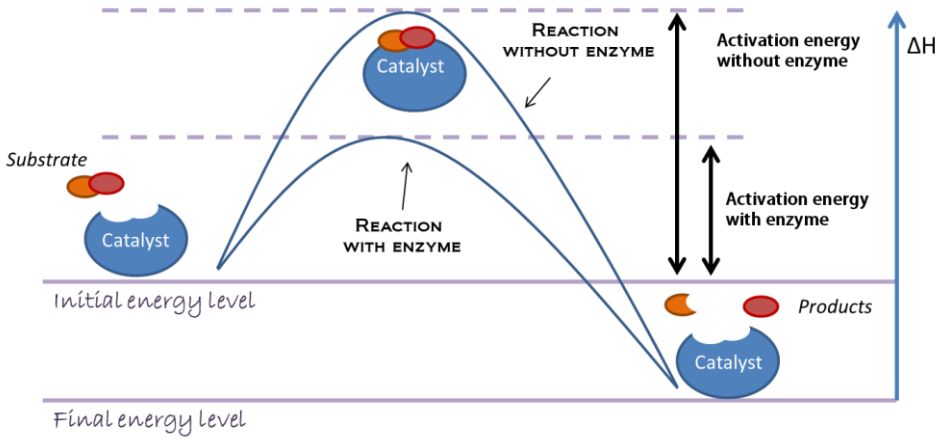

Figure 1.2 ***Scheme of a catalytic process.***

The most extended classification of enzymes is based on the reaction that they catalyze, which comprises 6 groups:[21]

Oxidoreductases: oxidation/reduction reactions.

Transferases: transfer of a functional group from one substrate to another.

Hydrolases: formation of two products from a substrate by hydrolysis.

Lyases: non-hydrolytic addition or removal of groups from substrates.

Isomerases: intramolecular rearrangement (isomerization).

Ligases: join together two molecules by synthesis of new C-O, C-S, C-N or C-C bonds with ATP cleavage.

Several oxidoreductases, also known as “redox enzymes”, have been used in this work for artificial photosynthesis: Hases, Laccase and PSI.

1.2.1 Hydrogenases (Hases)

Hases are metalloenzymes that catalyze molecular hydrogen evolution by the reduction of two protons, and the reverse reaction. These metalloenzymes have attracted immense interest because they are extremely active catalysts and can be used in fuel cells, electrocatalytic or photocatalytic devices and serve as model for synthetic catalysts.[22-25] Hases have shown an excellent electrocatalytic activity with a turnover frequency (TOF) up to 10,000 s^{-1} when they are attached to electrodes.[26] Hases can be classified in three groups according to the metal ion composition of their active site: NiFe, FeFe and Fe Hases. In the present work two types of NiFe Hases has been used: [NiFe] Hydrogenase from *Desulfovibrio gigas* (*Dg*[NiFe] Hase) and [NiFeSe] Hydrogenase from *Desulfovibrio vulgaris* Hildenborough (*Dv*[NiFeSe] Hase).

NiFe Hases are the most abundant group of Hases and are composed by a minimum of two subunits, known as the large and small ones (**Figure 1.3A**). The large subunit contains the NiFe active site and the small subunit includes the electron-transferring pathway based on one or more iron-sulphur clusters forming a chain from the protein surface to the active site .[27]

In the large subunit, the binuclear active site of NiFe Hases is formed by one Fe atom and one Ni atom coordinated by four cysteines. The Fe atoms are coordinated by inorganic ligands, 1 CO^- and 2 CN^-, which are detected by Fourier transform infrared spectroscopy **(**FTIR).[28] The Ni atom is coordinated by the S atoms of two bridging cysteines, also coordinated to the Fe atom, and by two other cysteines terminally bounded. The active site presents in same redox states another ligand bridging the Fe and Ni atoms, which is a hydride in the most reduced active states, or a hydroxyl in the oxidized inactive states. In the CO-inhibited state, an extrinsic CO is terminally coordinated to the Ni.[28] The active site scheme for a standard NiFe Hase is shown in **Figure 1.3B**.

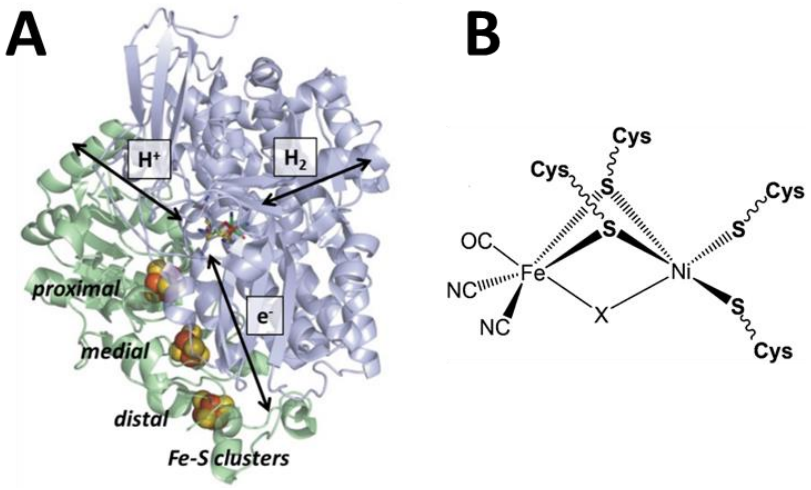

Figure 1.3 ***A) Scheme of a Hydrogenase showing the paths for H_2, H^+ and electrons. PDB 1H2R.***[29] ***B) Scheme of the active site of a [NiFe] Hase.***[30] *X represents the vacant site to which the substrates (H_2/H^+) or the inhibitors (O_2,CO) coordinate (either in terminal or bridging mode).*

In some cases, like in one of *D. vulgaris* hydrogenases, a terminal cysteine ligand of the Ni atom is replaced by a selenocysteine. Two different conformations of the [NiFeSe] Hase are obtained during its purification from *D. vulgaris* Hildenborough cells: the soluble form and the membrane form.[31] The higher amount of this enzyme is isolated in the membrane form, presenting a hydrophobic chain in the N-terminal region of the large subunit through which it associates to the cytoplasmic membrane, and the minor amount in the soluble form. The mentioned soluble form is the one used in this thesis. The two subunits of the [NiFeSe] Hase are 63 and 35 kDa in size.[32] A hydrophobic channel in the large subunit allows the molecular hydrogen to reach the active site, where the heterolytic separation of H_2 take place.[33,34] The protons are transferred to the exterior via cysteine, histidine and glutamate residues.[34] The small subunit contains the three $[4Fe4S]^{2+/1+}$ clusters, named proximal, medium and distal according to their positions, which allow the intramolecular electron transfer (IET). The electrons are exchanged with the enzyme´s redox partner (a cytochrome, organic dyes like viologens or an electrode) at the distal cluster. The short distances between clusters (0.5-0.7 nm) are crucial for the fast IET.[35,36] The region surrounding the distal cluster shows high variability. The charge distribution of the [NiFeSe] Hase is similar to those of other [NiFe] Hases from *Desulfovibrio* species, where glutamic residues predominate around the distal cluster.[37,38] The active site´s redox potential of these Hases is around – 400 mV (*vs.* SHE).[28]

The majority of the Hases are synthesized by anaerobic microorganisms, which make them highly sensitive to oxygen.[39,40] However, some Hases have been described that are less affected by carbon monoxide and/or oxygen, like NiFe Hydrogenase-1 from *Escherichia coli*[41] and the membrane-

bound NiFe Hases from *Ralstonia eutropha*[42] *and Aquifex aeolicus*.[43] The*Dv*[NiFeSe] Hase is also O_2 tolerant when electroproducing H_2 because of its fast reactivation at negative redox potential.[44,45]

1.2.2 Laccases

Laccase enzymes belong to the group of multicopper oxidases that contain four copper cations distributed in two redox sites. Laccases catalyze the reduction of O_2 to H_2O using several organic compounds as electron donors, such as *orto* and *para*-diphenol, aminophenol, polyphenol and lignin, and also are able to oxidize some inorganic compounds.[46,47] Laccases can be classified depending on their origin: produced by plants or by fungi. However, there have been also described some laccases that are able to oxidize diphenol derivatives in bacteria and insects.[48,49] Most laccases are extracellular enzymes, but some fungi also contain intracellular ones.[50] This location difference may be due to their physiological function.[51,52]

The main structural difference between laccases of different sources is in the substrate catalytic site.[53] Laccase molecules are monomeric and present three domains. Laccase's Cu atoms are distributed in two different sites of the enzyme: (i) the T1 site, which contains 1 Cu coordinated to 3 or 4 amino acid residues, is near the protein surface and receives the electrons from the donor compound during the catalytic reaction and then transfers the electrons one by one to the T2/T3 site; (ii) the T2/T3 site is formed by a cluster of 3 Cu and it is the catalytic center for the 4-electron reduction of O_2 to H_2O (**Figure 1.4A**).[54] The O_2 and the H_2O molecules have access to the T2/T3 sites through a channel from/to the protein surface. There is also an intramolecular electron pathway connecting the T1 and T2/T3 sites.[54]

The T1 center is the site that directly accepts electrons from the substrate oxidation. Laccases can directly oxidize the compounds with redox potentials lower than the T1 center one, so the T1 redox potential defines the efficiency of the laccase on the oxidation of the substrates. High redox potential laccases are highly interesting, as they are able to reduce oxygen at potentials above or near 0.7 V (*vs.* SHE) by direct electron transfer (DET) with electrodes.[55,56] The catalytic activity of laccases is irreversible when measured under the optimal conditions, at which the pH value is around 4. However, it has been already reported that a native laccase covalently attached to chemical modified graphite electrodes was capable of oxidizing H_2O to O_2 at neutral pH when a high overpotential of + 1.2 V (*vs.* SHE) was imposed at the electrode.[57]

Trametes hirsuta laccase (*Th*Lc) is a globular glycoprotein with fungal origin, classified as a high redox potential laccase according to its T1 center, which is 780 mV (*vs.* SHE).[47,58] The redox potential for the T2/T3 site of *Th*Lc is 400 mV (*vs.* SHE).[59,60] This laccase produces high catalytic current densities

and has high operational stability when attached to an electrode.[61] It has 70 kDa of molecular weight and 65x55x45 Å dimensions. Its structure contains 12% of carbohydrates.[62]

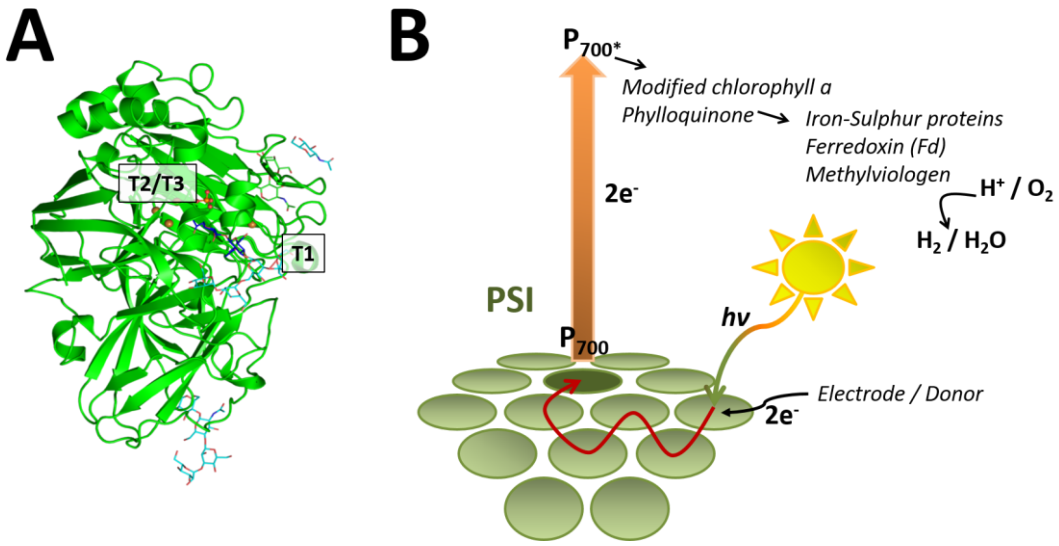

Figure 1.4 ***A) Scheme of a Laccase showing the T1 site and the T2/T3 Cu cluster. B) Scheme of Photosystem I and the electron pathway when illuminated.***

1.2.3 Photosystem I (PSI)

The PSI is a multisubunit membrane protein complex that plays a photosynthetic role and it is located in the thylakoid membranes of plants, algae and cyanobacteria. It catalyzes the transfer of an electron from the plastocyanin or cytochrome C6 on the luminal side to the ferredoxin or flavodoxin on the cytoplasmatic side of the thylakoids in chloroplasts (Figure 1.1). This protein has two main subunits, psaA and psaB. A special pair of chlorophyll-a molecules lies at the center of the structure which absorbs light at 700 nm. This special pair is denoted as P700. Upon excitation P700* transfers an electron through a chlorophyll and a bound quinone (Qa) to a set of 4Fe-4S clusters. From these clusters, the electron is transferred to the ferredoxin, a water-soluble mobile electron carrier located on the stroma, which is used for the reduction of $NADP^+$ catalyzed by FNR or for H_2 production catalyzed by a Hase. Therefore, PSI is capable of absorbing visible light by exciting low-energy electrons to high-energy ones, resulting in a considerable decrease on the overpotential needed for hydrogen evolution in presence of an adequate catalyst.[63] **Figure 1.4B** show the schematic flow of electrons when illuminating PSI.

Hases and *Th*Lc can be used as catalysts, for H_2 and O_2 evolution respectively, in the construction of the artificial photosynthetic systems. PSI can be used as a light absorber component, but also inorganic semiconductors can play this role. The properties of the semiconductors will be detailed below.

1.3 SEMICONDUCTORS

When classifying a material according to its conductivity it can be a conductor, an insulator or a semiconductor. A conductive material such as a metal has a low resistance to the electric current, whereas an insulator has a very high resistance. A semiconductor is a material where the conduction energy levels can be reached with an affordable energy amount.

In order to understand how a semiconductor works it is necessary to mention the "band theory for solids". A solid material is formed by large number of atoms, where the molecular orbitals overlap yielding energy bands. The electrons locate at the energy levels belonging to the band. The main energy bands of solid materials are the valence band (VB) and the conduction band (CB). The VB is occupied by the electrons in the fundamental state; while the CB will be empty if there is no excitation of the valence electrons. In a conductive material, the separation between the VB and CB is negligible, which means the electrons from the VB can be promoted to the CB with very low energy. In the case of insulators, the energy gap between bands is so large that the energy needed to promote the electrons from VB to CB is too high. However, in semiconductors it is possible to allow the electrons to be promoted between bands under certain conditions of pressure, light, temperature and/or presence of impurities (**Figure 1.5**).[64,65]

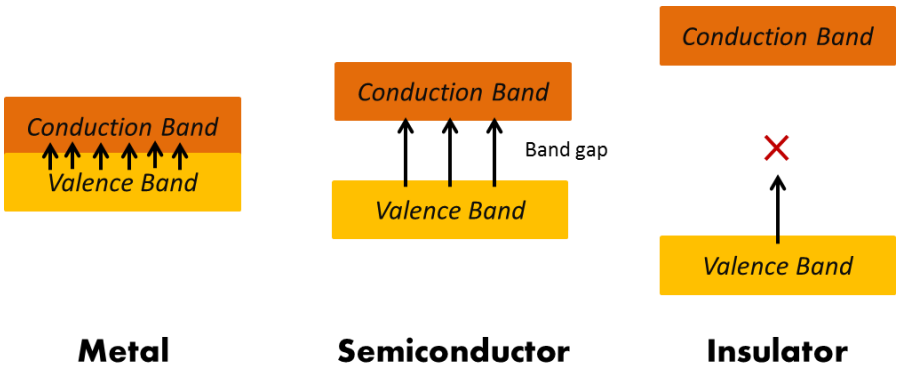

Figure 1.5 ***Scheme of metal, semiconductor and insulator enegy bands.***

1.3.1 The band gap

The difference of energies between the VB and CB in a semiconductor is known as band gap. In this space of energy there are no electrons. Therefore, the band gap is the minimum energy needed to promote an electron from the VB to the CB in semiconductors.

The band gap energy can be expressed in eV, which corresponds to a determined wavelength radiation (λ) in the spectrum of solar radiation (1), as correlated by the *Plank equation* (2):

$$\nu = \frac{c}{\lambda} \qquad (1)$$

$$E = h \cdot \nu \qquad (2)$$

Where ν is the frequency of the electromagnetic wave (s^{-1}), c is the value of light speed (299,792.458 $Km \cdot s^{-1}$). In the *Plank equation*, E corresponds to energy in eV and h is the Plank constant ($6.62607004 \cdot 10^{-34}$ $m^2 \cdot kg \cdot s^{-1}$).

Figure 1.6 shows the irradiance spectra of sunlight measured above the top regions of the Earth's atmosphere.[66] The three relevant band ranges along the solar radiation spectrum are ultraviolet, visible and infrared. Of the total light that reaches Earth's surface infrared radiation makes up 49.4% of it, while visible light provides 42.3%.[67] Ultraviolet radiation makes up just over 8% of the total solar radiation. Therefore, further approaches are focused on the use of materials able to use efficiently visible light. These include TiO_2 doped with anions (N or S) or cations (Cr, V, Fe); nitrides or oxinitrides like Ta_3N_5, TaON; the perovskites $LaTiO_2N$ and $LaNbON_2$; oxides like $BiVO_4$, Cu_2O, WO_3 or Fe_2O_3; or sulphides like $CuGaS_2$, CdS, In_2S_3, $ZnIn_2S_4$, SnS_2 or MoS_2.[68-73]

The current in a semiconductor occurs via mobile or "free" electrons and holes, collectively known as charge carriers. When a semiconductor is irradiated the pair electron-hole is created, where the electron is excited to the CB and a hole is created in the VB. Although the natural tendency of an excited electron is the relaxation back to the VB, it may be accepted by a catalyst, for example a Hase in this thesis. The created holes may be filled by a holes' scavenger present in the electrolyte or a catalyst for water oxidation, for example a Laccase in this thesis.

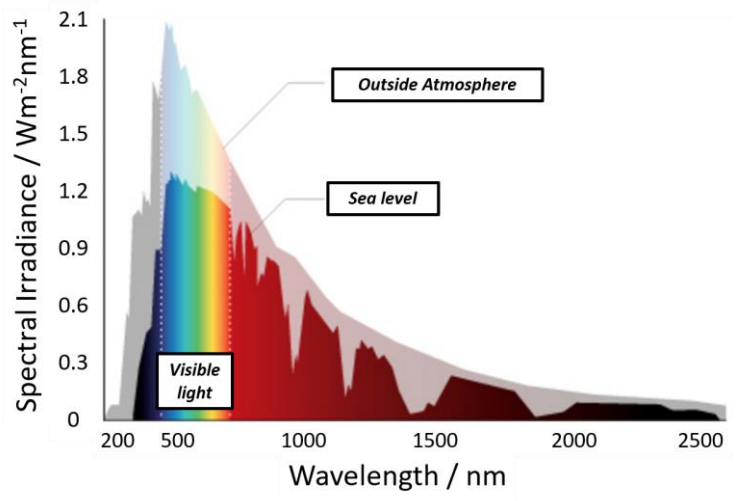

Figure 1.6 ***Spectral irradiance vs photon wavelength.*** *Figure adapted from Fondriest Environmental, Inc. "Solar Radiation and Photosynethically Active Radiation." Fundamentals of Environmental Measurements*[74]

Many metal-sulphide semiconductors have attracted much attention due to their band gaps being in the energy range of visible light radiation and their CB energy level situated above of that required for reducing protons to H_2. In **Figure 1.7** are shown the energy bands for several conductors.[75]

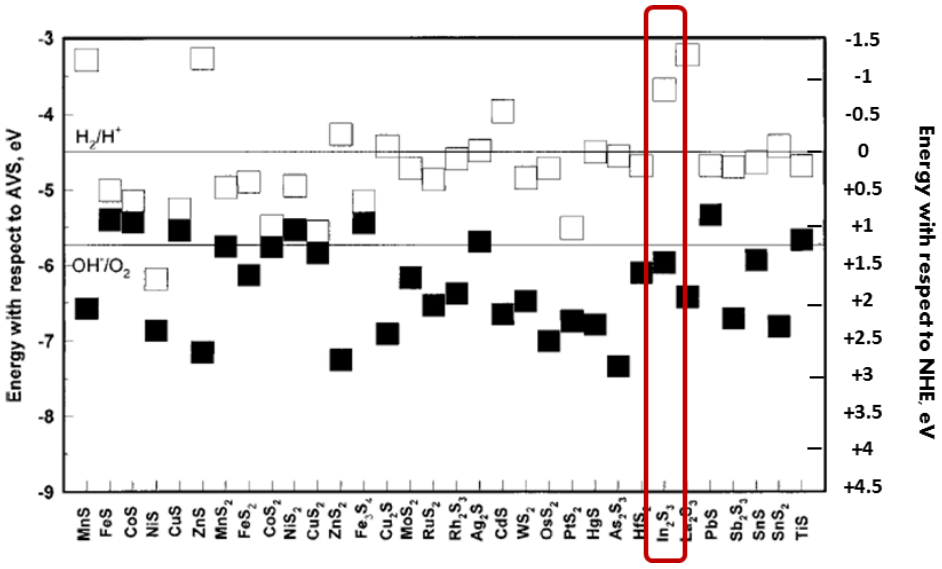

Figure 1.7 ***Energy levels for conduction and valence bands of semiconductors at pH 0,*** *extracted from Xu, Y.; Schoonen, M. A. A. (2000), The absolute energy positions of CB and VB of selected semiconducting minerals, Am. Mineralogist.*[75] *The In_2S_3 VB and CB energy bands are plotted inside the red rectangle. The two grey lines represent the standard redox potentials of H_2/H^+ and OH^-/O_2.*

In semiconductor physics, the band gap of a semiconductor can be defined as a direct band gap or an indirect band gap. The minimal-energy state in the CB and the maximal-energy state in the VB are each characterized by a certain crystal momentum. The band gap is called "direct" if the momentum of electrons and holes is the same in both the CB and the VB; an electron can directly emit a photon. In an "indirect" gap, a photon cannot be emitted because the electron must pass through an intermediate state and transfer momentum to the crystal lattice.

1.3.2 n-type and p-type semiconductor

An important property to take in account when working with semiconductors in photoelectrochemistry is the type of majority charge carriers formed in the material when irradiated. Based on this, there are two types of semiconductors: n-type ones when electrons are the majority charge carriers behaving as donors of charge, and p-type ones when holes are the majority charge carriers behaving as acceptors of charge.[76]

In an n-type semiconductor, the Fermi level lies closer to the CB than to the VB. Oppositely, the Fermi level lies closer to the VB than the CB for p-type semiconductors. In electrochemical processes n-type semiconductors will be used in oxidation reactions at the electrode, whereas p-type semiconductors will be used in reduction reactions. This behavior is related to the band bending when the semiconductor is in equilibrium with the electrolyte.[76]

1.3.3 Band bending and flat band potential

When a semiconductor is placed in contact with an electrolyte, electric current initially flows across the junction until electronic equilibrium is reached, where the Fermi energy of the electrons in the solid (E_F) is equal to the redox potential of the electrolyte (E_{redox}). In consequence, the charge distribution on the junction differs from the bulk material, and this effect is known as the space-charge layer. On the electrolyte side, this corresponds to the electric double layer: the compact Helmholtz layer followed by the diffuse Gouy–Chapman layer.[76-78] On the semiconductor side of the junction the nature of the band bending depends on the position of the Fermi level in the solid. [77-78]

Band bending refers to the local changes in the energy offset of a semiconductor's band structure near the junction, due to these space charge effects. The band diagram in **Figure 1.8** shows the electron energy states of a semiconductor´s CB (E_c), VB (E_v) and E_F versus the distance from the surface, before and after the contact with an electrolyte. The degree of band bending depends on the

relative Fermi levels of the material and the electrolyte, and on the charge carrier concentrations of the materials forming the junction. In the p-type semiconductor the bands bend upwards, while in n-type the bands bend downwards. In an n-type semiconductor, the band bending facilitates the electrons to move to the bulk of the material, whereas the holes migrate to the interface with the electrolyte. In p-type semiconductor, the band bending facilitates the electrons to migrate to the electrolyte interface, whereas the holes move to the bulk.

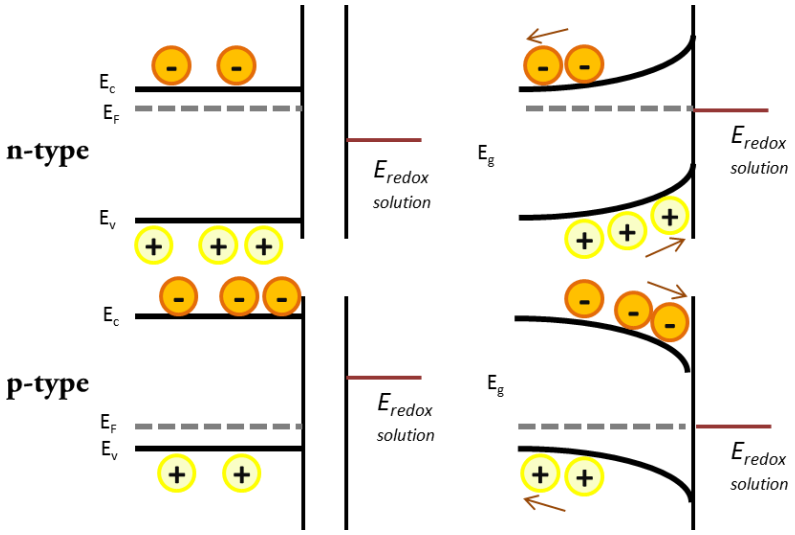

Figure 1.8 ***N-type and p-type semiconductor band bending in contact with an electrolyte*****.**

The flat band potential of a semiconductor is a very useful value in photoelectrochemistry as it facilitates location of the energetic position of the VB and CB edges of a given semiconductor material. It is obtained by measuring the capacity of the semiconductor-electrolyte junction at different applied potentials.[78]

1.3.4 In_2S_3 semiconductor

The semiconductor In_2S_3 (indium (III) sulfide) is frequently used as a buffer layer in photovoltaic solar cells[79-82] or water splitting photochemical cells,[83] because of its interesting electron-handling properties. This semiconductor is also interesting because it has low toxicity and is easily synthesized by solvothermal reaction with no further modification. [83]

The In_2S_3 was the first indium compound ever described, being reported in 1863.[84] In_2S_3 is an inorganic compound with "rotten egg" odor. In_2S_3 features tetrahedral In(III) centers linked to four sulfide ligands. Three different structures or polymorphs are known: α-In_2S_3 with defect cubic structure, β-In_2S_3 with defect spinel tetragonal structure and γ- In_2S_3 with layered structure. In β-In_2S_3

the sulfide anions are closely packed in layers, with octahedrally-coordinated In(III) cations present within the layers, and tetrahedrally-coordinated In(III) cations between them. A portion of the tetrahedral interstices is vacant, which leads to defects in the spinel. Two subtypes of β-In_2S_3 are described: in the T-In_2S_3 subtype the tetragonally-coordinated vacancies are in an ordered arrangement, whereas the vacancies in C-In_2S_3 are disordered. The latter subtype, in presence of a noble metal catalyst, shows activity for photocatalytic H_2 production.[85]

In_2S_3 is a n-type semiconductor with gap energy of 2-2.3 eV, which corresponds to a $\lambda \approx 500$ nm light absorption. Therefore, In_2S_3 is a suitable material to absorb visible light photons to excite the VB electrons to the CB. It is known that its CB potential is - 0.8 V (*vs*. RHE),[75,86] which is negative enough for the H_2 evolution reaction.[75,86] On the other hand, the VB potential is positive enough for the O_2 production reaction. Both bands energies are represented in Figure 1.7. However, when working with semiconductors in electrochemistry, the n or p type property of the material will determine the possibility of exchanging electrons with the electrode on either reductive or oxidative reactions. In_2S_3 is a n-type semiconductor, which limits the use of this material for oxidation reactions at the electrode.

A photochemical study has revealed a carrier mobility value for In_2S_3 that is in the same range as compounds frequently used in photoelectrodes, such as the metal oxides semiconductors Cu_2O, WO_3 and $BiVO_4$.[87,88] In this thesis, In_2S_3 will be either used for photocatalytic production of H_2, coupled to Hase activity in aqueous solution, and for photoelectrochemical O_2 production, using *Th*Lc immobilized on an electrode as catalyst.

The transfer of charge carriers between light absorber and catalyst for photocatalytic water splitting can be considered a critical step in artificial photosynthetic systems. Moreover, when the hybrid photocatalyst is built on an electrode the electron transfer (ET) between light absorber and electrode is also one of the main concerns for maximizing the efficiency.

1.4 ELECTRON TRANSFER

1.4.1 Fundaments

The charge transfer takes place in the interface between an electrode, made with a conductor or semiconductor material, and the electrolyte solution, where the electric charge is transferred through ions. [89-93]

When an electrode is polarized the ions from the electrolyte diffuse to the surface to counter the charges created in the electrode and, in the interface, is formed what is known as electrical double-layer.[94] The presence of a double layer in the electrode/electrolyte induces a capacitance (C_d), which is a non-faradaic process. When the applied potential (E) on the electrode varies,[92,93] the distribution of the charges at the double layer changes with time (dq/dt) and in consequence a capacitive current (i_c) is measured. If we make the approximation of considering the system as an ideal capacitor then:

$$C = \frac{q}{E}$$

$$i_c = \frac{dq}{dt} = C_d \, x \frac{dE}{dt}$$

In faradaic processes, the ET between the solution and the electrode involves a redox reaction. A basic electrochemical reaction is defined as:

$$O + ne^- \rightleftarrows R$$

where O is the oxidized species, R is the reduced species, and n is number of electrons involved in the reaction. The relation between O and R concentrations and the free energy is:

$$\Delta G = \Delta G° + RT \ln \frac{[R]}{[O]}$$

Where R is the gas constant (8.3145 J·mol^{-1}·K^{-1}), T (K) is the temperature and $\Delta G°$ (J·mol^{-1}) is the standard Gibbs free energy change. From the Gibbs free energy change, the redox potential can be derived:

$$\Delta G^{\circ} = -nFE^{\circ\prime}$$

Where $E^{\circ\prime}$ is known as the standard electrode potential, and F is Faraday's constant (96485 C·mol^{-1}).

The potential of the **thermodynamic** equilibrium in faradaic processes is determined by the *Nernst* equation that correlates redox potential on the electrode with the concentration of *O* and *R* species in the interface and the $E^{\circ\prime}$ of the redox reaction.

$$E = E^{\circ\prime} - \frac{RT}{nF}\ln\frac{[R]}{[O]}$$

Kinetic aspects of the redox reactions are defined by the *Butler-Volmer* equation in conditions of non-equilibrium:

$$i = i_{\mathrm{o}}\left[e^{\frac{(1-\alpha)nF\eta}{RT}} - e^{\frac{(-\alpha)nF\eta}{RT}}\right]$$

Where i is the net current (A), i_o is the exchange current, α is the ET coefficient characteristic for each redox system and η is the applied overpotential (V).

The current intensity on the electrode is also controlled by **mass transport** from the bulk of the electrolyte to the electrode surface. The most important modes of transport in electrochemistry are the *diffusion of the redox species* that create a concentration gradient at the electrode/electrolyte interface, the *migration of the ions* due to electric field applied at the electrode and the *convection* due to agitation of the electrolyte or rotation of the electrode.

In faradic process two types of electrochemical cells are defined: galvanic and electrolytic cells.[92,93]

- In *galvanic cells,* a redox reaction occurs spontaneously when two electrodes are connected externally by an external circuit and share the same electrolyte, or their respective electrolytes are separated by a barrier that allows ion transport.

- In *electrolytic cells,* the redox reaction is non-spontaneous and an external energy source is applied to generate a potential difference across the cell and force the electrochemical reactions to take place. For electrochemical studies, a three electrode system is commonly used.

In the three electrodes electrochemical cell, the reaction of interest takes place on the working electrode (WE). In order to determine the potential on the WE it is used a Reference electrode (RE) which has a stable and well-known electrode potential. The conventional RE is the standard hydrogen

electrode (SHE) and by definition its potential is equal to 0.000V at all temperatures. However, the silver/silver chloride electrode (Ag/AgCl 3M KCl), with a potential in standard conditions of + 0.222 V (*vs.* SHE), or the standart calomel electrode (SCE KCl $_{sat}$), with a potential in standard conditions of + 0.240 V (*vs.* SHE), are normally used as RE. The third electrode on the electrochemical cell is the auxiliary or Counter Electrode (CE) which provides the circuit over which current is either applied or measured to balance the reaction occurring at the working electrode. The most common CE is Pt wire electrode.

One of the most extended applications of electrochemical cells is the fuel cells. A conventional fuel cell set up consists in two half-cells connected in series by a conductive electrolyte containing anions and cations. One half-cell includes a negatively polarized electrode to which cations migrate (Cathode). The other half-self includes an electrode positively polarized to which anions migrate (Anode). Redox reactions are then taken place in the electrode: reduction in the cathode and oxidation in the anode.

The potential of a cell (E_{cell}) is defined as the difference between the potential of the cathode (E_c) and the potential of the anode (E_a):

$$E_{cell} = E_c - E_a$$

Another application of electrochemical cells is the development of Photoelectrochemical cells or PECs. This type of cell electrolyzes water to H_2 and O_2 by irradiating the anode with electromagnetic radiation (**Figure 1.9**).

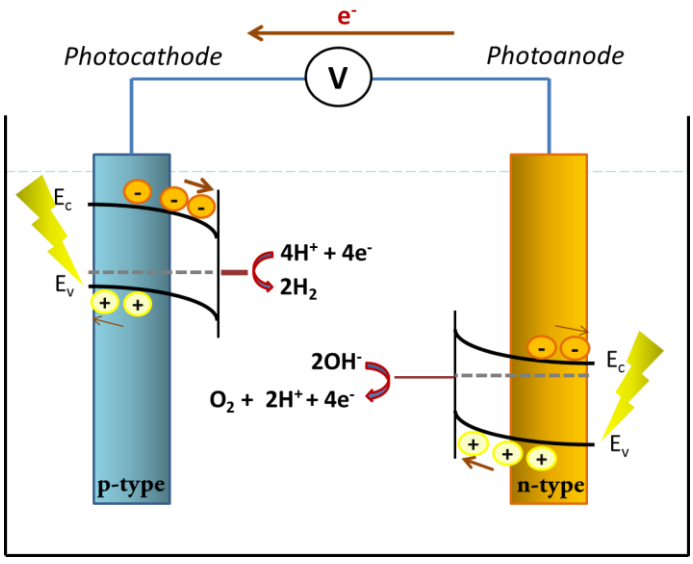

Figure 1.9 ***Scheme of a photoelectrochemical cell (PEC).*** *The reaction in the anode corresponds to photoproduction of O_2 and in the cathode, to photoproduction of H_2.*

For an efficient photoelectrocatalyst the interface between light absorber, catalyst and electrode must be optimal to allow fast ET between them and the reactive species in the solvent. When enzymes are used as light absorber and/or catalyst, the ET between these components and/or the electrode is often mediated by a redox compound in solution or by a redox polymer, and is defined as mediated electron transfer (MET).[95] However, when the ET is directly from the Oxidized/Reduced species to the catalyst and the electrode it is defined as DET. In order to achieve efficient DET, the functionalization of surfaces to orientate and anchor enzymes is the most useful approach. [95-100]

1.4.2 Enzymes immobilization

Several strategies can be applied to attach efficiently enzymes to electrodes and/or semiconductors for efficient ET at the interface (**Figure 1.10**):

- Physical adsorption of the enzyme on the material surface.
- Surface functionalization of the material for covalent binding of the enzyme.
- Co-immobilization of enzymes and hydrogels on the material (cross-linking).

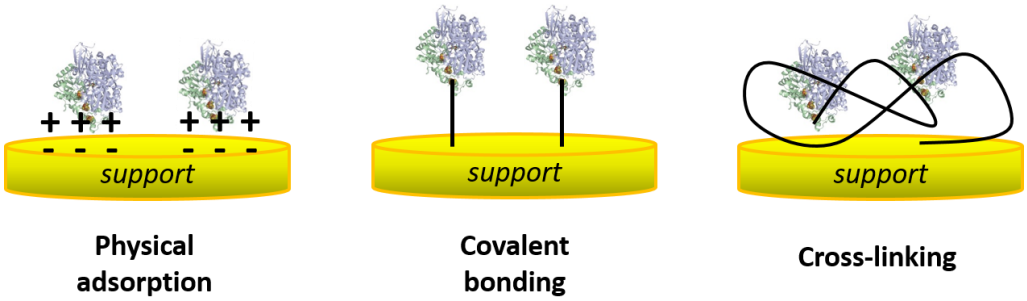

Figure 1.10 ***Scheme of three enzymatic immobilization strategies: physical adsorption, covalent bonding and cross-linking hydrogel*.**

Physical adsorption of the enzyme on the surface of the electrode or semiconductor material is based on electrostatic interactions, van der Waals forces and/or hydrogen bridges. The main factors that affect to this interaction are the pH of the solution, ionic strength and the roughness and porosity of the surface of the support.

The immobilization of enzymes on **functionalized surfaces** favors the correct orientation of the biocatalysts due to different types of interactions: electrostatic ones, hydrophobic ones, hydrogen bridges, disulfide bridges, etc. Functionalization also allows formation of covalent bonds between the

enzyme and the support.[101,102] The covalent immobilization process is based on the reaction of the functionalized groups generated on the surface of the electrode with the functional groups of the enzyme. It is known that this kind of immobilization can also prevent the enzyme from its denaturalization.[103]

The functionalization of the electrode surface, among many other methods, can be done by formation of self-assembled monolayers (SAM)[103] or disulfide bonds formation of thiol molecules. The thiols adsorption on gold and other solid supports[104-107] is spontaneous, with high rate of organization, compaction and stability.[103] The surface functionalization through diazonium aromatic salts is also an extended approach for enzymes immobilization. The electrochemical reduction of this molecules on the electrode surface yields in a covalent bond -C-X between the aryl ring of the molecule and the electrode support (X), which is interesting for its high stability.[108,109]

Redox hydrogels are cross-linked polymer network structures capable of swelling in water and present an electron-conducting phase, where water-soluble biomolecules can dissolve and diffuse.[110] Redox hydrogels conduct electrons by self-exchange reactions of electrons through collisions between reduced and oxidized centers bound to the backbone of the cross-linked polymer networks.[111] In many cases enzymes have been integrated in cross-linked redox hydrogels. [112-117]

2. OBJECTIVES

2. OBJECTIVES

The main objective of this thesis is the development of inorganic/biological hybrid systems for photo-water splitting by combining a visible light absorber component with a catalyst, either in solution or on an electrode surface. For this goal, the study and optimization of the interface between absorber and catalyst is necessary to efficiently transfer the photo-excited electrons from one to the other.

The aim of the first photosystem is the H_2 photoproduction from protons on an electrode that incorporates a biological light absorber, the photosystem I (PSI) complex extracted from spinach, and the [NiFe] Hydrogenase (Hase) from *Desulfovibrio gigas* electrically wired by a hydrogel of organometallic redox polymers.

The aim of the second hybrid-photosystem is also the H_2 photoproduction from protons but using In_2S_3 semiconductor as light absorber combined with [NiFeSe] Hase from *Desulfovibrio vulgaris* Hildenborough using a sacrificial electron donor in solution.

The aim of the third hybrid-photosystem is the O_2 photoproduction from water on electrodes by depositing the In_2S_3 semiconductor on a FTO substrate and further covalent attachment of *Trametes hirsuta* Laccase to it.

Some additional objectives to achieve these goals are:

- Study of the stability of PSI and *Dg*[NiFe] Hase immobilized on electrodes by entrapment in redox polymers.
- Synthesis and characterization of the In_2S_3 semiconductor.
- Characterization of the *Dv*[NiFeSe] Hase soluble form.
- Functionalization of electrodes with aminophenyl groups for enzyme covalent immobilization.
- Modification of FTO electrodes with In_2S_3 particles and its further functionalization for the covalent immobilization of Laccase.

3. MATERIALS AND METHODS

3. MATERIALS AND METHODS

3.1 REAGENTS AND MATERIALS

All the reagents were used as received without further purification and are listed here:

Sodium phosphate monobasic dihydrate 99%, sodium phosphate dibasic dihydrate 99.5%, sodium chloride 99.5%, calcium chloride dihydrate 99%, methyl viologen dichloride hydrate 98% (MV), sucrose, dimethyl sulfoxide (DMSO), bis(cyclopentadienyl)cobalt (III) hexafluorophoshate 98% (Cc-monomer), poly(ethylene glycol)diglycidyl ether (PEGDE), $InCl_3$ 99.999%, thiourea 99%, sodium sulfite 98%, TRIS (hydroxymethyl)-aminomethane 99%, 2-[4-(2-hydroxyethyl) piperazin-1-yl] ethanesulfonic acid 99.5% (HEPES), 4-aminothiophenol 97% (4-ATP), 2,2'-Azino-bis (3-ethylbenzothiazoline-6-sulfonic acid) diammonium salt 98% (ABTS), 2-(N-Morpholino) ethanesulfonic acid hydrate, 4-Morpholineethanesulfonic acid (MES hydrate) 99.5%, 4-nitrophenyldiazonium perchlorate (4-Dz), tetrabutylammonium tetrafluoroborate 99.0%, sodium meta-periodate 99.8%, N-(3-dimethylaminopropyl)-N'-ethylcarbodiimide hydrochloride (EDC), Type I horseradish peroxidase 147 $U \cdot mg^{-1}$ (HRP) and Triton X100 were purchased from Sigma-Aldrich. Magnesium chloride hexahydrate 99.9%, ethanol absolute 99.5%, acetonitrile and acetone 99.5% was purchased from Scharlau. Sodium acetate 99.5% and N-hydroxysuccinimide 97.0% (NHS) were purchased from Fluka. Sodium hydrogen carbonate 99.999%, di-sodium hydrogen phosphate 12-hydrate 99.0-102.0%, sodium di-hydrate phosphate 2-hydrate 99.0-102.0% and HCl 37% were purchased from Panreac. Sodium dithionite 87% was purchased from MERK. All the water solutions were prepared with MilliQ deionized water (18.2 MΩ · cm). Grey dielectric paste was supplied by Gwent Group.

The gases used were H_2 99.999%, 20 % H_2: 80% Ar mixture, O_2 99.999%, CO 99.999% and Ar 99.999% supplied by Air Liquide and N_2 99.999% bottle supplied by AGA.

The electrode supports used were: 2 mm-diameter polycrystalline gold disk from Bioanalytical Systems, Inc. (BASi), 5 mm-diameter polycrystalline gold rotating disk from Pine Instruments, fluorine-doped tin oxide coated glass (FTO) from Sigma-Aldrich and low density graphite 99.999% rods of 3.05 mm diameter (LDG) from Alfa Aesar.

3.2 EXTRACTION AND PURIFICATION OF THE ENZYMES

Four enzymes were used in this thesis work: the PSI, the *Dg*[NiFe] Hase, the *Dv*[NiFeSe] Hase and the *Th*Lc. The extraction and purification protocols for each enzyme are described here.

3.2.1 PSI enzymatic complex

The extraction of PSI was carried out at the group of Professor Dr. Lo Gorton of the Center for Molecular Protein Science (CMPS) in Kemicentrum of Lund University during a three-month secondment.

The PSI extract was obtained from *Spinacia oleracia*. 200 g of spinach baby leaves were mixed into 500 mL of an aqueous solution containing 50 mM sodium phosphate, 500 mM sucrose and 10 mM NaCl pH 7.4. The mixture was homogenized in a mixer for 1 min, followed by filtration through 4 layers of nylon net (25 µm mesh) supported on a strainer. The filtered solution was then centrifuged at 2,500 g for 5 min and resuspended in fresh buffer. The dispersion was centrifuged again at 2,500 g for 5 min, and then resuspended in 500 mL of 50 mM sodium phosphate buffer pH 7.4 containing 50 mM sucrose and 10 mM NaCl. This solution was centrifuged and resuspended twice in the same buffer. The final pellet was resuspended in 120 mL of 50 mM sodium phosphate buffer pH 7.4 containing 150 mM NaCl. The extract was treated with a French press at 1,000 psi at low flow for 10 min for the thylakoids fragmentation. The resulting material was collected and ultracentrifuged at 40,000 g for 30 min. The supernatant was transferred to new tubes and centrifuged at 100,000 g for 1 h. The pellet was resuspended in 10 mM sodium phosphate, 100 mM sucrose and 5 mM NaCl pH 7.4 to a final volume of 3 mL. Finally, DMSO was added to the sample at a final concentration of 5 % (v/v). The sample was divided into aliquots of 20 µL and frozen at -80°C. The extraction procedure used produced enrichment of the stroma lamella of thylakoids, which is rich in PSI.[118,119] The final PSI enriched membrane fraction concentration was 0.6 mg chlorophyll (a+b)/mL. Chlorophyll determination was made spectrophotometrically in 80 % acetone.[120]

3.2.2 *Desulfovibrio gigas* [NiFe] Hydrogenase

Dg[NiFe] Hase was purified at the Institute de Biologie Structurale et Microbiologie, CNRS, Marseille, according to a previously-published protocol and kindly supplied by Prof. Dr. Claude Hatchikian.[121] The final concentration of Hase, determined by Bradford protein assay, was 7.7 mg/mL in 100 mM phosphate buffer pH 7.6.

3.2.3 *Desulfovibrio vulgaris* Hildenborough [NiFeSe] Hydrogenase

Dv[NiFeSe] Hase soluble form was purified by the Bacterial Energy Metabolism laboratory of Dra. Inês A. C. Pereira at the Instituto de Tecnologia Química e Biológica (ITQB), Universidade Nova de Lisboa, Portugal. [122]

10 g of *Desulfovibrio vulgaris* cells were resuspended in 10 mL of 20 mM TRIS pH 7.6 with DNAse, followed by 3 cycles of French press at 1000 psi to disrupt the cells. The solution was centrifuged for 15 min at 10,000 rpm at 4°C. The supernatant was separated and ultracentrifuged for 1 h and 30 min at 42,000 rpm at 4°C. The soluble fraction was collected and filtered through a 0.22 nm porous membrane. The enzyme purification was continued by FPLC chromatography using an AKTA Q-Sepharose 16/10 column (Column volume = 25 mL), finally eluted in 20 mM TRIS pH 7.6 containing 1 M NaCl. The fraction obtained was purified afterwards using an affinity column. The washing buffer was 100 mM TRIS-HCl pH 8 containing 150 mM NaCl and the elution buffer was 100 mM TRIS pH 8 containing 150 mM NaCl and 2.5 mM desbiotin. The fractions collected were 20, 25 and 30% of elution buffer, which correspond to the most concentrated and pure enzyme fraction. These fractions were concentrated using a 30 kDa pore size Diaflon membrane. The concentration was measured by the Bradford protein assay and purity checked by Acrilamide/SDS Gel electrophoresis (**Figure 3.1**). The purified Hase 5.8 mg/mL was kept in 20 mM TRIS-HCl pH 7.6 at -80°C.

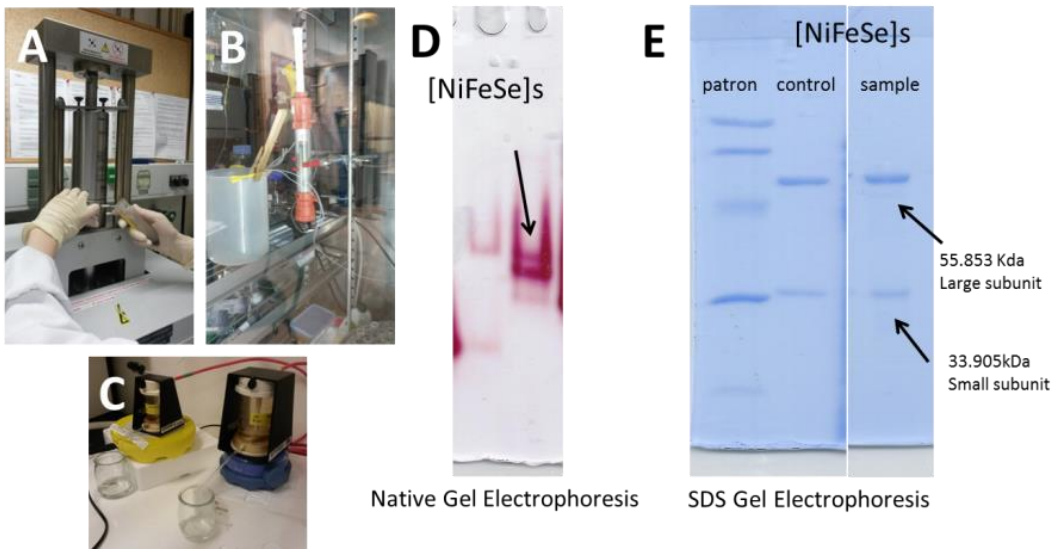

Figure 3.1 Purification of *Dv*[NiFeSe] Hase. *A) French press, B) chromatography, C) concentration, D) Native Gel electrophoresis and E) SDS Gel electrophoresis steps.*

3.2.4 *Trametes hirsuta* laccase purification (*ThLc*)

The *Th*Lc, strain 56, was used from a frozen stock purified at the Moscow State University of Engineering Ecology as previously reported,[123] which was kindly supplied by Professor Dr. Sergey Shleev. The enzyme concentration was determined using the Bradford method,[124] calibrated with BIO-RAD (Bio-Rad Laboratories) and bovine serum albumin. *Th*Lc was stored at -80°C in 100 mM phosphate buffer pH 6.0 at a concentration of 5.8 mg/mL.

3.3 SYNTHESIS OF In_2S_3 SEMICONDUCTOR

In this thesis, the semiconductor In_2S_3 was used as light absorber in combination with *Dg*[NiFe] Hase for H_2 evolution, and with *Th*Lc for O_2 evolution.

The polycrystalline powder of In_2S_3 was synthetized by a known hydrothermal procedure[125] in collaboration with the Nanostructured Catalysts for Energy Group of Professor Dr. José Carlos Conesa in the Instituto de Catálisis y Petroleoquímica (ICP).

"Hydrothermal synthesis" method for single crystals synthesis is based on the solubility of minerals in hot water under high pressure. Following this procedure, a Teflon-lined steel high-pressure reactor, as shown in **Figure 3.2**, was filled with 50 mL of aqueous solution containing 148 mM $InCl_3$ and 178 mM thiourea. 80 µL of 37 % HCl were added and the reactor was set into a stove at 453 K (180°C) during 48 hours. Then the product was collected and centrifuged during 15 min at 20°C and 7000 rpm using a BECKMAN Coulter Avanti J-E centrifuge with a JA 25.5 rotor. The supernatant was discarded and the pellet was redispersed in 40 mL MilliQ·H_2O. This process was repeated twice in order to increase the purity of the precipitate. Finally, another centrifugation-redispersion cycle was carried out using EtOH to remove as much water as possible from the precipitate. The resulting pellet was dried for 12 hours at 60°C. The reaction yield was 80 %.

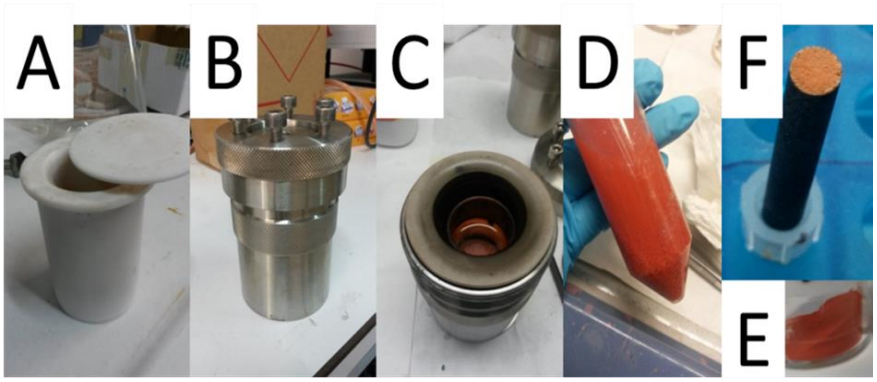

Figure 3.2 ***Hydrothermal synthesis of In_2S_3.*** *A) 125 mL Teflon container where the 50 mL vessel with the reagents is placed, B) high-pressure reactor, C) precipitated product, D) washing process, E) dried powder and F) powder deposited onto the bare low density graphite rod for the electrochemical measurements.*

3.4 MODIFICATON OF ELECTROACTIVE SURFACES

LDG and FTO electrodes were modified with In_2S_3.

3.4.1 In_2S_3-LDG electrode

The LDG rod was polished using sandpaper and then immersed in H_2O:EtOH 1:1 solution during 10 min in an ultrasound bath. Then In_2S_3 semiconductor, synthetized as described in **section 3.3**, was deposited on a LDG electrode as follows: a 30 mg/mL In_2S_3 suspension on EtOH was prepared; 6 µL of it were deposited onto a clean LDG rod, and dried at 100°C under vacuum during 2 hours (Figure 3.2F).

3.4.2 In_2S_3-FTO electrode

2x1cm FTO glass electrodes were cleaned by immersion into water and 15 min ultrasound treatment. Afterwards the electrodes were washed with EtOH, immersed into acetone and treated for 15 min with ultrasounds. The electrodes were further washed with EtOH and ultrasounds were applied during 15 min in the same solvent. Then the electrodes were let to dry. Afterwards the electrodes were masked with dielectric paste leaving exposed 0.196 cm^2 of active surface.

In parallel a 4 mg/mL suspension of In_2S_3 in EtOH was prepared and treated with ultrasounds during 20 min. 7 µL of the In_2S_3 suspension were dropped on the FTO electrodes and let to dry for 5 min. The dropping-drying process was performed a total of 5 times and let to dry overnight. Finally, a copper wire was connected to the FTO with conductive adhesive tape (**Figure 3.3**).

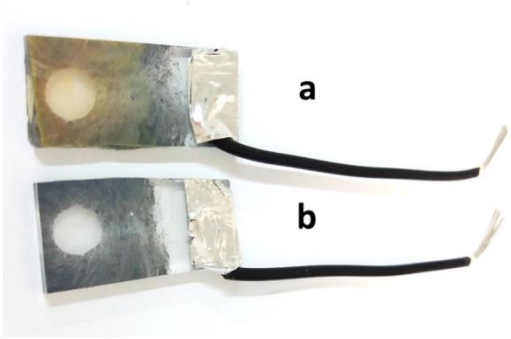

Figure 3.3 ***(a) FTO/In_2S_3 and (b) bare FTO electrodes.***

3.5 PREPARATION OF REDOX POLYMERS

Three redox polymers, shown in **Figure 3.4**, were tested to wire the PSI to the *Dg*[NiFe] Hase on a gold electrode for H_2 photoproduction.

3.5.1 Osmium redox polymer

The Osmium polymer ([Os(2,2'-bipyridine)$_2$(polyvinylimidazole)Cl]$^+$) (Os-PVI) was kindly donated by Professor Dr. Dónal Leech from the School of Chemistry, National University of Ireland at Galway, Ireland. The polymer synthesis has already been reported.[126] The standard potential of the Os-PVI is +420 mV (*vs.* SHE). Os-PVI was dissolved in MilliQ·H_2O up to a concentration of 10 mg/mL, sonicated for 2 h and then it was stored at 4°C for further use.

3.5.2 Viologen redox polymer

The viologen-pendant linear poly(ethylenimine) redox polymer (MV-LPEI) was synthesized and kindly donated by Professor Dra. Shelley Minteer from the Department of Chemistry, University of Utah, Salt Lake City, USA, as previously reported.[127,128] MV-LPEI was dissolved in MilliQ·H_2O at a concentration of 2.5 mg/mL and sonicated for 4 h; the dissolved MV-LPEI was stored at 4°C.

3.5.3 Cobaltocene redox polymer

The cobaltocene redox polymer (Cc-BPEI) was synthesized and kindly donated by Professor Dra. Shelley Minteer from the Department of Chemistry, University of Utah, Salt Lake City, USA, as already reported.[128] Cc-BPEI was dissolved in MilliQ·H_2O at a concentration of 2.5mg/mL, sonicated for 1 h and stored at 4°C.

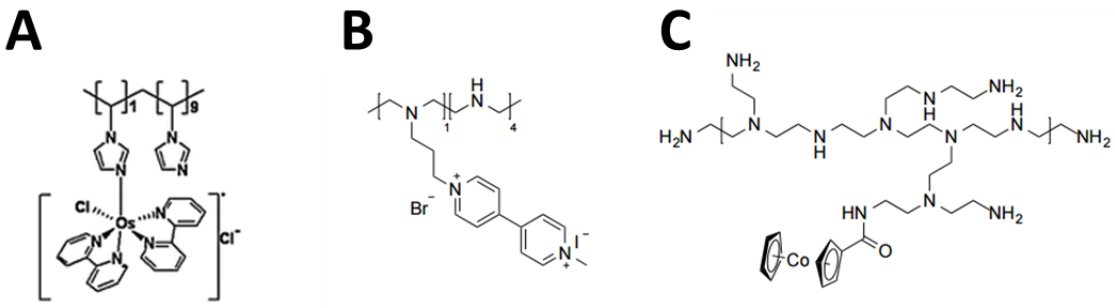

Figure 3.4 ***A) Os-PVI, B) MV-LPEI and C) Cc-BPEI redox polymers structures.***

3.6 EXPERIMENTAL CONDITIONS AND TECHNIQUES

3.6.1 PSI – Hydrogenase for H_2 photoelectroproduction

3.6.1.1 Electrode modification

2 mm-diameter polycrystalline gold disk electrode was cleaned with Piranha solution (3:1 H_2SO_4:H_2O_2) for 15 min. This step must be done with caution since hydrogen peroxide and sulfuric acid react violently and highly exothermically. Then it was polished with 1.0 µm alumina slurry. The polishing step was repeated with 0.3 µm and 0.05 µm alumina slurries and sonicated for 10 min in 1:1 EtOH:H_2O solution. Afterwards 25 scans of cyclic voltammetry (CV) from 0.2 to -1.3 V (*vs.* SHE) in 0.5 M NaOH at scan rate of 200 mV/s were applied. Then 25 scans from 0.2 to 1.7 V (*vs.* SHE) at a scan rate of 200 mV/s in 0.5 M H_2SO_4 were applied.

The redox polymers were electrochemically evaluated by drop-coating 2 µL of each polymer on the surface of a gold electrode. After drying, the initial electrochemical measurements were performed in a 10 mM sodium phosphate buffer at pH 7.5 containing 10 mM NaCl and 5 mM $MgCl_2$ after O_2 removal by N_2 bubbling for 30 min.

The stability of PSI on the electrode was studied by PSI immobilization on clean gold electrodes together with Os-PVI. First 2 µL of Os-PVI were dropped on the gold electrode and dried for 5 min. Meanwhile the following solution (PSI mix) was prepared: 10 µL of 0.6 mg/mL PSI was mixed with 1 µL of Triton (1/100) and 1 µL of PEGDE (0.12 mg/mL). The use of a detergent such as Triton favored the accessibility to the PSI donor side (P700) in the purified extract. After allowing the Os-PVI to adsorb for 5 min, 2.5 µL of the PSI mix were added and left to incubate additionally for 15 min. Following incubation, the modified electrode was covered with a Spectra/Por®1 Dialysis membrane (MWCO: 6-8 kD) before the electrode could reach dryness.

Electrode modification with redox polymers, PSI and *Dg*[NiFe] Hase was accomplished in a step-wise fashion. Initially, a 1 µL drop of Os-PVI was deposited on a clean electrode. After allowing the Os-PVI to adsorb for 5 min, 1.5 µL of the PSI mix was deposited onto the electrode and allowed to incubate at room temperature for 15 min. Another solution comprising 1.5 µL of 7.7 mg/mL Hase mixed with 1.5 µL of 2.5 mg/mL MV-LPEI or 1.5 µL of 2.5 mg/mL Cc-BPEI and 0.5 µL of 0.12 mg/mL PEGDE was prepared and 2 µL of it was deposited onto the modified electrode and allowed to incubate further for 15 min. Following incubation, the modified electrode was covered with an osmotic membrane before the electrode could reach dryness. Control experiments in the absence of either PSI or Os-PVI on a clean gold electrode were performed also.

For studying H^+ transport to *Dg*[NiFe] Hase through the Cc-BPEI polymer a 5 mm-diameter

rotating polycrystalline gold disk electrode (Pine Instruments) was used. It was cleaned following the same protocol as described above. Each electrode was modified with a 14 µL mixture of 6 µL of 7.7 mg/mL Hase, 6 µL of 2.5 mg/mL Cc-BPEI and 2 µL of 0.12 mg/mL PEGDE and allowed to incubate at room temperature for 15 min.

3.6.1.2 Measurements' conditions

Electrochemical measurements for H_2 photoelectroproduction were performed in a three-electrode cell, with a refrigeration glass jacket, using Ag/AgCl (KCl sat.) as RE and a Pt wire as CE. A typical electrolyte solution comprised 10 mM sodium phosphate buffer, 10 mM NaCl, 5 mM $MgCl_2$ and 1 mM MV at pH 7.5.

For photoelectrocatalytic H_2 production experiments, O_2 was first removed from the electrolyte by bubbling with N_2 for 30 min. On the other hand, for the studies of PSI stability the buffer was bubbled with O_2 to act as the final electron acceptor. MV in solution was used to mediate electron transfer from PSI to *Dg*[NiFe] Hase for H_2 production to compare with the ability of the redox polymers for MET. Photocurrent measurements for H_2 production were performed at 40°C, although PSI studies for O_2 reduction were performed at 25°C. Photoelectrochemical measurements were performed using a solar light simulation Fiber liter MI-150 Lamp from Dolan-Jenner Industries, placed at ~5 cm from the electrode surface. The light intensity was set at 40 mW/cm^2. All CVs were performed at a scan rate of 10 mV/s. The current density values were calculated considering the geometrical area of the electrode, which is 0.0314 cm^2. Each measurement was performed between 3 to 5 times in order to evaluate the reproducibility of the electrode preparation for PSI incorporation. Even though the catalytic behavior was reproducible, the magnitude of catalytic current varied from electrode to electrode. Representative CVs are shown.

For diffusional studies of H^+ to *Dg*[NiFe] Hase through Cc-BPEI polymer, experiments were performed in a M-Braun anaerobic chamber (O_2 content ≤ 0.1 ppm). The electrochemical cell contained as electrolyte 30 mL of 10 mM phosphate buffer, 10 mM NaCl and 5 mM $MgCl_2$, at pH 7.5 and 40°C. It was used as RE a SCE and as CE a Pt wire. The O_2 was removed from the electrolyte by bubbling N_2 for 30 min. CVs were recorded at 10 mV/s from -0.2 to -0.51 V (*vs.* SHE). Activity's stability was tested by chronoamperometry at -0.51 V (*vs.* SHE). The rotation speed was controlled at 0 rpm, 100 rpm, 500rpm and 1000 rpm. Measurements were controlled by a PG30 Autolab Potentiostat/Galvanostat from Ecochemie. Temperature was kept at 40°C using a MultiTempIII thermostatic water recirculation system from Pharmacia Biotech.

3.6.2 In_2S_3 – Hydrogenase for H_2 photoproduction

3.6.2.1 FTIR measurements

The FTIR spectra were recorded at 2 cm^{-1} resolution and by averaging 1024 scans from 4000 to 800 cm^{-1} using a Bruker Tensor 27 Fourier transform spectrometer, equipped with a mercury cadmium telluride detector and a purge gas system (Whatman) for removal of CO_2 and H_2O. Temperature of the cell was kept at 25°C using a thermostatic recirculation bath CC230 from Huber.

Dv[NiFeSe] Hase sample was first concentrated up to 117 µM by ultrafiltration using Amicon 50K. The measurements were performed in a transmission CaF_2 cell with 82 µm path length. Three different states of the Hase were measured: as isolated, reduced and reoxidized. For the as isolated state of the Hase, 25 µL of the enzyme 117 µM solution were added to the FTIR cell. For obtaining the reduced state of the Hase, the as-isolated sample was deoxygenated by three cycles of vacuum-argon in a vial with a rubber Suba Seal septum (Sigma-Aldrich). Then, 1 µL of 10 mM sodium dithionite, for every 50 µL of Hase solution, was added through the septum with a gas-tight syringe (SGE Analytical Science) to reduce residual O_2 and finally kept under 1 atm H_2 atmosphere for 25 min at room temperature. The sodium dithionite solution was prepared in a special vial with two tubes, keeping the reagent separately from the buffer 20 mM TRIS pH 8 until O_2 was removed by doing three cycles of vacuum-argon before mixing. For obtaining the reoxidized state, the reduced Hase solution was exposed to air overnight and kept at 4°C.

3.6.2.2 Electroactivity of *Dv*[NiFeSe] Hase in gold electrode

Rotating gold disk electrodes from PINE with 5 mm diameter were used for the electroactivity study of *Dv*[NiFeSe] Hase. First the electrodes were cleaned by immersion in piranha solution (3:1 H_2SO_4:H_2O_2) during 15 min. Then the electrodes were polished with 1.0 µm alumina solution. The polishing step was repeated with 0.3 µm and 0.05 µm alumina solution and sonicated for 10 min in 1:1 EtOH:H_2O solution. Afterwards 25 scans from 0.2 to -1.3 V (*vs.* SHE) in 0.5 M NaOH at scan rate of 200 mV/s were applied. Then 25 scans from 0.2 to 1.7 V (*vs.* SHE) at a scan rate of 200 mV/s in 0.5 M H_2SO_4 were applied.

Once the gold electrodes were clean, a 4-ATP SAM was obtained by immersing the electrodes in an EtOH solution containing 1 mM of 4-ATP and incubated overnight (**Figure 3.5**). After 4-ATP SAM was formed on the electrode's surface it was rinsed carefully with 100 mM Phosphate buffer pH 7. 6 µL of the 5.8 mg/mL *Dv*[NiFeSe] Hase was deposited on the surface and let it to incubate for 30 min. Then it was let to react during 90 min with 5.5 µL of 14 mM EDC and 4.5 µL of 21 mM NHS prepared in

MES 10 mM pH 6. An amide bond is formed between amino groups of the 4-ATP SAM and the carboxylic residues at the Hase surface (Figure 3.5). Then the modified electrode was immersed in 100 mM Phosphate buffer pH 7 with slow stirring for 5 min in order to remove the non-attached Hase to the electrode surface.

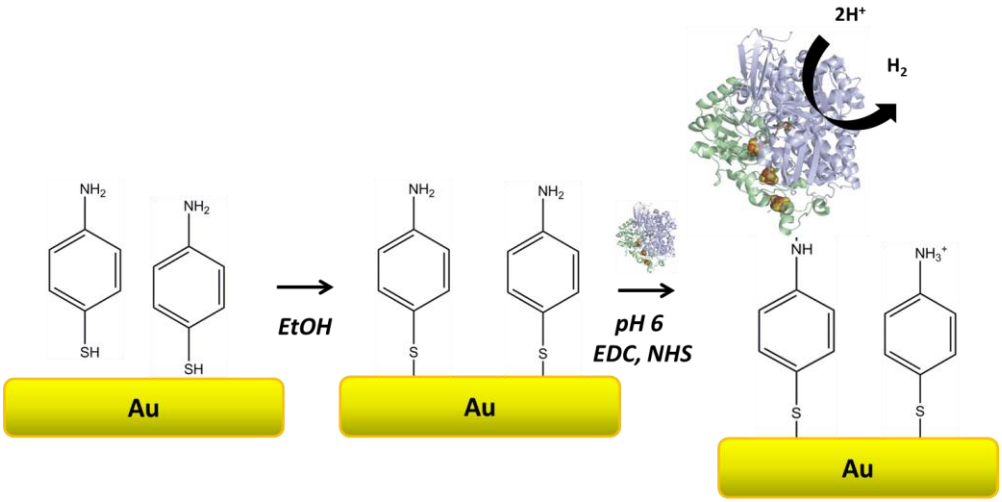

Figure 3.5 ***Functionalization of gold electrode with 4-ATP SAM*** *by immersing the electrode in 4-ATP in EtOH solution overnight. Then* ***immobilization of Hase*** *by covalent bond with EDC and NHS 90 min incubation at pH 6.*

The electrochemical measurements were performed in 100 mM Phosphate buffer at pH 7. All the measurements were performed inside the anaerobic chamber. Previously, O_2 was removed from the electrolyte by bubbling N_2 for at least 30 min. A three-electrode electrochemical cell with refrigerated glass jacket was used, connected to a thermostatic water recirculation system MultiTempIII from Pharmacia Biotech set at 30°C. A SCE was used as RE, and a Pt wire as CE. CV was used to characterize the kinetics and inhibition properties of the *Dv*[NiFeSe] Hase. Scans from -0.40 to 0.45 V (*vs.* SHE) were performed. For the study of the H_2 oxidation, H_2 was bubbled into the electrolyte during 30 min, and then the current for DET was measured by CV. Rotation was applied for mass transport limitation studies. Then the electrolyte was changed to 100 mM Phosphate buffer pH 7 containing 1 mM MV redox mediator to study the MET between Hase and electrode. For inhibiting the *Dv*[NiFeSe] Hase 1000 µL of CO-saturated buffer were added to the solution since CO binds to the enzyme´s active site, blocking its activity. The reversible *Dv*[NiFeSe] Hase activation was studied upon the addition of 50 µL of O_2-saturated buffer, which was used to remove the CO from the active site. This inhibition process was monitored by chronoamperometry at -0.45 V (*vs.* SHE) and 500 rpm electrode rotation. The current densities were calculated considering the geometrical area of the electrode, which is 0.196 cm^2. Each measurement was performed three times. The electrochemical

measurements were controlled by a PG30 Autolab Potentiostat/Galvanostat from Ecochemie. Representative CVs and chronoamperometry are shown.

3.6.2.3 Mass spectrometer measurements

The H_2-production activity of the *Dv*[NiFeSe] Hase was measured by membrane-inlet quadrupole mass spectrometry from Pfeiffer Prisma. The output signal of the mass spectrometer for each mass value expressed as a current signal is proportional to the partial pressure of the corresponding gas in the reaction vessel.[129] The rate of H_2 production in the reactor solution was measured by monitoring the evolution of mass 2 signal, which corresponds to H_2, with time at the spectrometer. The output signal of the spectrometer for mass 2 was calibrated first by saturating the reactor solution with 100 % H_2.

The **catalytic activity** of the *Dv*[NiFeSe] Hase was measured in a 10 mL solution of 50 mM TRIS pH 7.0 containing 0.1 M MV. The solution was purged with 100 % Ar and then the reactor was closed, leaving no gas phase inside. 10 µL solution of as isolated 0.166 µM Hase were injected to the reactor through a rubber septum with gastight syringes (SGE Analytical Science). The reaction was initiated by injecting 2 µL of 1 M sodium dithionite into the vessel for reducing the MV. The activity in U/mg protein was calculated from the maximum slope of the curve of the H_2 output signal. The activity was also measured for previously activated Hase sample. The activation process consisted on adding 1 µL of 10 mM sodium dithionite to 50 µL of anaerobic enzyme solution in a glass vial with a rubber Suba Seal septum (Sigma-Aldrich) and then incubated under 100% H_2 atmosphere during 25 min at room temperature.

For **photoactivity** measurements of the inorganic/enzymatic hybrid system, 22.1 µmol In_2S_3 particles and 0.26 pmol of *Dv*[NiFeSe] Hase, were mixed and placed into the reaction vessel. The effect on the photoactivity of the incubation time of semiconductor with Hase before the catalytic measurement was studied. The incubation times monitored were 1, 2, 3, 4, 6 and 22 hours. The suspension was mixed at 60 rpm speed on a roller mixer (SRT9D) at 4°C. Each set of In_2S_3-Hase mixture after incubation was placed in the reactor vessel connected to the mass spectrometer, which was closed avoiding the presence of a gas phase, for measuring the photoproduction of H_2. The Hase was activated by bubbling the solution with a 20% H_2: 80% Ar gas mixture during 10 minutes. Afterwards 100% Ar was bubbled to remove all the H_2 from the solution (monitored by the decrease of mass 2 signal). The reactor was illuminated with white light coming from a Solar simulator 450W Xenon lamp. The distance from the light source to the reactor was 40 cm. A scheme of the instrumental set up is shown in **Figure 3.6**. A black box covered the experimental setup to minimize photons reaching the reaction vessel except those from the Xe lamp. The light source power was measured with a Delta

OHM HD 2302.0 LightMeter, yielding 1.5 ± 0.1 W/m^2 within the range 315 – 400 nm and 368 ± 1 W/m^2 within the range 400 – 1050 nm. Control experiments were performed in absence of either semiconductor or Hase under equal setup conditions.

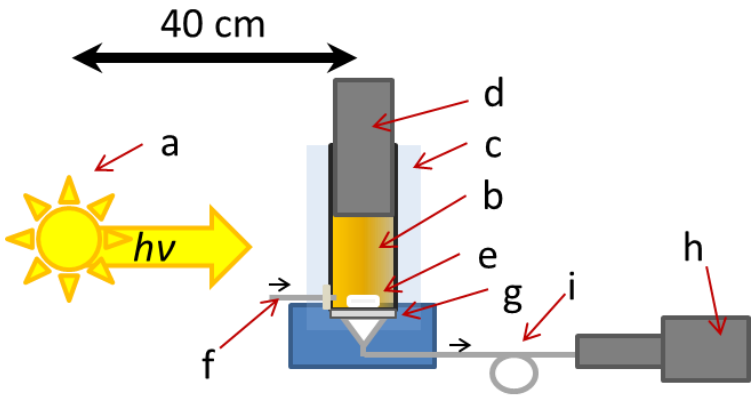

Figure 3.6 ***Scheme of the instrumental set up for photoproduction of H_2 measurements****: (a) light source, (b) 10 mL reaction vessel, (c) thermostated jacket, (d) plunger, (e) magnet, (f) canal fitted with a septum plug (gas or reagent introduction), (g) Teflon membrane, (h) mass spectrometer and (i) trap with liquid N_2.*

To determine the amount of active Hase attached to the In_2S_3 after the incubation time the samples were let to precipitate. The precipitated fraction was collected and resuspended in fresh buffer, and then the photoactivity was measured.

3.6.3 In_2S_3 – Laccase for O_2 photoelectroproduction

3.6.3.1 Electrode modification

The development and characterization of FTO/In_2S_3/*Th*Lc electrodes was made in two main steps: (i) the modification of FTO with In_2S_3, which was done as described in **section 3.4.2** and (ii) the attachment of the *Th*Lc. This last step of modification of the electrode and the conditions of measurements are described here.

3 µL containing 5.8 mg/mL of *Th*Lc in 100 mM phosphate buffer pH 6.0 were added to 33 µL of 47 mM $NaIO_4$ and let to incubate in ice during 30 min, in order to oxidize the hydroxyls of the glucosaccharides present on the surface of the laccase to aldehydes.[130] Then 54 µL of 100 mM phosphate buffer were added to the solution to increase the pH up to 7.

Two different strategies were tested: (i) physical adsorption and (ii) covalent immobilization on FTO/In_2S_3 electrodes.

For *Th*Lc physical adsorption on FTO/In_2S_3 electrodes, 15 µL of *Th*Lc solution was deposited on the electrode surface and let to adsorb for 120 min.

For *Th*Lc covalent immobilization on FTO/In_2S_3 electrodes, two different aromatic linkers were tested: 4-ATP and aminophenyl groups. The binding of 4-ATP to the FTO/In_2S_3 electrodes by forming a disulphide bond was studied by immersion of the electrodes in 1 mM 4-ATP EtOH solution overnight. The modification of the FTO/In_2S_3 electrodes with aminophenyl groups was done by electrochemical reduction of 4-nitrophenyldiazonium perchlorate (4-Dz).[108,109] First electrochemical grafting of nitrophenyl groups to the FTO/In_2S_3 electrodes was performed by recording two CVs from 0.8 to 0.1 V (*vs.* SHE) at 100 mV/s scan rate in 5 mL of CH_3CN containing 2 mM 4-Dz and 100 mM Bu_4NBF_4. The modified electrodes were rinsed thoroughly with EtOH and taken into the electrochemical cell containing a 9:1 mixture of H_2O:EtOH. Two CVs were recorded from 0.2 to -1.2 V (*vs.* SHE) at 100 mV/s scan rate to reduce the pendant nitro-phenyl groups to aminophenyl ones (**Figure 3.7**).[109]

15 µL of the *Th*Lc solution were deposited on the surface of the FTO/In_2S_3 electrodes modified with 4-ATP or aminophenyl groups at room temperature and let to incubate for 45 min. During this time, the aldehyde groups of the glucosaccharides of the laccase react with the amino groups of the modified support forming an imino bond. Afterwards 13.5 µL of 14 mM EDC and 11.2 µL of 21 mM NHS were added to the electrode and let to react 90 min at room temperature in MES 10 mM pH 6. An amide bond is formed between the amino groups of the 4-ATP or aminophenyl groups and the carboxylic groups of glutamic and aspartic residues on the Laccase's surface (Figure 3.7). After the reaction, the electrode was rinsed with 100 mM phosphate buffer pH 7.1 and taken to the electrochemical cell for the measurements.

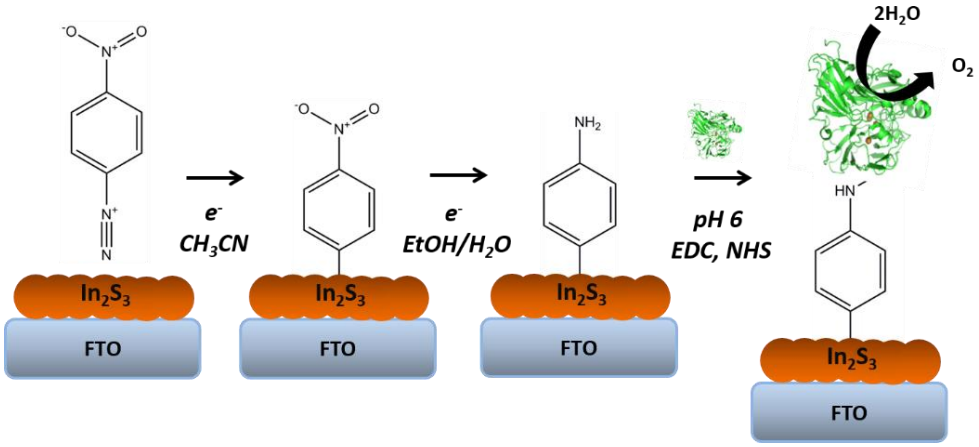

Figure 3.7 ***Functionalization of FTO/In_2S_3 electrodes with electrodeposited 4-Dz and covalent immobilization of Laccase.***

Immobilization of *Th*Lc on clean FTO was done as control experiment following the same methods described for the immobilization on FTO/In_2S_3 electrodes.

3.6.3.2 Measurements conditions for O_2 photoproduction

A three-electrode electrochemical cell with a Ag/AgCl (3 M NaCl) as RE and a Pt wire as CE was used. The electrochemical cell was filled with 30 mL phosphate buffer 100 mM pH 7.1 electrolyte and had refrigeration glass jacket connected to a thermostatic water recirculation system Haake SC150 from Thermo set at 30°C. Experiments were performed under Ar atmosphere. The electrochemical measurements were controlled by a PG30 Autolab Potentiostat/Galvanostat from Ecochemie. The current density values were calculated considering the geometrical area of the electrodes, which was 0.196 cm^2. All electrochemical measurements were repeated at least 4 times and the shown CV and chronoamperometry results correspond to typical results.

Illumination was carried with a LOT Quantum Design 150W Xenon Lamp setting the output power at 8.5 A. The light source was placed at ~28 cm from the working electrode. UV was filtered by a 1 mm thick polycarbonate layer or by optical filters from Andover Corporation. Measurements were averaged both in front and behind the electrochemical cell for each case. The light source power was measured with a Delta OHM HD 2302.0 LightMeter, yielding 200 ± 10 W/m^2 within the range 315 – 400 nm and 2500 ± 100 W/m^2 within the range 400 – 1050 nm.

The O_2 produced in the electrochemical cell for FTO/In_2S_3 powder was monitored with an O_2 microsensor from Unisense (Oxy Meter OX-NP-17180) placed at ~1.5 mm distance from the WE.

3.6.3.3 H_2O_2 determination

Direct water oxidation at the FTO electrode surface may produce H_2O_2 in addition to O_2. To determine the amount of H_2O_2 formed after applying chronoamperometries at different potentials to a bare FTO electrode, the electrolyte was collected and spectrophotometric determination monitored at λ = 414 nm was done with a UV-2401 PC SHIMADZU spectrophotometer following a known procedure.[131] The measurements were performed after mixing in a cuvette 890 μL of sample, 100 μL of 9.1 mM ABTS and 10 μL of 1 mg/mL HRP and letting to react during 8 min at room temperature.

3.6.3.4 *Th*Lc activity

*Th*Lc activity was determined by following ABTS oxidation at λ = 414 nm using the same spectrophotometer as for H_2O_2 determination. The cuvette contained 2.25 mL of 100 mM phosphate buffer pH 4.4, 250 μL of 9.1 mM ABTS and variable amounts of sample. First a calibration line was obtained by adding different amounts of fresh laccase solution to the cuvette. To check the amount of active laccase covalently attached to the FTO/In_2S_3 electrode the working area of the modified electrode was immersed in a cuvette side that did not interfere with the light path. Measurements of the activity before and after the photoelectrochemical experiments were done to determine the amount of active enzyme remaining attached to the electrode. Also, the electrolyte-leaked laccase was determined by concentrating the electrolyte solution after the photochronoamperometry by 3 cycles of centrifugation at 4000g using Centricon 3K filters. The concentrated solution was taken to 5 mL of 100 mM phosphate buffer pH 4.4. 2.5 mL of the concentrate were used for UV-Vis determination with the proper amount of ABTS.

3.7 CHARACTERIZATION TECHNIQUES

For In_2S_3 semiconductor characterization X-Ray Diffraction (XRD), scanning electron microscopy (SEM), transmission electron microscopy (TEM), UV-Vis spectrometry, FTIR, inductively coupled plasma optical emission spectrometry (ICP-OES), Brunauer-Emmett-Teller (BET) method for surface area calculation and electrochemical impedance spectroscopy (EIS) were used and are detailed here.

XRD of the synthesized In_2S_3 powder was performed with a Philips X'Pert Pro PANalytical diffractometer (Cu-Kα, λ= 0.1541874 nm). The samples were scanned from 4 to 90 degrees and the accumulation time was 20s. No previous sample treatment was needed.

SEM was performed with a TM-1000 Tabletop Hitachi including an X-ray Dispersive Energy detector (EDX).

TEM was performed at a point resolution of 0.19 nm with a 200KV JEOL 2100 transmission electron microscope, equipped with an Oxford Instruments EDX analyzer. Samples were prepared by taking the powder into an ethanol-filled Eppendorf and immersed during 15 min into an ultrasound bath. 20 µL of the sample were deposited on a carbon film-coated 200 mesh copper TEM grid (Electron Microscopy Sciences) and let to dry.

The **UV-Vis** spectrum of the powder was measured using a double beam UV-Vis-NIR Varian Cary 5000 spectrometer.

The **FTIR** spectra were recorded at 2 cm^{-1} resolution and averaging 1024 scans from 4000 to 800 cm^{-1} using a Bruker Tensor 27 Fourier transform spectrometer, equipped with a mercury cadmium telluride detector and a purge gas system (Whatman) for removal of CO_2 and H_2O. Temperature of the cell was kept at 25°C using a thermostatic recirculation bath CC230 from Huber.

The chemical analysis by **ICP-OES** was performed with an Optima 3300 DV Perkin Elmer spectrometer.

The **Surface area** of In_2S_3 particles was measured using BET method calculation with Isotherms of Absorption ASAP2020 Micromeritics equipment, after 100 h of N_2 degasification at room temperature.

EIS measurements were controlled by an Autolab Potentiostat/Galvanostat Ecochemie PGSTAT30 with a Frequency Response Analysis (FRA) module. A three-electrode cell configuration was used with an aqueous electrolyte containing 0.1 M sodium carbonate, 0.1 M sodium acetate and 0.1

M sodium sulfite in the pH range of 4-10. The WE was prepared by depositing 6 µL of a 30 mg In_2S_3 suspension in 1 mL of EtOH onto a clean LDG rod, and dried at 100°C under vacuum during 2 hours. The RE was Ag/AgCl (3M NaCl) from BAS and a Pt wire (0.5 mm diameter, Goodfellow) was used as CE. The capacitance was measured at 1000 Hz and 0.482 V (*vs.* SHE). CV studies were performed with the same cell configuration.

4. RESULTS AND DISCUSSION

4. RESULTS AND DISCUSSION

In this section are presented the results obtained on the three artificial photocatalysts studied in this thesis: (i) PSI-Hase combination for H_2 production, (ii) In_2S_3-Hase hybrid for H_2 production and (iii) In_2S_3-Laccase hybrid for O_2 evolution.

4.1 PSI – HYDROGENASE FOR H_2 PHOTOELECTROPRODUCTION

Development of a cathode for bioelectrochemical photoproduction of H_2 is the first objective of this thesis. To achieve this goal the strategy was to combine PSI from spinach's thylakoids as light absorber able to reduce a biocatalyst, with the [NiFe] Hase from *Desulfovibrio gigas*. This system was developed on a gold electrode modified with two redox hydrogels, which allowed the electron transfer from the electrode to the PSI and then from the PSI to the Hase for H_2 evolution, as represented in **Figure 4.1.1**.

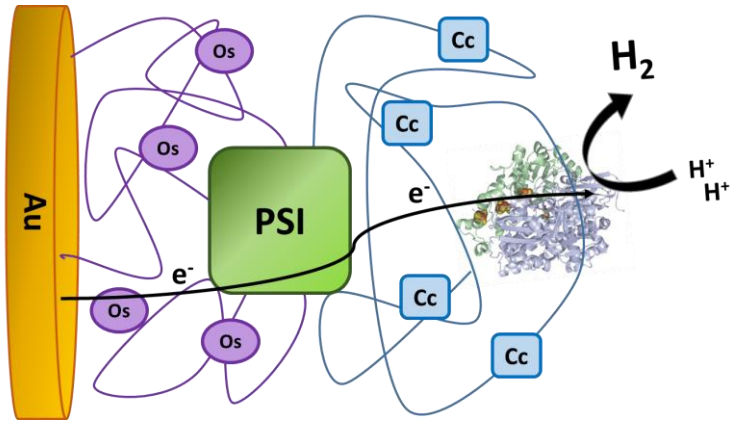

Figure 4.1.1 ***Scheme of PSI-Hase photoelectrocatalyst connected through redox polymers on gold electrode for H_2 photoproduction.*** *"Os" represents Os-PVI polymer, "Cc" represents Cc-BPEI polymer.*

First of all, the characterization of the redox formal potential of the polymers was performed. PSI stability and Hase electroactivity were also studied.

4.1.1 Redox polymers characterization

Os-complex modified polymers have been extensively used to connect redox enzymes,[116,117,132] DNA molecules,[133] bacterial cells,[134,135] thylakoids,[136] PSI[7] and PSII[137] to electrode surfaces. Here Os-PVI was selected to connect the PSI to the gold electrode. Redox polymers loaded with pending viologen have been extensively used for O_2 scavenging while simultaneously mediating H_2 electrooxidation by Hase, since its redox potential is not negative enough to reduce the Hase in the H_2 evolution reaction.[138] MV-LPEI and Cc-BPEI redox polymers, which have a negative formal redox potential, were tested to wire the *Dg*[NiFe] Hase to the PSI and to favor the transfer of excited electrons for H_2 evolution. The chemical structure and preparation method of Os-PVI, MV-LPEI and Cc-BPEI are shown in **section 3.5**.

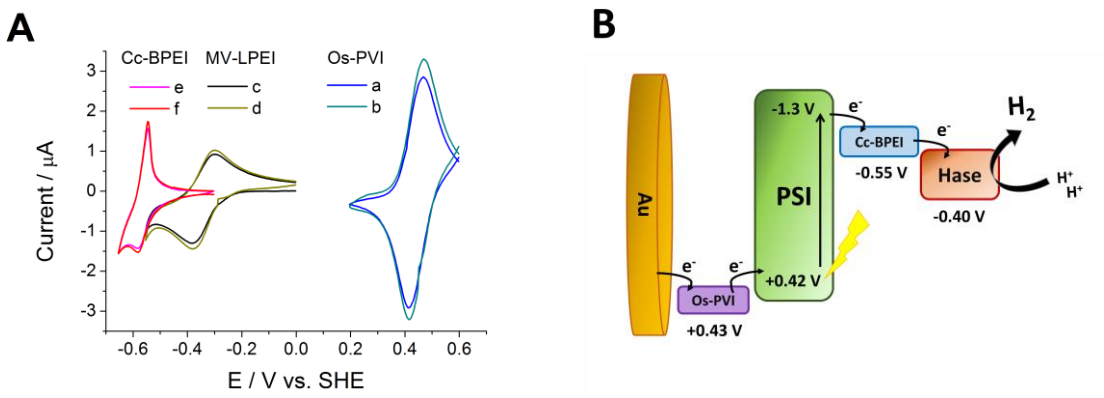

Figure 4.1.2 ***A) CVs of gold electrodes*** *modified with either Os-PVI under illumination (a) and dark (b) conditions, MV-LPEI under illumination (c) and dark (d) conditions or Cc-BPEI under illumination (e) and dark (f) conditions. CVs recorded at 10 mV/s, in 10 mM sodium phosphate buffer containing 10mM NaCl and 5 mM $MgCl_2$ at pH 7.5.* ***B) Scheme of the electron pathway*** *from gold electrode to PSI and the Hase, through Os-PVI and Cc-BPEI redox polymers.*

The experimental formal potential of the three polymers was determined by cyclic voltammetry. The CVs for each of three polymer-modified gold electrodes under light and dark conditions are shown in **Figure 4.1.2A.** The Os-PVI exhibited a formal potential of + 430 mV (*vs.* SHE), whereas the MV-LPEI exhibited a quasi-reversible redox couple with a formal potential of -340 mV (*vs.* SHE). The redox potential of *Dg*[NiFe] Hase active site for H_2-production is -430 mV (*vs.* SHE) at pH 7.5.[28] According to the redox potentials measured, the Os-PVI and the MV-LPEI were suitable for their

intended purposes of wiring PSI and O_2 scavenging, respectively. Illumination did not result in a significant change in the behavior of the redox polymer. Cc-BPEI exhibited a formal redox potential of -550 mV (*vs.* SHE), which was negative enough to facilitate H_2 evolution (almost overlapping the overpotential of H_2 evolution at the gold electrode surface). Cc-BPEI had a considerably more negative redox potential than MV-LPEI and may be able to work simultaneously as a redox mediator between PSI and Hase, in addition to acting as an O_2 scavenger. A scheme of the electron pathway from gold electrode to the Hase is represented in **Figure 4.1.2B**.

4.1.2 Operational stability of PSI

PSI can perform a gain in the overpotential from +0.42 V to -1.3 V (*vs*. SHE) when illuminated.[63] The photoelectrochemical stability *in operando* of the PSI co-immobilized with the Os-PVI (Au/Os-PVI/PSI) on the electrode was monitored by CV and chronoamperometry in the presence of 1 mM MV in solution. Under illumination the exited electrons of P700* of the PSI are able to reduce MV, which simultaneously reduce O_2 as the final electron acceptor. An increase in the current density under illumination is observed in **Figure 4.1.3A**, with an onset potential around +0.27 V (*vs*. SHE). A chronoamperometry at 0.15 V (*vs.* SHE) showed that PSI retained 50% of its activity after 10 min of continuous exposure to light (**Figure 4.1.3B**), which was consistent with reported results.[4]

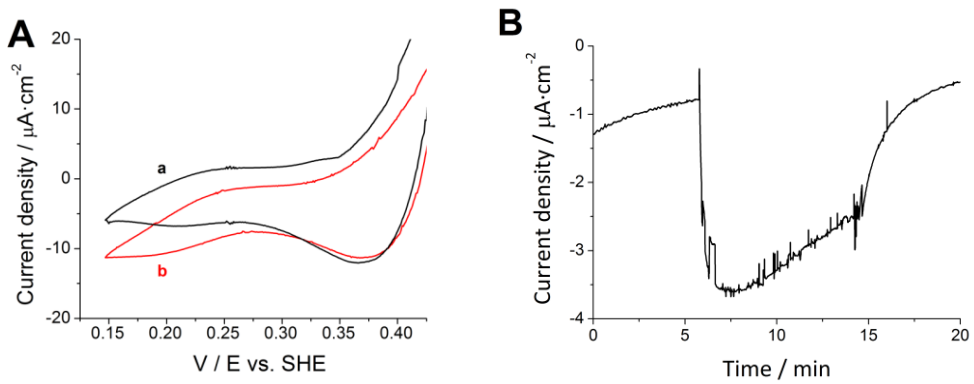

Figure 4.1.3 ***Photoelectrochemical stability in operando of the PSI.*** *(A) CV of an Au/Os-PVI/PSI electrode under dark (a) and illumination (b) conditions at 10 mV/s. (B) Chronoamperometry of Au/Os-PVI/PSI electrode recorded at 0.15 V (vs. SHE). The light was switched ON from min 5 to min 15. Performed in 10 mM sodium phosphate 10 mM NaCl, 5 mM $MgCl_2$ and 1 mM MV pH 7.5 at 25°C.*

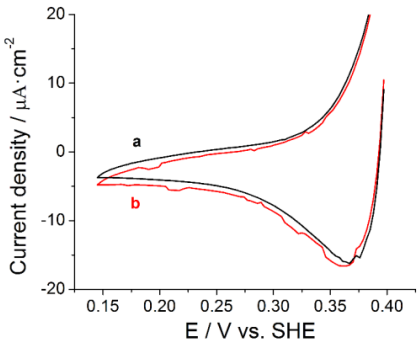

Figure 4.1.4 ***CV of an Au/Os-PVI/PSI electrode in the absence of O_2*** *under dark (a) and illumination (b) conditions. Recorded at 10 mV/s in 10 mM sodium phosphate buffer containing 10 mM NaCl, 5 mM $MgCl_2$ and 1 mM MV pH 7.5 at 25°C.*

The removal of O_2 as the final electron acceptor cancelled the previously observed photocurrents, whereby PSI could no longer reduce a suitable electron acceptor in the electrolyte solution (**Figure 4.1.4**).

4.1.3 H_2 photoproduction by PSI-Hase on gold electrode

The electrodes modified with PSI and Hase in absence of O_2 use protons as final electron acceptors to produce H_2 when illuminated. Different set of experiments were performed testing several combinations according to the redox polymer connecting PSI and Hase, in presence or absence of soluble mediator MV in the solution (**Figure 4.1.5).**

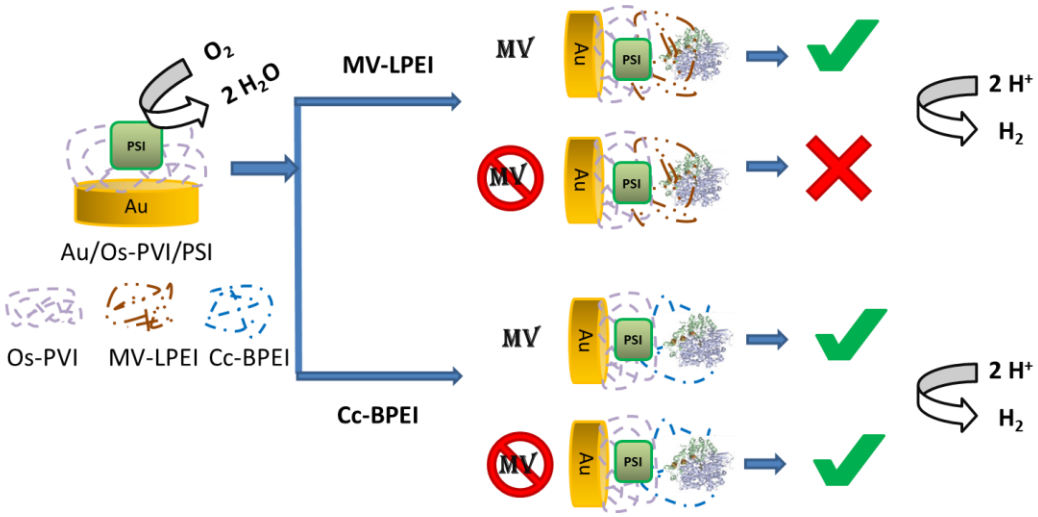

Figure 4.1.5 ***Scheme of the experiments performed combining PSI and Hase wired with MV-LPEI or Cc-BPEI redox polymer in presence or absence of the soluble mediator MV for H_2 evolution.***

Initially, Os-PVI mixed with PSI was deposited on the surface of a gold electrode and then a mixture of MV-LPEI and *Dg*[NiFe] Hase was placed on top, in order to build the full construction Au/Os-PVI/PSI/MV-LPEI/Hase as detailed in **section 3.6.1.1**. The MV-LPEI polymer was tested because viologens have been reported in many cases as electron mediators for Hase activity, either as a redox-polymer component or free in solution.[28,138-140] As can be observed in **Figure 4.1.6A**, a clear electrocatalytic effect appeared when illuminating the modified electrode in presence of 1 mM MV in solution. The onset potential for the photocatalytic production of H_2 by the Au/Os-PVI/PSI/MV-LPEI/Hase electrode can be estimated. When illuminated, the photocatalytic production of H_2 started at ca. +250 mV (*vs.* SHE), indicating that a catalytic replenishment of soluble $MV^{+\cdot}$ was taking place due to the activity of PSI and thus allowing H^+ reduction activity of Hase. It should be noted that the magnitude of the catalytic currents of the whole system varied from one electrode to other due to the low operational stability of PSI; therefore, representative CVs are shown. Under dark conditions there is no driving force for MV^{2+} reduction, thus, no subsequent cathodic current increase at such a high redox potential is observed.

Further experiments were performed in absence of soluble MV. As shown in **Figure 4.1.6B**, *Dg*[NiFe] Hase seemed unable to undergo efficient MET with MV-LPEI in absence of soluble MV; the CV only showed a very slight increase in the cathodic current when the modified electrode was illuminated. The resulting currents suggested that the electron-transfer kinetics for H^+ reduction activity were not as good as those reported for other Hases connected to a viologen-loaded redox polymer for H_2 oxidation.[138] Note, however, that in this case the MET process is thermodynamically uphill, whereas in the work by Plumeré and co-workers the MET was a downhill process.[138] Another possible explanation is that the system was not scavenging the residual O_2 at high-enough rate.

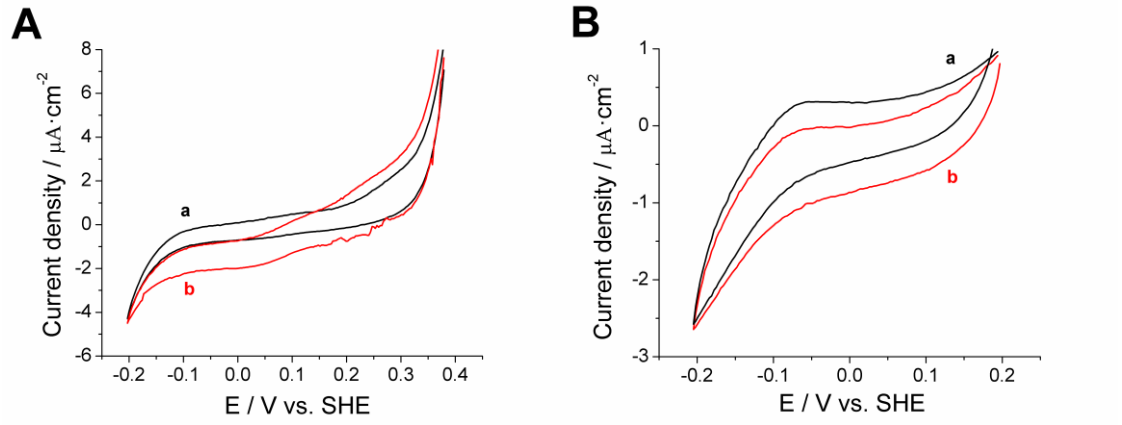

Figure 4.1.6 ***CVs of an Au/Os-PVI/PSI/MV-LPEI/Hase*** *electrode under dark (a) and illumination (b) conditions at 10 mV/s; A) in presence and B) in the absence of 1 mM soluble MV. Recorded at 10 mV/s in 10 mM sodium phosphate buffer containing 10 mM NaCl and 5 mM* $MgCl_2$ *pH 7.5 at 40°C.*

Once it was confirmed that soluble MV was needed in the solution to successfully transfer the excited electrons from PSI to the *Dg*[NiFe] Hase, the photocurrents measured on the CVs with and without MV-LPEI immobilized on the electrode were compared, in presence of soluble MV (**Figure 4.1.7A**). Illumination of the modified electrode containing MV-LPEI yielded higher photoactivity, demonstrating the advantage of using both redox polymers to facilitate and protect the photoelectrochemical process. When an electrode was prepared lacking *Dg*[NiFe] Hase but containing PSI, Os-PVI and MV-LPEI, as well as 1 mM soluble MV, H_2 production did not take place (**Figure 4.1.7B**).

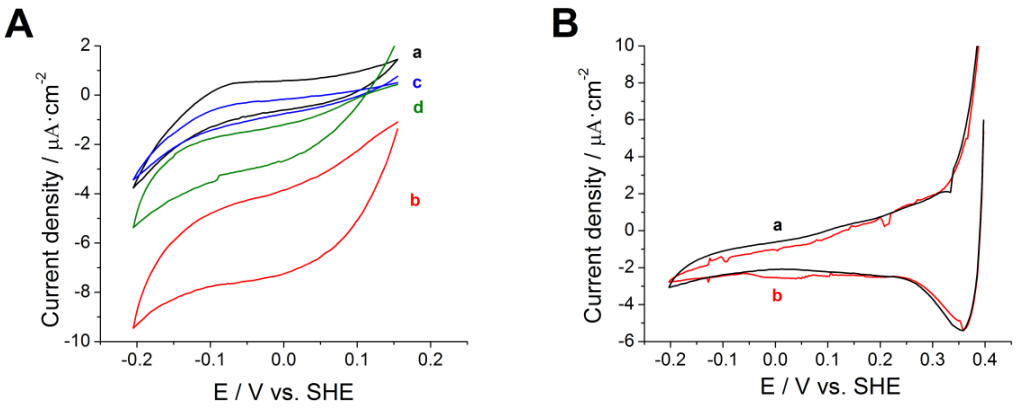

Figure 4.1.7 ***A)*** *CVs of an Au/Os-PVI/PSI/MV-LPEI/Hase electrode (a,b) and Au/Os-PVI/PSI/Hase electrode (c,d), under dark (a,c) and illumination (d,b) conditions.* ***B)*** *CV of a modified electrode lacking Hase under dark (a) and illumination (b) conditions. All CVs were run in 10 mM sodium phosphate buffer containing 10 mM NaCl, 5 mM $MgCl_2$ and 1 mM MV pH 7.5 at 40°C.*

In order to achieve the photoproduction of H_2 without MV redox mediator in the solution, another set of experiments was performed by the substitution of MV-LPEI with Cc-BPEI. The current densities developed by the electrode under illumination and dark conditions were recorded in two different electrolyte solutions, either in the absence or presence of soluble MV as an additional electron mediator (**Figure 4.1.8A**). Interestingly, Cc-BPEI greatly improved the performance of the photobioelectrochemical system without the need of an external mediator, which is attributed to the more negative redox potential of the cobaltocenyl radicals of the polymer compared to that of MV-LPEI.

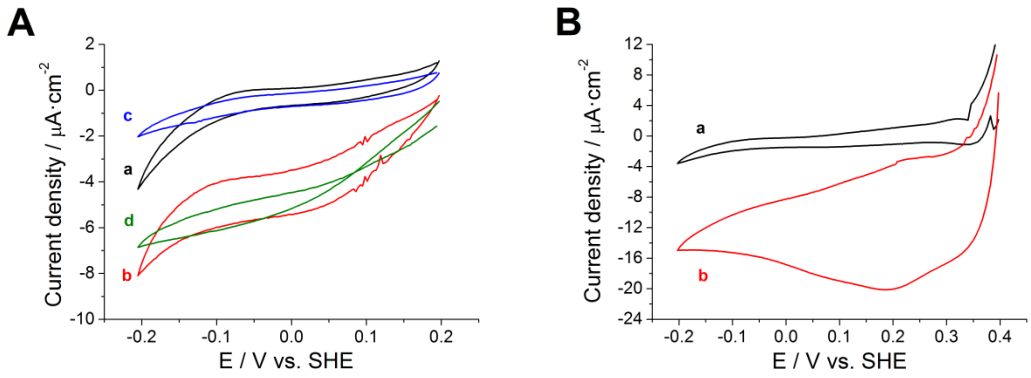

Figure 4.1.8 ***CVs of Au/Os-PVI/PSI/Cc-BPEI/Hase A)*** *Dark (a, c) – light (b, d) in presence (a, b) or absence (c, d) of 1 mM soluble MV.* ***B)*** *Onset potential in absence of 1 mM soluble MV under dark (a) and illumination (b) conditions. Recorded at 10 mV/s in 10 mM sodium phosphate buffer containing 10 mM NaCl and 5 mM $MgCl_2$ pH 7.5 at 40°C.*

The onset potential was measured by CV in absence of soluble MV (**Figure 4.1.8B**). Illumination of the electrode caused a significant cathodic catalytic process that started at +380 mV (*vs.* SHE) approximately.

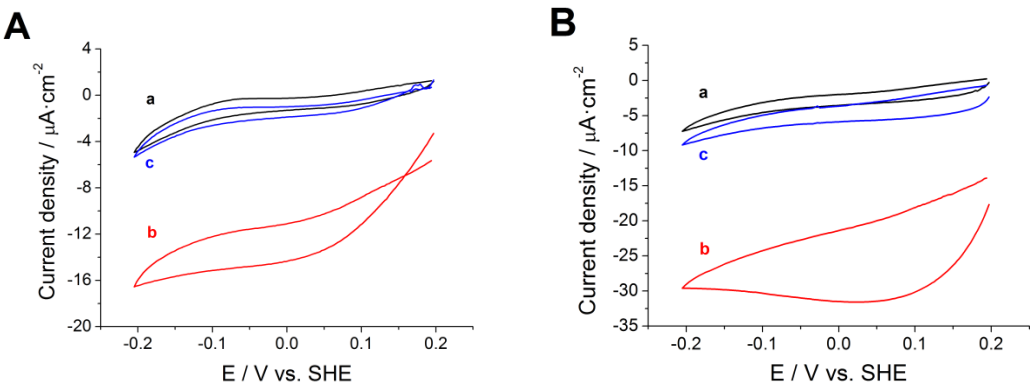

Figure 4.1.9 ***Dg[NiFe] Hase inhibition.*** *CVs under dark (a), illumination (b) and illumination in presence of CO in solution (c) for:* ***A)*** *Au/Os-PVI/PSI/MV-LPEI/Hase and* ***B)*** *Au/Os-PVI/PSI/Cc-BPEI/Hase modified electrodes. Recorded at 10 mV/s in 10 mM sodium phosphate buffer containing 10 mM NaCl, 5 mM $MgCl_2$ and 1 mM MV pH 7.5 at 40°C.*

Further experimental evidence of the involvement of *Dg*[NiFe] Hase in the photoelectrocatalytic wave was obtained by studying its inhibition of an Au/Os-PVI/PSI/MV-LPEI/Hase electrode by carbon monoxide (CO).[28] As can be observed in **Figure 4.1.9A** for the Au/Os-PVI/PSI/MV-LPEI/Hase electrode, the reductive current density increased when irradiation was turned ON but the addition of CO resulted in a significant decrease of the photocatalytic effect to almost the value in the

dark. The same response was observed when using Cc-BPEI redox polymer in the full modified electrode (**Figure 4.1.9B**). Addition of CO in the electrolyte inhibits the activity of the Hase because it binds to the enzyme´s active site.[28] These experiments confirmed that the cathodic current was indeed produced by the Hase activity and thus related to H_2 production.

Control experiments were performed in absence of Cc-BPEI but in presence of 1 mM soluble Cc-monomer. The CV of the monomer in solution shows a cathodic peak at a very similar potential as that of the polymer, although the signal is irreversible in the case of the monomer (**Figure 4.1.10A)**. In consequence, the system yielded much lower photocurrents densities when using the soluble Cc-monomer instead of the Cc-polymer, shown in **Figure 4.1.10B**.

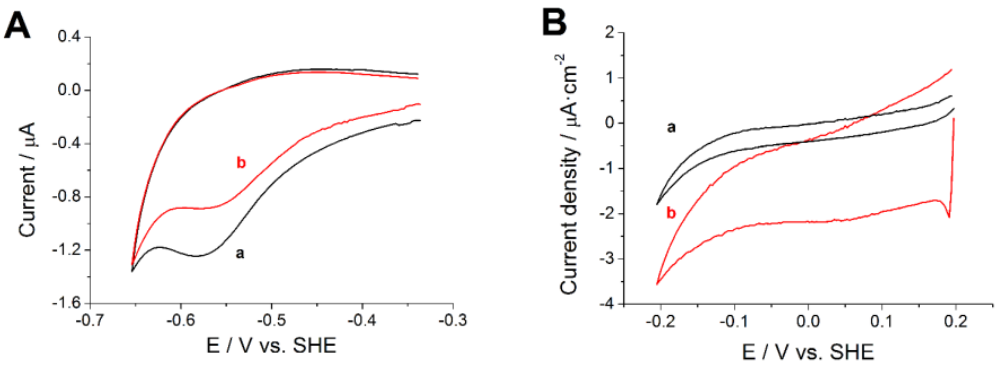

Figure 4.1.10 ***Cc-monomer CVs. A)*** *CVs for clean bare gold electrode under dark (a) and illumination (b) conditions performed in a typical electrolyte containing 1 mM soluble Cc-monomer.* ***B)*** *CVs for an Au/Os-PVI/PSI/Hase modified gold electrode under dark (a) and illumination (b) conditions. CVs recorded at 10 mV/s in 10 mM sodium phosphate buffer containing 10 mM NaCl, 5 mM $MgCl_2$ and 1 mM soluble Cc-monomer pH 7.5 at 40°C.*

The amount of H_2 produced and the PSI turnover frequency were determined by performing the CVs in the bipotentiostat mode. Since a ring-disk electrode was not available, the proton reduction CVs of the Au/Os-PVI/PSI/Cc-BPEI/Hase modified gold electrode were measured while a second working electrode, a Pt wire placed ~1 mm from the surface of the first working electrode (**Figure 4.1.11A**), was set at a constant potential of + 0.4 V (*vs.* SHE), at which the H_2 is oxidized.

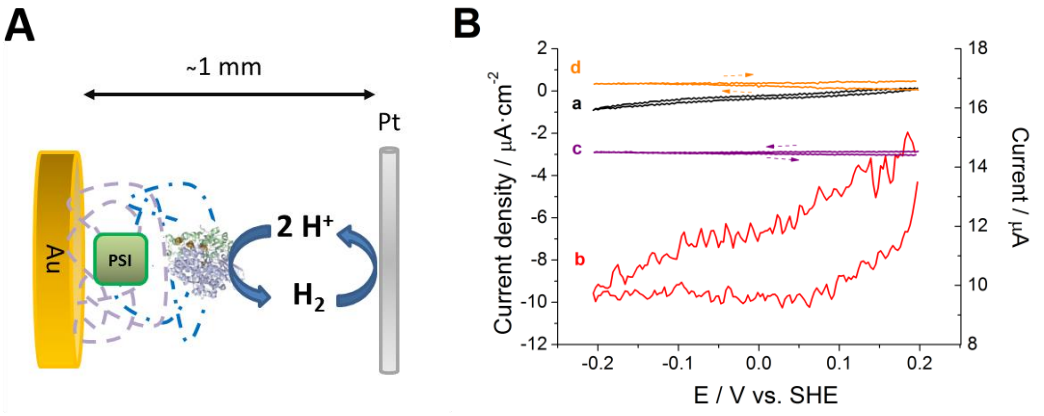

Figure 4.1.11 ***H_2 determination in bipotentiostat mode. A)*** *Schematic set up.* ***B)*** *The left axis corresponds to the CV for the Au/Os-PVI/PSI/Cc-BPEI/Hase modified electrode recorded at 5 mV/s under dark (a) and illumination (b) conditions, and the right axis corresponds to the chronoamperometry at + 0.4 V (vs. SHE) for a wire Pt electrode placed at 1 mm distance from the Au-modified electrode under dark (c) and illumination (d) conditions.*

In this setup, the H_2 produced in the modified gold electrode could be detected through its oxidation in the Pt electrode, as shown in **Figure 4.1.11B.** Under light illumination an increase in the oxidation of H_2 at the Pt electrode was observed. The control experiment without Hase showed no significant photocurrent in the CV under illumination, as can be observed in **Figure 4.1.12A**, meanwhile in the Pt wire electrode no H_2 oxidation was detected under illumination.

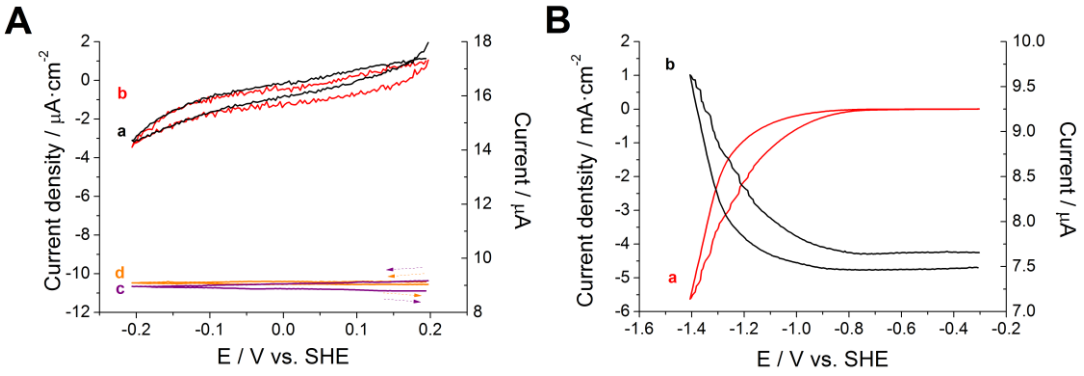

Figure 4.1.12 ***H_2 determination in bipotentiostat mode****.* ***A)*** *The left axis corresponds to the CV for the Os-PVI/PSI modified electrode recorded at 5 mV/s under dark (a) and illumination (b) conditions, and the right axis corresponds to the chronoamperometry at + 0.4 V (vs. SHE) for a wire Pt electrode placed at 1 mm distance from the Au-modified electrode under dark (c) and illumination (d) conditions.* ***B)*** *The left axis corresponds to the CV for the clean Au electrode at 5 mV/s (a) and the right axis corresponds to the chronoamperometry at + 0.4 V (vs. SHE) for a wire Pt electrode placed at 1 mm distance from the Au electrode (b).*

The amount of H_2 produced by Au/Os-PVI/PSI/Cc-BPEI/Hase modified gold electrode was calculated from the integration of the chronoamperometric curve, measured on the Pt electrode, during the 80 first seconds, which corresponds to the 5 mV/s linear sweep voltammetry from +0.2 to -0.2 V (*vs.* SHE) applied at the gold electrode. The charge resulting of this integration was transform to mol of H_2 following the *Faraday's law*:

$$M = \frac{1}{F} \cdot \frac{Q}{n}$$

where *M* is mol of substance, *F* is the Faraday constant, *Q* is the charge and *n* is the number of equivalents/electrons involved on the reaction.

Since the detection of H_2 may be underestimated due to mass transport limitation of the H_2 molecules from the working electrode to the Pt, calibration of the system was performed with a clean gold electrode as the main working electrode and a Pt wire as the second WE shown in **Figure 4.1.12B**. Using the *Faraday's law* equation, when 8.9 nmol of H_2 were produced at the gold electrode, only 2.3 nmol of H_2 were oxidized at the wire Pt electrode, so the H_2 produced by the system was almost 4 times the H_2 detected on the Pt eletrode. Several modified electrodes were tested yielding to an average H_2 production of 83 ± 4 pmol H_2/s. The TOF based on the molecular weight (200 kDa) and the amount of PSI on the electrode yield a rate equals to 3 s^{-1}.

4.1.4 Diffusional limitation studies using redox polymers

The hybrid PSI-Hase connected by Os-PVI and Cc-BPEI redox polymers has been shown to be able to photoproduce H_2 without the need of MV in solution. The photocurrent measured in the CV when illuminating the modified electrode clearly decreased at potentials lower than 0.2 V (Figure 4.1.8B). A reason for this decrease could be that the reaction could be limited by mass transport of protons. In order to confirm if there was some limitation by mass transport, gold disk electrodes were modified with CC-BPEI and Hase, and rotation was applied. The amount of *Dg*[NiFe] Hase and Cc-BPEI polymer was scaled for modifying the rotating gold disk as described in **section 3.6.1.1**. The onset potential for the electrocatalytical H_2 evolution by the *Dg*[NiFe] Hase using Cc-BPEI redox polymer as mediator was clearly observed at ≈-0.40 V (*vs.* SHE) (**Figure 4.1.13A**). Before applying rotation to the electrode, the stability versus time of the Cc-BPEI/Hase modified electrode was checked by chronoamperometry at -0.51 V (*vs*. SHE) at 0 rpm, shown in the inset of Figure 4.1.13A. After 18 min of reductive potential application, time required for fully activating the Hase, the cathodic current reached -2 µA and was stable during at least another 15 min.

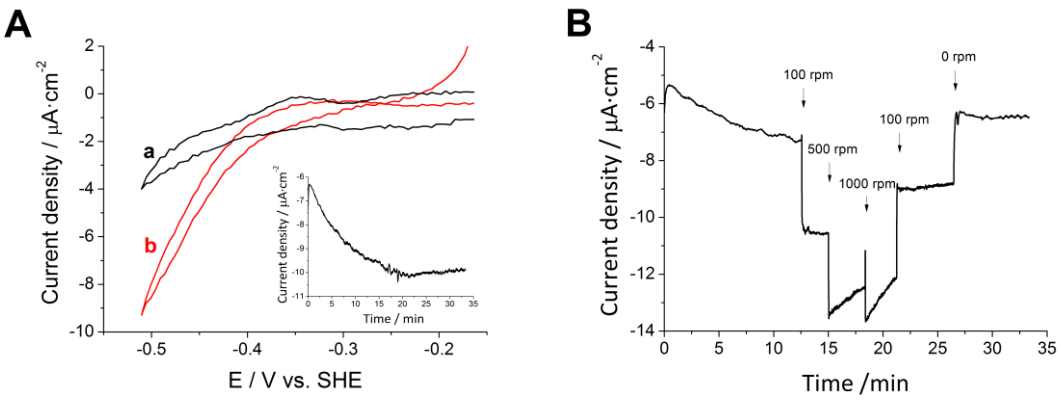

Figure 4.1.13 ***A)*** *CVs for bare Au (a) and Au/Cc-BPEI/Hase (b) electrodes at 10 mV/s. inset: chronoamperometry of Au/Cc-BPEI/Hase electrode at -0.51 V (vs. SHE).* ***B)*** *Chronoamperometry of Au/Cc-BPEI/Hase electrode at -0.51 V (vs. SHE). Arrows represent the moment when the electrode rotation speed was changed. Rotational speeds applied were 0 rpm, 100 rpm, 500 rpm and 1000 rpm. Performed in 10 mM sodium phosphate buffer containing 10mM NaCl and 5 mM $MgCl_2$ pH 7.5 at 40°C.*

In order to study the mass transport limitation of proton reduction by the Cc-BPEI/Hase modified electrode, the rotational speed of the electrode was varied between 0 rpm, 100 rpm, 500 rpm and 1000 rpm in a chronoamperometry performed at -0.51 V (*vs.* SHE). It can be observed in **Figure 4.1.13B** a significant increase in the current when rotation at 100 rpm was applied. After 2 minutes the current was stable, the rotation speed was increased until 500 rpm. Again, the current increased instantly but this time a significant decrease on the reductive current was observed after 2.5 min. The decrease on the negative current was even faster when 1000 rpm was applied. These results, obtained for the Hase/Cc-BPEI system, suggest that the diffusion of H^+ from the bulk of the electrolyte to the Hase through the polymer was rate-limiting the system because the current increased with the electrode rotation rate. However, when higher rotational speed was applied a decrease on the current was observed suggesting that the interaction between electrode surface and Cc-BPEI/Hase was not strong enough.

4.1.5 Discussion

Wiring PSI with *Dg*[NiFe] Hase for produce H_2 from H^+ and light faces several challenges. First of all, these biocatalysts are difficult to connect via DET to either an electrode or between each other. Secondly, the presence of O_2 typically inhibits most Hases. Our system's approach faced these challenges by the addition of two redox polymers: a redox polymer with a positive redox potential that facilitated the wiring of PSI and an additional redox polymer with a very negative potential that scavenged O_2[138] while simultaneously reducing Hase, which in turn can reduce H^+ to produce H_2.

The transfer of electrons to a gold electrode was successful for each of the three polymers, which were studied independently for their formal potential determination.

The stability of PSI is known to be poor when working outside of the cell, *i.e.* immobilized on an electrode surface.[141] The stability against light illumination of the PSI evaluated by mixing it with Os-PVI on a gold electrode was not much better than the one previously reported,[4] losing 50% of its activity after 10 min of illumination. On the other hand, the bound stability of the *Dg*[NiFe] Hase mixed with the polymer Cc-BPEI on the gold electrode surface was acceptable and yielded stable cathodic current for longer than 30 min. Therefore, the PSI stability was clearly a limitation for long term H_2 photoproduction. Another limiting factor was the diffusion rate of protons to the Hase through the redox polymer, which was minimized by applying rotation to the electrode. However, the electrode rotation decreased the stability of the immobilized Hase/Cc-BPEI due to the weak interaction between the redox polymer and the gold surface.

ET from PSI to Hase was not significantly efficient when using MV-LPEI as wire in absence of soluble MV, because the formal potential of that polymer is more positive than that of the *Dg*[NiFe] Hase active site (at pH 7.5), which is able to produce H_2 at almost the thermodynamic potential.[28] However, the electrochemical process for H_2 evolution improved significantly when both soluble MV and MV-LPEI were present, the first one providing enough driving force for proton reduction at pH 7.5, whereas the MV-LPEI polymer protected the photoelectrochemical process by reducing residual O_2 in the system. ET while illuminating from the PSI to the *Dg*[NiFe] Hase without soluble MV mediator was achieved when Cc-BPEI redox polymer was used to wire the PSI to Hase. This result confirms that both challenges, scavenging O_2 while simultaneously reducing Hase, can be achieved by using a very negative potential redox polymer to connect PSI and Hase.

The H_2 photoproduction on the electrode could be measured with an onset potential of + 250 mV (*vs.* SHE) in the case of MV-LPEI and soluble MV, and + 380 mV (*vs.* SHE) approximately in case Cc-

BPEI, which is 830 mV more positive than that of the MV redox mediator, suggesting the ET between PSI and Cc-BPEI redox centers is more efficient.

Regarding the TOF of the photosystem with Cc-BPEI polymer, the H_2 evolution calculated rate based on the molecular weight (200 kDa) and the amount of PSI on the electrode, which was the limiting step due to its poor stability, was 3 s^{-1}, and yield a H_2 production of 83±4 pmol H_2/s. However, the TOF was probably underestimated since the concentration of PSI mixed in the construction was considered as pure enzyme, although it was an enriched PSI extract. A next step to improve the H_2 photoproduction by Hase could be the use of alternative light absorbers which show higher stability, like semiconductor materials.[142]

Previous studies targeting the connection of PSI to electrodes for photocurrent generation have been published,[4,5] and in many cases based in cross-linked redox hydrogels.[113-115] However, most of these studies have not focused in H_2 photoproduction for energy storage. An interesting reported study proposed Pt as catalyst for this goal,[115] but we have achieved the H_2 bioelectrochemical photoproduction of H_2 avoiding the use of precious-metal-based catalysts.

4.2 In_2S_3 – HYDROGENASE FOR H_2 PHOTOPRODUCTION

The second approach for H_2 evolution was based on the formation of a hybrid photocatalyst that combined an inorganic semiconductor able to absorb in the visible light spectral range, instead of PSI, with a Hase for protons reduction.

Since the stability of PSI was limiting the efficiency of the system PSI-Hase described in the previous **section 4.1**, In_2S_3 semiconductor was the light absorber material synthetized and used for this purpose. Its characterization results are shown in this section. The biocatalyst used for the proton reduction in this case was the *Dv*[NiFeSe] Hase soluble form (*Dv*[NiFeSe]$_s$ Hase). For several years the group had been working with this enzyme in its native membrane form.[44,143,144] Herein, the active site of the soluble form was firstly studied by FTIR and then its electroactivity studied by its immobilization in gold electrodes.

Once both components of the hybrid photocatalyst, In_2S_3 and *Dv*[NiFeSe]$_s$ Hase, had been characterized they were mixed to form the hybrid system for H_2 photoproduction in solution, monitored by mass spectrometer. Schematic representation of the hybrid photocatalyst is shown in **Figure 4.2.1**.

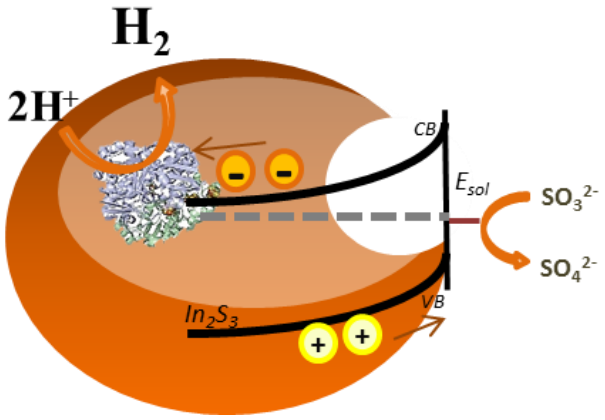

Figure 4.2.1 ***In_2S_3-Hase hybrid for photocatalytic production of H_2.*** *The Hase is represented inside a pore of In_2S_3 aggregate. When the In_2S_3 is illuminated the exited electrons at the CB are transferred to the Hase for H_2 production. The holes created on the VB of In_2S_3 migrate to the interface with the electrolyte and oxidize the holes scavenger (sacrificial donor), that is Sulfite.*

4.2.1 In_2S_3 powder characterization

The In_2S_3 powder obtained by the hydrothermal synthetic route described in **section 3.3** displayed an orange-reddish color and was characterized by different techniques. TEM and SEM were used to determine the geometry and size of the powder particles. The TEM images in **figure 4.2.2.A**, **B** show two typical In_2S_3 particles ranging 50-100 nm in diameter, with near-hexagonal shape. It could also be appreciated that the particles comprise several crystalline domains, separated by typical grain boundaries. SEM revealed spherical particle aggregation with a broad distribution of sizes, which ranged from 2 to 15 µm of diameter (**Figure 4.2.2C,D**).

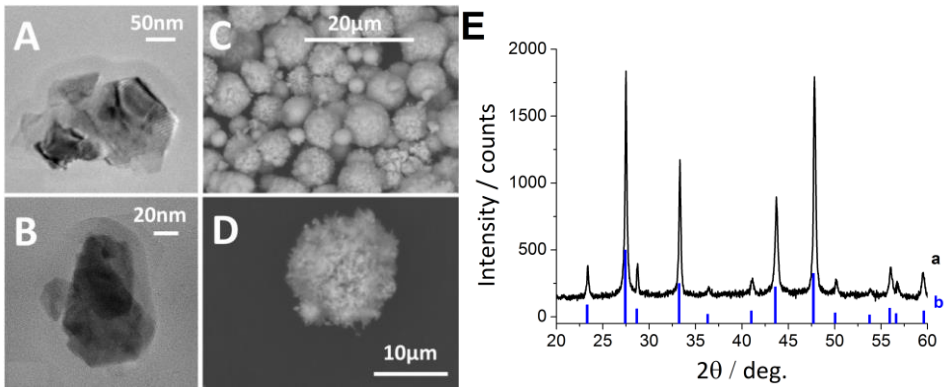

Figure 4.2.2 ***A, B) TEM images*** *showing two different particles of In_2S_3.* ***C, D) SEM images*** *from In_2S_3 powder aggregates.* ***E) XRD Diffractogram*** *obtained from the synthesized In_2S_3 (a) and XRD reference pattern of α-In_2S_3 (ref. code 01-084-1385) (b).*

The XRD diffractogram, displayed in **Figure 4.2.2E**, shows in (a) the experimental XRD from the powder and in (b) the reference diffractogram (ref. code 01-084-1385), of cubic α-In_2S_3. The latter is a spinel structure with disordered cation vacancies, usually obtained in this type of preparations instead of the thermodynamically more stable tetragonal β-In_2S_3 form, which differs from it only in having the cation vacancies ordered according to a specific pattern. No characteristic diffraction peaks from possible impurities such as InS, In_2O_3, S, sulfate and nitrate were detected, indicating a phase-pure In_2S_3 product. The diffractogram was thus in agreement with the reference pattern and yielded a crystal domain size of ca. 37.2 nm, also in agreement with the TEM observed crystal size and similar value as previously reported,[125,145] using Scherrer's equation:

$$\tau = \frac{k\lambda}{\beta cos\theta}$$

Where τ is the mean size of the ordered (crystalline) domains, which may be smaller or equal to the grain size, *K* is a dimensionless shape factor, with a typical value of about 0.9 for sphere shape,

λ is the X-ray wavelength, β is the line broadening at half the maximum intensity (FWHM, in radians) and ϑ is the Bragg angle (in degrees).

The In_2S_3 powder was characterized by a diffuse reflectance UV-Vis spectrum (**Figure 4.2.3A**). A common and simple method for determining whether the band gap of the In_2S_3 is direct or indirect is transforming the UV-Vis spectrum values to a *Tauc* plot. The *Tauc* plot shows *hv* (the energy of the light) on the abscissa and $(\alpha hv)^{1/m}$ on the ordinate, where α is the absorption coefficient of the material. The value of the exponent m denotes the nature of the transition. For direct allowed transition the value of m is ½ and for indirect transition m is 2. The resulting plot has a linear regime which denotes the onset of absorption. Thus, extrapolating this linear region to the abscissa yields the energy of the optical band gap of the material. The extrapolation of the linear region for In_2S_3 measurement yielded a 2.1 eV band gap, as deduced from the linear segment in the region above the gap when $(\alpha hv)^2$ was plotted against the photon energy, thus evidencing a direct band gap (**Figure 4.2.3B**). This result corresponds to the visible range and is in agreement with the value obtained for In_2S_3 powder in earlier works[125,145,146] and close to the 2.0 eV value measured for a well-crystallized material.[147]

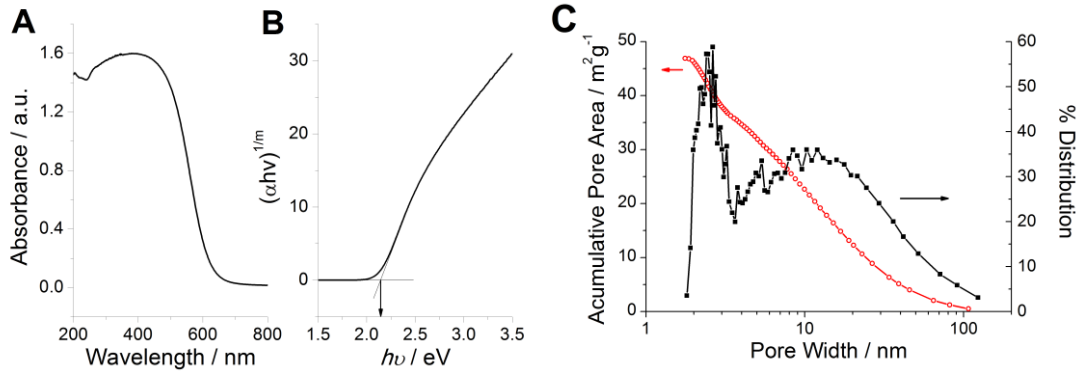

Figure 4.2.3 ***A) UV-Vis absorbance spectrum of In_2S_3. B) Plot of direct band gap of In_2S_3,*** *where α corresponds to absorption coefficient, h to Plank Constant, υ to incident photon frequency and m to the transition (m=1/2 for direct transition). The arrow marks the band gap value of the semiconductor.* ***C) BJH adsorption*** *(red circles) and pore area distribution (black squares) of In_2S_3.*

The specific area of the In_2S_3 powder was measured using the Brunauer-Emmett-Teller (BET) method, obtaining a value of 40.6 ± 0.3 m^2/g and a total pore volume of 0.168 cm^3/g. The average pore width was 16.5 nm. The pore area distribution is shown in **Figure 4.2.3C**.

The surface charge on the In_2S_3 was studied by deposition of the semiconductor particles on LDG electrodes and measuring the interfacial capacitance versus the solution pH by impedance

experiments.[148] The LDG/In_2S_3 electrode showed a capacitance maximum at pH 7 (**Figure 4.2.4A**), which suggested that surface groups have a pKa value around 7.[148,149] Moreover, the capacitance values decreased more when the pH was changed to acidic values than when changed to basic ones. These results suggest that the semiconductor particles were almost with a nul net surface charge at pH 5 or lower, whereas there was a negative net charge at neutral pH.[148]

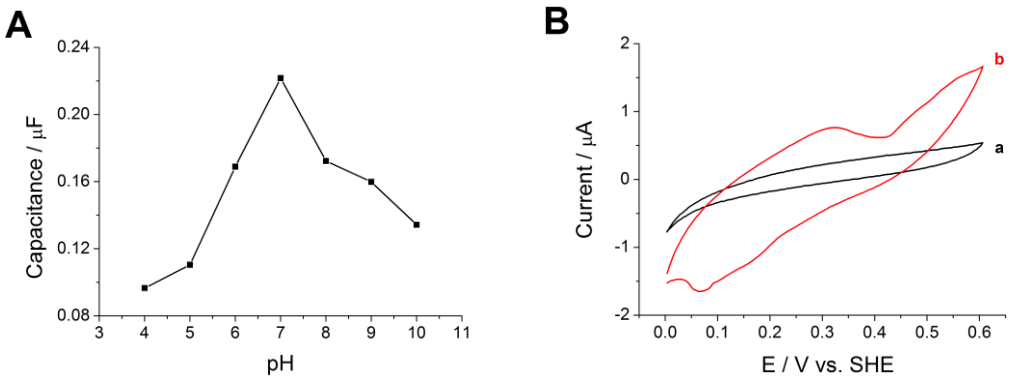

Figure 4.2.4 ***A) Capacitance versus solution pH for In_2S_3 deposited onto a LDG electrode****. Measured at 1000 Hz and 0.482 V (vs. SHE), in a 0.1 M sodium carbonate, 0.1 M sodium acetate and 0.1 M sodium sulfite aqueous solution at different pH values****. B) CV of bare LDG rod (a) and LDG/In_2S_3 (b) electrode.*** *Recorded at 2 mV/s in phosphate buffer 100 mM pH 7.5 at 25°C.*

Although the CB energy level of In_2S_3 has been reported,[75,86] we evaluated the redox potential of the semiconductor (**Figure 4.2.4B**), despite it is not a reversible system. A mid-point redox potential of ≈ + 0.2 V (*vs.* SHE) is estimated from the peak potentials difference of the oxidation and reduction waves measured by CV under illumination.

After characterizing the In_2S_3 as absorber component of the hybrid photocatalyst, the catalyst component *Dv*[NiFeSe]$_s$ Hase was also characterized. The *Dv*[NiFeSe]$_s$ Hase was expressed, extracted and purified by ITQB group. It was studied first by FTIR to check if its active site behaved as the native membrane form one (*Dv*[NiFeSe]$_m$ Hase) previously characterized by our group.[44,143] Then the Hase's activity was characterized by electrochemical and mass spectrometer techniques.

4.2.2 *Dv*[NiFeSe]$_s$ Hase FTIR characterization

The active site of NiFeSe Hases (**Figure 4.2.5A)** has a CO ligand and two CN^- coordinated to the Fe atom, which give clear vibrational bands between 2150 and 1900 cm^{-1} in the FTIR spectrum.[32,150] In [NiFe] hydrogenases the intense bands in the 1900-1960 cm^{-1} range are assigned to the CO ligand. The

CN^- ligand bands are less intense and appear around 2050-2100 cm^{-1}. A shift on the position of these bands is observed when the redox state of the active site changes.[28]

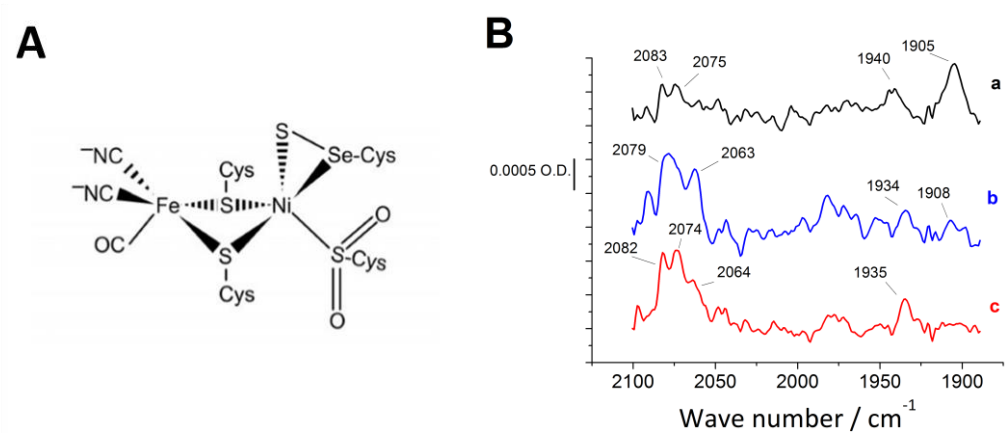

Figure 4.2.5 ***A) Scheme of the active site structure in Dv[NiFeSe] Hase*** *when in the as-isolated oxidized state.*[31] ***B) FTIR spectra for the recombinant Dv[NiFeSe]$_s$ Hase:*** *as isolated (a), reduced with 1 µL of 10 mM sodium dithionite under 1 atm H_2 atmosphere for 25 minutes (b) and reoxidized in air (c).*

FTIR measurements in a standard transmission cell for liquids of *Dv*[NiFeSe]$_s$ Hase were compared with those of the native membrane form reported previously.[44,143] The spectra for the as isolated, reduced and reoxidized redox states are shown in the **Figure 4.2.5B**. The conditions of the FTIR measurements are detailed in experimental **section 3.6.2.1**.

The previous published FTIR data for *Dv*[NiFeSe]$_m$ Hase showed two Isoforms: I and II,[44,143] which should be present also in the *Dv*[NiFeSe]$_s$ Hase. The FTIR bands of the *Dv*[NiFeSe]$_m$ Hase active site are shown in **Table 4.2.1**, reported by De Lacey et al.[143] A shift of 1-2 cm^{-1} on the position of the band is due to slight changes in electronic density of the active site. The as isolated *Dv*[NiFeSe]$_s$ Hase spectrum fitted quite well with those reported for the isoforms I and II of *Dv*[NiFeSe]$_m$ Hase (ν(CO) vibrations at 1905 cm^{-1} and at 1940 cm^{-1} respectively). The bands in the CN^- region (2075 cm^{-1} and 2083 cm^{-1}) also fitted with those of Ni-IS isoform I. When reducing *Dv*[NiFeSe]$_s$ Hase with sodium dithionite under H_2 atmosphere the bands suffered the expected shift, as the frequencies observed for the ν(CO) vibrations at 1934 cm^{-1} and 1908 cm^{-1} are almost equal to those of the Ni-R isoforms I and II, respectively. Regarding to the $\nu(CN^-)$ bands at 2063 cm^{-1} and 2079 cm^{-1}, they matched well with the NI-R isoforms I and II, too. After reoxidizing the *Dv*[NiFeSe]$_s$ Hase with air the band that appears at 1935 cm^{-1} could correspond to overlapping of CO bands due to Ni-R still present in the solution and to Ni-OX (isoform I). The bands in the CN^- region at 2082 cm^{-1} and 2074 cm^{-1} can be assigned to the Ni-OX redox state from isoform I and isoform II respectively, but clearly the band at 2064 cm^{-1} suggests that

still Ni-R from both isoforms is present in the solution. These results suggest that the *Dv*[NiFeSe]$_s$ Hase might have not been totally reoxidized after exposition to air.

Table 4.2.1 ***Vibrational frequencies of the Fourier transform IR bands of Desulfovibrio vulgaris Ni-Fe-Se hydrogenase (native membrane form) active site at different redox states. Values reported by De Lacey et al.***[143]

Redox state	Isoform I		Isoform II	
	ν(CO) / cm^{-1}	ν(CN$^-$) / cm^{-1}	ν(CO) / cm^{-1}	ν(CN$^-$) / cm^{-1}
Ni-IS	1904	2076, 2085	1939	2079, 2094
Ni-OX	1938	2084, 2095	1944	2074, 2012
Ni-TR	1925	2078, 2092	?	?
Ni-C	1915	2083, 2094	1900	2068, ?
Ni-R	1933	2064, 2079	1909	2064, 2079

The FTIR characterization of the Hase confirmed that the active site of the *Dv*[NiFeSe]$_s$ Hase behaved as the *Dv*[NiFeSe]$_m$ Hase when reducing and oxidizing it. The activity of this *Dv*[NiFeSe]$_s$ Hase was then characterized by electrochemistry.

4.2.3 Electroactivity of *Dv*[NiFeSe]$_s$ Hase on gold electrode

The activity of the *Dv*[NiFeSe]$_s$ Hase was studied electrochemically. The Hase was covalently attached to a 4-ATP SAM built on a gold disk electrode as described in **section 3.6.2.2**. The electroactivity of the Hase for the oxidation of H_2 was measured by cyclic voltammetry in an electrolyte saturated with H_2. These experiments were performed in anaerobic conditions to avoid the O_2 inactivation of the enzyme, although this [NiFeSe] Hase is described as an O_2-tolerant Hase under reductive conditions.[151] The CVs were recorded at 20 mV/s in 100 mM phosphate buffer pH 7 and the temperature was set to 30°C. The CVs are shown in **Figure 4.2.6A**. The first CV was recorded in absence of H_2. Since there was no H_2 in the electrolyte to be oxidized no increase in the current was detected (Fig.4.2.6A, line a), although a reductive current more negative than -0.35 V (*vs.* SHE) was recorded corresponding to proton reduction by the Hase. Then H_2 was bubbled to the electrolyte during 50 min. After this time, CV was recorded under 1 atm of H_2. A slight increase of the anodic current was observed corresponding to the catalytic effect of H_2 oxidation by the Hase but rapidly decreased due to inactivation by the positive potential (Fig.4.2.6A, line b).[152] The Hase was not fully activated just in presence of H_2 so a redox potential of -0.607 V (*vs.* SHE) was applied under H_2 for 1 hour to facilitate its activation (Fig.4.2.6A, line c). After this activation time, a CV was recorded with higher increase of

the current and much lower deactivation by the positive potential. The inhibition of the Hase activity was also tested by adding CO in the electrolyte to block its active side,[28] which was definitely inhibited as it is shown in line d, Fig.4.2.6A.

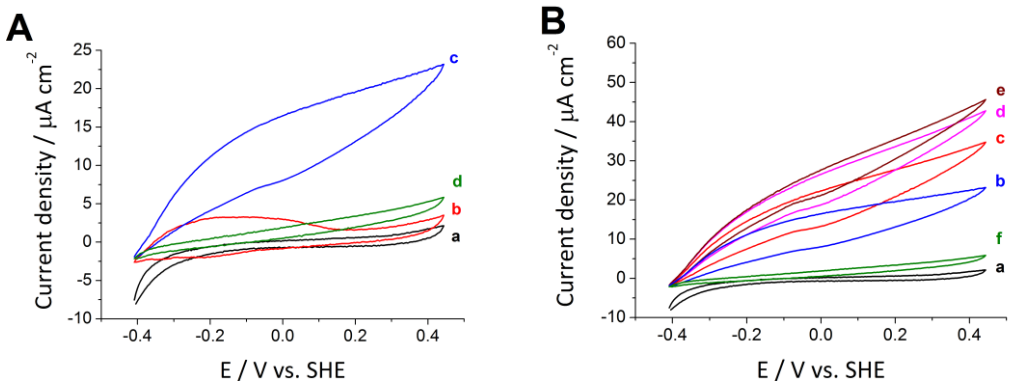

Figure 4.2.5 ***Electro-activity of [NiFeSe] Hase attached covalently through a 4-ATP SAM to gold electrode. A)*** **Stationary voltammetry:** *CV under N_2 (a), under H_2 (b), after 1 hour at -0.607 V (vs. SHE) applied potential under H_2 (c) and inhibition by adding 100 µL of CO-saturated buffer (d). No rotation was applied to the electrode.* ***B) Diffusional mass control study****: CVs under N_2 (a) and under H_2 (b-f). A rotational speed of 0 rpm (a,b), 500 rpm(c), 1000 rpm (d), 1500 rpm (e) and 0 rpm after adding CO (f) was applied to the electrode. All CVs were recorded at 20 mV/s in 100 mM phosphate buffer pH 7 at 30°C.*

Once the Hase was fully activated the mass transport limitation of the system was studied. The controlled rotation of the electrode was needed to evaluate the diffusional limitation of the substrate (H_2), recording CVs at 20 mV/s. In **Figure 4.2.6B** the CVs with rotational speed of 0, 500, 1000 and 1500 rpm are shown. When increasing the rotation of the electrode from 0 to 500 rpm, the oxidative catalytic current increased due to the faster transport of the substrate, the H_2, to the electrode surface (Fig.4.2.6B, line b and c). The results at 0 rpm indicated that the mass transfer of the substrate was limiting the catalytic process. An increase in the current was again observed upon increasing rotation from 500 to 1000 rpm (Fig.4.2.6.B, line d). However, rotating at 1500 rpm (Fig.4.2.6.B, line e) did not yield higher currents of H_2 oxidation, thus the diffusional limitation was avoided at around 1000rpm rotational speed. Under those conditions the ET between the Hase and the electrode was most probably the limiting step as the catalytic oxidative current increased greatly with the overpotential.[98] These results show that there was DET between Hase and electrode, reaching a similar oxidative current than with *Dv*[NiFeSe]$_m$ Hase.[144,153]

To check the correct oriented immobilization of Hase on the gold electrode the H_2 oxidation electroactivity was measured in presence of MV as redox mediator in the electrolyte.[28,138-140] As shown

in **Figure 4.2.7A,** mass transport was also limiting the process since higher catalytic currents were recorded when rotating at 1000 rpm compared to 0 rpm (line c and b respectively). Also in presence of MV higher catalytic currents were reached, confirming that not all the Hase immobilized on the electrode was well oriented for DET (Fig.4.2.7A, line d and c).

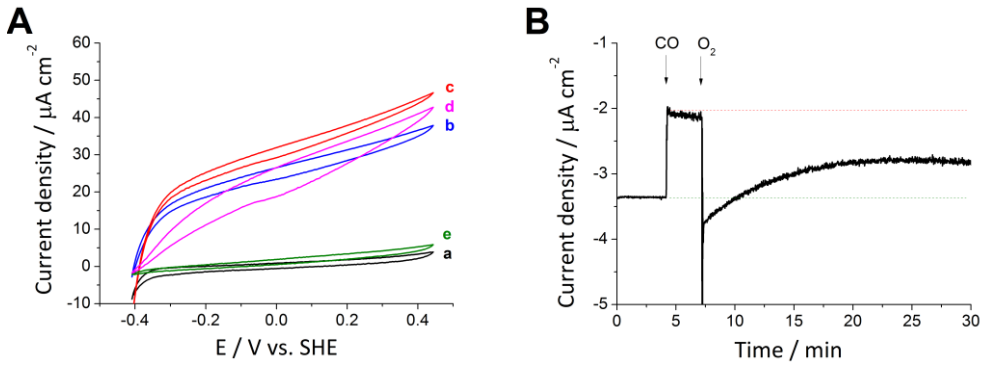

Figure 4.2.7 ***A) Diffusional mass control and MET kinetic study of Dv[NiFeSe]$_s$ Hase*** *attached covalently through 4-ATP SAM to a gold electrode. CVs under 1 atm N_2 and 0 rpm (a), under 1 atm H_2 and 0 rpm (b), under H_2 and 1000 rpm with 1 mM MV (c), under H_2 and 1000 rpm without MV in solution (d) and under H_2 and 0 rpm adding CO (e). Recorded at 20 mV/s.* ***B) Chronoamperometry at -0.45 V of H_2 production by Dv[NiFeSe]$_s$ Hase*** *inhibited by CO and its reactivation by removing CO by O_2. Measurements recorded in 100 mM phosphate buffer pH 7 at 30°C.*

To study the reversible activation of the *Dv*[NiFeSe]$_s$ Hase after its inactivation with CO, compared to *Dv*[NiFeSe]$_m$ Hase, a chronoamperometry was performed at -0.45 V (*vs.* SHE) and 500 rpm. The chronoamperometry, shown in **Figure 4.2.7B**, was performed under N_2 atmosphere and, once the current reached the equilibrium for H_2 production, 1 mL of CO-saturated buffer was added near the electrode surface. Inhibition by CO caused the decrease of the cathodic current. To remove the CO bound to the active site 50 µl of O_2 saturated buffer was added near the electrode surface. O_2 is able to replace the CO from the active site and, due to the negative potential applied during the chronoamperometry, the *Dv*[NiFeSe] Hase can be reactivated as reported in previous works.[151] A fast increase in the negative current was recorded corresponding to direct O_2 reduction on the gold surface. Once all the O_2 was removed by the N_2 purge, the current reached an equilibrium that corresponded to H_2-production catalyzed by the reactivated enzyme. As can be observed in the Figure 4.2.7B, the reduction current was smaller than before the CO inhibition, reaching just the 60% of the initial current. This result suggests that the recombinant *Dv*[NiFeSe]$_s$ Hase does not behave as the native membrane form, whose electrocatalytical activity is totally reversible after inhibition with CO and reactivation with O_2 under applied negative potentials.[151]

4.2.4 H_2-production by *Dv*[NiFeSe]$_s$ Hase measured by mass spectrometry

The specific activity for H_2-production, using reduced MV as electron donor, was measured for each of the as-isolated, reduced and reoxidized states of *Dv*[NiFeSe]$_s$ Hase by mass spectrometry as described in **section 3.6.2.3**. The **Figure 4.2.8A** shows a typical measurement recording mass 2 in the mass spectrometer for monitoring H_2 evolution *vs.* time in the reactor solution. The output signal of the spectrometer is proportional to the partial pressure of H_2 in the reaction vessel.[129] The activity of the enzyme was calculated from the slope maximum, taking in account the amount of Hase injected in the reactor vessel.[129]

Specific activity determination of the *Dv*[NiFeSe]$_s$ Hase as isolated was measured first at ITQB, since it was expressed, extracted and purified there, by Gas Chromatography (GC) yielding 4060 ± 80 µmol H_2/(min·mg Hase). Once at ICP, the activity of as-isolated *Dv*[NiFeSe]$_s$ Hase measured by mass spectrometer yielded 770 ± 40 µmol H_2/(min·mg). Therefore, the *Dv* [NiFeSe]$_s$ Hase lost 80% of its activity after one week kept in ice. Nevertheless, its activity increased to 3800 ± 200 µmol H_2/(min·mg) by previously reducing the Hase sample. The activity of the reoxidized Hase was then measured after leaving the sample under air overnight, yielding 2800 ± 900 µmol H_2/(min·mg). Therefore, Hase was more active after it was reduced with sodium dithionite and activated under H_2 atmosphere for 25 minutes, which is in agreement with the electrocatalytic measurements for H_2-oxidation (Figure 4.2.6A) and with the FTIR experiments that showed that the reduced Hase was in the active Ni-R state under those conditions (Figure 4.2.5B).

Prior to any photoactivity measurement, the effect of 0.2 M sulfite on the specific activity of the enzyme was measured. Sodium sulfite was selected as hole scavenger for the hybrid In_2S_3-Hase photocatalyst according to published work.[154] The specific activity for H_2 production of *Dv*[NiFeSe] Hase under these conditions was 1140 ± 45 µmol H_2/(min·mg Hase). In absence of sulfite the specific activity of the enzyme was 3800 ± 200 µmol H_2/(min·mg Hase), indicating that sulfite decreased 3-fold the catalytic turnover of the Hase. This great decrease of the activity in presence of sulfite could be explained by the increase of the ionic strength, which has been reported to affect considerably the H_2-production and uptake activities of Hases using MV as redox partner.[155,156]

4.2.5 Photocatalytic H_2 production by In_2S_3 - Hase hybrid

To monitor the H_2 production by the hybrid photocatalyst with the mass spectrometer, both In_2S_3 and Hase were mixed as detailed in **section 3.6.2.3**. In order to be sure that the kinetics of the

overall photocatalytic process were not limited by the photochemical properties of the semiconductor the measurements were done with a great excess of In_2S_3 over the amount of attached Hase.

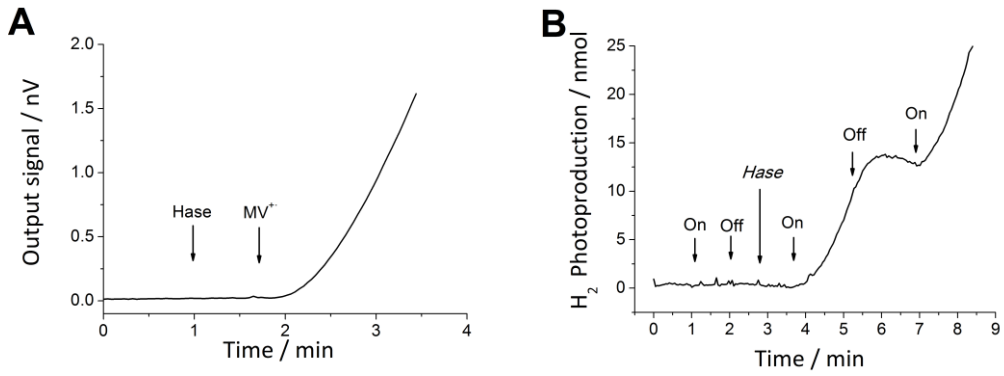

Figure 4.2.8 ***A) Typical output signal in mass spectrometer*** *measurements monitoring mass 2 corresponding to H_2 signal.* ***B) Photocatalytic production of H_2 by Dv[NiFeSe] Hase mixed with In_2S_3 particles*** *monitored by mass spectrometry. The arrows mark the times at which the lamp was turned on or off, and when Hase was injected into the reactor vessel.*

First the O_2 was removed by purging the solution with 20% H_2: 80% Ar gas mixture during 10 minutes, which activates at the same time the *Dv*[NiFeSe] Hase. Then the H_2 was removed by bubbling with 100% Ar until the H_2 signal decreased and stabilized, reaching the background level. Then the vessel was closed in such way that no gas phase remained in the reaction vessel. The measurement started with the reactor containing only 22.1 µmol In_2S_3 particles dispersed in an aqueous buffer containing 50 mM TRIS-HCl and 0.2 M sodium sulfite, the electron donor, at pH 7. The photoactivity recorded for the hybrid In_2S_3 - Hase experiment is shown in **Figure 4.2.8B,** in which is represented the monitorised signal for H_2. The solution was illuminated from minute 1 to minute 2 with no production of H_2 during that time frame. Afterwards 0.26 pmol Hase sample was injected inside the reaction vessel under dark conditions, allowing 1 min to mix with the In_2S_3 particles under magnetic stirring. When the light was switched on again H_2 production was observed almost immediately. Switching off the light source, at minute 5, interrupted the H_2 production inside the reactor, and after a delay period the H_2 production monitored started to decrease. When the illumination was restored, at minute 7, the photobiocatalytic H_2 production rate also was restored. When irradiated the steady state rate of the photocatalytic system was 292 µmol H_2/(min·mg Hase), whereas in the absence of light the H_2 production was negligible. This kinetic experiment showed that the photoexcited electrons that populate the In_2S_3 CB were directly transferred to the *Dv*[NiFeSe] Hase's active site successfully (DET), thus allowing it to catalyze the reduction of two protons to H_2.

The photobioactivity towards H_2 production was also tested for either In_2S_3 or Hase as stand-alone catalyst, **Figure 4.2.9A.** Both cases demonstrated to be unable to produce H_2 by just illumination. In the control experiment with the Hase (Fig.4.2.9A, line a) reduced MV was introduced at min 4, yielding H_2 production in the absence of light, showing that the Hase was active under these conditions. Regarding the control with In_2S_3 (line b), at min 4 of the experiment Hase was added, which turned into H_2 production detection only when the reactor was illuminated. These control experiments showed that the photobioproduction of H_2 needs both components, In_2S_3 and *Dv*[NiFeSe] Hase.

The efficiency of the hybrid photocatalyst was just 25.6%, comparing the photoactivity (292 µmol H_2/(min·mg Hase)) with the specific activity in the solution using $MV^{+\cdot}$ as electron donor (1140 ± 45 µmol H_2/(min·mg Hase)). In order to increase this efficiency, the interaction between the In_2S_3 particles surface and the Hase distal cluster had to be improved. Since In_2S_3 particles possess high porosity, the next strategy to improve the DET between In_2S_3 and Hase was incubating the mixture of both components, In_2S_3 and Hase, at 4°C in a roller mixer. Several preparations with increasing incubation periods from 0 to 22 h were tested, and afterwards their catalytic activity towards H_2 photosynthesis was measured. **Figure 4.2.9B** shows the comparison between an experiment with no previous incubation time (a) and another experiment where the incubation time was 3 h prior to the experiment's run (b). Both samples were exposed to the lamp illumination during the same period of time, from min 1 to min 3. As it can be observed, the longer incubation period yielded a higher H_2 production.

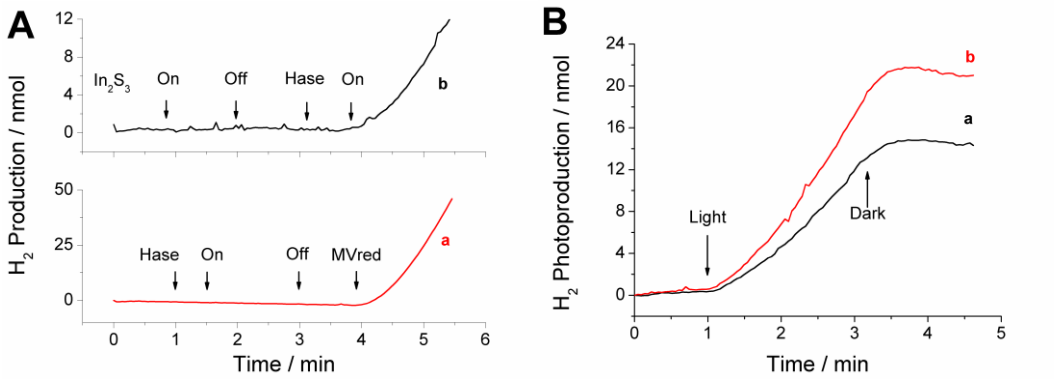

Figure 4.2.9 ***A) Negative controls of photoactivity*** *monitoring H_2 by mass spectrometry with only Dv[NiFeSe] Hase (a) and only In_2S_3 (b). The arrows mark the time when the light is switched on or off and the moment when 10 µL of 0.166 µM Hase or 2 µL of 1 M sodium dithionite were injected into the vessel to reduce the 1 mM MV present in solution.* ***B) Incubation effect on the photocatalytic production of H_2 by Dv[NiFeSe] Hase in combination with In_2S_3 particles****. The lines represent H_2 evolution with no previous incubation (a) and after 3 h of incubation at 4°C in a roller mixer (b).*

The dependence of the specific activity of the Hase for H_2 photobioproduction on the incubation time with the semiconductor is shown in **Figure 4.2.10A** (striped bars). In general, a longer incubation period yielded a higher photobioproduction of H_2, except for the overnight incubation period that proved too long. The highest photobioproduction rate was measured after an incubation time of 6 hours, which was 672 µmol H_2/(min·mg Hase).

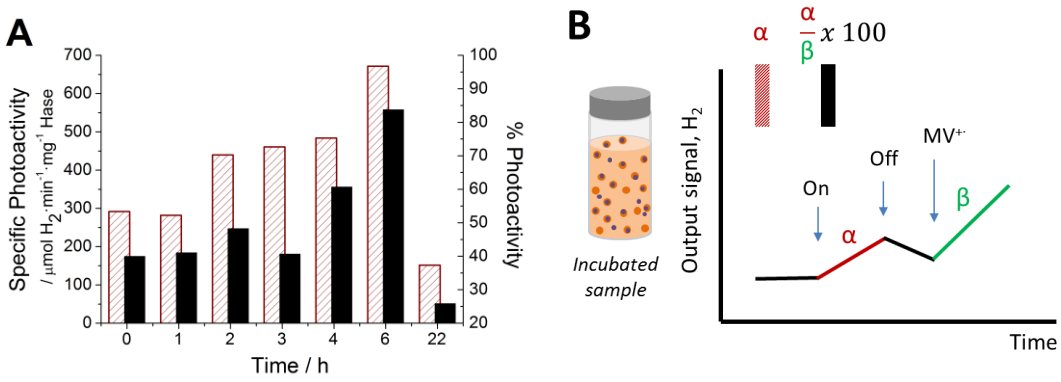

Figure 4.2.10 ***A) Incubation dependence of photocatalytic production of H_2 by Dv[NiFeSe] Hase in combination with In_2S_3 particles.*** *Striped column bars represent the specific activity of H_2 photoproduction by Hase after different incubation times. Black column bars represent the % of photoactivity of Hase compared to the specific activity of the sample measured with reduced MV as electron donor.* ***B) Scheme of the measurement process on mass spectrometer.*** *α represents the specific photoactivity of Hase corresponding to striped column bars from A), β is the specific activity measured with reduced MV after measuring the photoactivity on the same sample, β contains α plus Hase that is not photoactive.* $\frac{\alpha}{\beta} * 100$ *is represented in A) by black column bars.*

The H_2 photobioproduction rate for each sample was compared with the H_2 production rate driven by reduced MV instead of light measured after the photoactivity, as shown in **Figure 4.2.10B**. For these measurements, the light was turned off and 1 mM MV and 0.2 mM sodium dithionite were injected into the reactor. This comparison of catalytic activities allows determining for each sample the efficiency of the photoexcited electron exchange between the In_2S_3 and Hase (Figure 4.2.9A, black bars). The initial efficiency of the photocatalytic system with no previous incubation time was 40%, whereas the 6-hour incubation sample yielded 84% H_2-photobioproduction rate efficiency; this means that the irradiated In_2S_3 supplies enough excited electrons to the enzyme. Overnight incubation was not an improvement. The photobioproduction decreased to 152 µmol H_2/(min·mg Hase) after 22 hours incubation, whereas the activity with reduced MV for this sample was 93% of the initial activity of the Hase before incubation with the semiconductor. This result corresponds to 26% photocatalytic

efficiency, indicating that an excess of incubation time scarcely deteriorates the Hase, but it does the In_2S_3 and/or its interface with the Hase.

A study of the enzyme ratio attached to the In_2S_3 particles after incubation was performed on fresh samples. After their incubation time, the samples were let to sediment during 2 hours. The supernatant was then separated from the semiconductor powder sedimented at the bottom. The solid was redispersed with 10 mL of fresh buffer (50 mM TRIS-HCl 0.2 M sodium sulfite pH 7). The H_2 production activity of both fractions was measured by mass spectrometry using 1 mM MV as electron donor. **Figure 4.2.11A** represents the percentage of H_2 production obtained with the supernatant fraction (bars white area), the semiconductor particles fraction (bars grey area) and the percentage of photoactivity in the In_2S_3 particles fraction compared to the Hase activity measured in the same fraction with reduced MV (black bars). The measurements were performed as represented in **Figure 4.2.11B.**

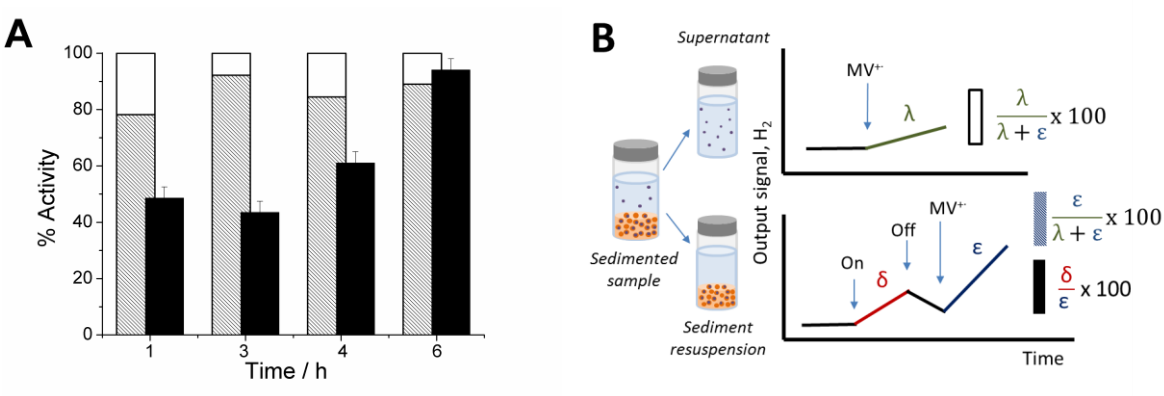

Figure 4.2.11 A) Percentage of Dv[NiFeSe] Hase activity retained by In_2S_3 particles after incubation periods of 1, 3, 4 and 6 hours. *The white and grey bar areas represent the % of Hase activity (measured with reduced MV) in the supernatant and In_2S_3 particles fractions respectively. Black bars represent the % of H_2 photobiocatalytic production in the In_2S_3 particles fraction compared to the Hase activity with reduced MV; the error was measured during H_2 production. Measurements were done at 37°C in 50 mM TRIS-HCl 0.2 M sodium sulfite pH 7.* ***B) Scheme of the measurement processes in mass spectrometer.*** *λ represents the specific activity of Hase in the supernatant fraction, δ is the specific photoactivity in the sediment particles fraction, and ε is the specific activity measured with reduced MV in the sediment particles fraction after measuring the photoactivity on the same sample.*

The total H_2 production activity (sum of the amount obtained with the supernatant and redispersed fractions) measured with reduced MV for samples incubated 1 h, 3 h, 4 h and 6 h was 687 µmol H_2/(min·mg Hase), 1150 µmol H_2/(min·mg Hase), 798 µmol H_2/(min·mg Hase) and 802 µmol H_2/(min·mg Hase) respectively. These results confirmed that the enzyme maintained at least 75.4% of

the initial activity after the incubation and the H_2 photobioproduction assay. The sample incubated during 1 h presented 78% of its MV-related enzymatic activity in the In_2S_3-bound fraction, and 49% of it was photocatalytically active. Sample 3 h showed an increase of the MV-related enzymatic activity in the In_2S_3-bound fraction up to 92%, whereas only 44% of it was photoactive. Sample 4 h retained 85% of the MV-related enzymatic activity within the In_2S_3-bonded fraction, showing an increase up to 61% of the photobiochemically produced H_2. Sample 6 h showed an 89% MV-related enzymatic activity in the In_2S_3-bonded fraction and 94% of it was photoactive. A schematic representation of the % of Hase attached to the In_2S_3 and % of Hase photoactive is shown in **Figure 4.2.12** for samples after 1h and 6h incubation.

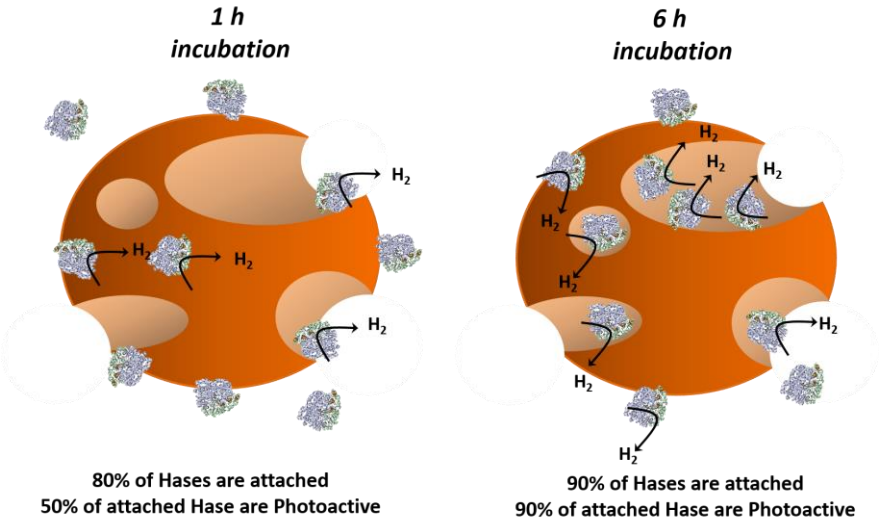

Figure 4.2.12 ***Scheme of % Hase attached and % Hase photoactive after 1h and 6h incubation time.***

4.2.6 Discussion

The characterization of In_2S_3 powder with XRD revealed that the semiconductor obtained was In_2S_3 in its cubic conformation, which is the photoactive form,[85] with an average crystal domain size of 37 nm. Hexagonal nanocrystal shape was determined by TEM. SEM images showed that the aggregate particles were flower like spheres, mostly about 10 µm diameter, and with high level of porosity. The most common pore size was around 16.5 nm diameter. The direct band gap value obtained by UV-VIS spectroscopy at 2.1 eV was the expected one for this material,[75,86] which is thus useful for absorbing light within most of the visible range.

The characterization of the *Dv*[NiFeSe]$_s$ Hase by FTIR confirmed that its active site behaves similar as the membrane form Hase, but its electroactivity when inhibited with O_2 is not as reversible as that of the *Dv*[NiFeSe]$_m$ Hase immobilized on an electrode,[151] yielding just 40% of the initial activity after the O_2 inhibition (Fig. 4.2.7B). However, H_2-production activity in solution monitored by mass spectrometer yield similar TOFs as the *Dv*[NiFeSe]$_m$ Hase when reduced with MV.

The impedance spectroscopy results on LDG/In_2S_3 electrode indicated that at pH 7 the semiconductor surface had a negative charge, thus preventing massive aggregation of particles in solution. The *Dv*[NiFeSe] Hase has an optimal H_2-production activity at the pH range 6-7 using reduced MV as electron donor,[32] so the incubation of enzyme and semiconductor particles was done at pH 7. The Hase has great affinity for the semiconductor, as after 1 h incubation most of the active enzyme was attached to the semiconductor particle fraction and not in the solution one. Therefore, the formation of an In_2S_3/Hase hybrid indeed took place. Such high affinity for the attachment with a semiconductor had also been reported for the [NiFeSe] Hase from *Desulfomicrobium baculatum* with TiO_2 particles.[157]

Illumination of the mixture of In_2S_3 and Hase with visible light, monitored in situ in aqueous solution by membrane-inlet mass spectrometry, clearly led to immediate production of H_2 with a high rate. Therefore, In_2S_3 was able to excite electrons from its VB to its CB with visible light, use the sulfite in solution as holes scavenger and transfer the excited electrons to the attached Hase, which catalyzes the reduction of 2 protons to H_2. This confirmed that the CB has a high enough energy level for thermodynamically favoring the donation of electrons to the Hase, which has a redox potential of approximately -0.4 V (*vs*. SHE) to drive its catalytic activity.[143] Indeed, the flat-band potentials measured for In_2S_3 films on FTO are between -0.7 and -0.9 V (*vs.* SHE).[158] Although the presence of sulfite in the solution decreased the specific activity of the Hase in 3-fold, the In_2S_3 had no toxicity against the Hase since after 22h of incubation the specific activity of the Hase was still 93% of the initial

activity. Control experiments lacking Hase or In_2S_3 in the solution confirmed that the photocatalytic activity required both the presence of In_2S_3 and Hase.

The retention of Hase by In_2S_3 was fast, showing high affinity between both, since the proportion of Hase retained after only 1 h of incubation was similar to that retained after 6 h (Fig. 4.2.11A). At 1h, 80% of Hase was attached to In_2S_3 but its photoproduction rate just reached the 49% of the overall activity. This result indicates a poorly efficient ET from the CB to the Hase active site; electron transfer was rate-limiting. The efficient photocatalysis with redox metalloenzymes not only requires favorable thermodynamics, but fast kinetics of ET from the semiconductor surface to the exposed redox site of the enzyme (the distal 4Fe4S cluster in the case of Hases).[159] The best photocatalytic results were obtained after 6 hours of incubation of Hase with the In_2S_3 under mild stirring. Under those conditions, 84% of photocatalytic efficiency was reached when comparing with the total Hase specific activity in solution and on the semiconductor surface, whereas it increased up to 94% when considering only attached Hase. Therefore, an optimal In_2S_3-Hase interface was obtained in which the photocatalytic process was not rate-limited by ET between semiconductor and enzyme.

Fast interfacial kinetics of ET has been obtained by adsorption of Hases on rough graphite electrode surfaces with pore diameters slightly larger than the size of the enzyme molecule,[160] suggesting that the enzyme molecule immobilized inside a pore will have its distal 4Fe4S cluster at a distance of the electrode surface adequate for fast DET, independently of its orientation.[160] The pore analysis of the In_2S_3 indicated an average diameter of 16.5 nm, which is big enough to host the *Dv*[NiFeSe] Hase molecules with a diameter around 5 nm.[31] Therefore, the insertion of the enzyme into the semiconductor pores is favored. The increase in the photobiocatalytic efficiency after a 6 h incubation period may be explained by the slow insertion of the Hase molecules into suitable pores, favoring the contact between the Hase and the surrounding semiconductor and decreasing the importance of Hase orientation for fast ET upon irradiation of the In_2S_3-Hase catalytic tandem. In this way, the highest TOF of the *Dv*[NiFeSe] Hase measured in the system for H_2-photobioproduction was 986 s^{-1}. This value equals the highest one measured by Brown *et al.* using CdS nanorods and a [FeFe] Hase as photocatalyst hybrid.[14]

4.3 In_2S_3 - LACCASE FOR O_2 PHOTOELECTROPRODUCTION

In **section 4.1** has been described the development of a bioelectrochemical photocatalyst based on the co-immobilization of PSI and Hase on gold electrode for a **H_2 evolution cathode**. This section shows the development of a hybrid photocatalytic system for an **O_2 evolution anode**, thus studying the other electrode required for a complete photoelectrochemical device.

Since In_2S_3 studied in **section 4.2** managed to absorb visible light by creating electron-hole pairs that could be involved in either H_2 or O_2 evolution, and according to its n-type nature as semiconductor and its LUMO position, In_2S_3 was selected as light absorber component for O_2 photoelectrochemical production. Laccase acted as the biocatalyst for water oxidation. Herein, the last approach of this thesis was based on the hybrid In_2S_3 – Laccase deposited on an FTO substrate electrode for the photoelectrochemical production of O_2 (**Figure 4.3.1**).

Several strategies were studied to optimize the interface between the *Th*Lc and the In_2S_3 semiconductor to successfully achieve DET.

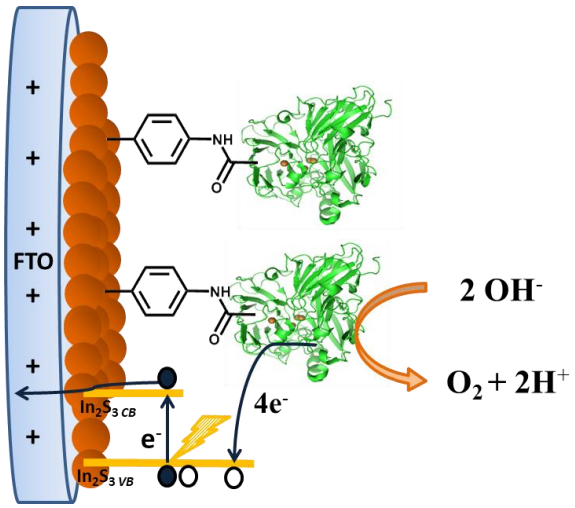

Figure 4.3.1 ***In_2S_3-ThLc hybrid for photocatalytic production of O_2 on a FTO electrode.***

4.3.1 Characterization of FTO/In_2S_3 and FTO/In_2S_3/*Th*Lc electrodes

Drop-cast In_2S_3-deposition on FTO substrate electrodes was performed as described in **section 3.6.3.1**. The FTO substrate was chosen because its translucency under visible light, its easy manipulation and affordability. The translucency of the substrate electrode was needed since the experiments were performed by illuminating from its back side.[161]

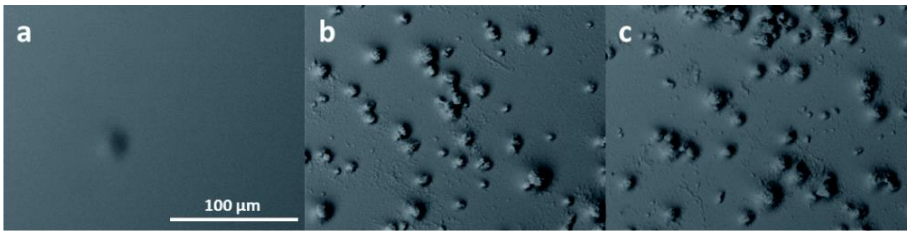

Figure 4.3.2 ***SEM images*** *of bare FTO (a), FTO/In_2S_3 (b), FTO/In_2S_3/ThLc (c) electrodes.*

The synthesis of the polycrystalline In_2S_3 used for electrode modification was described and characterized in **section 3.3** and **4.2.1** respectively.[162] Clean samples of FTO, FTO/In_2S_3 and FTO/In_2S_3/*Th*Lc were visualized by SEM (**Figure 4.3.2)**. As a result of the In_2S_3 deposition on the FTO surface the roughness increased. The further modification with the laccase did not yield any significant change at this scale, as expected taking into account the much smaller size of laccase molecules[163] than that of the In_2S_3 particles.[162]

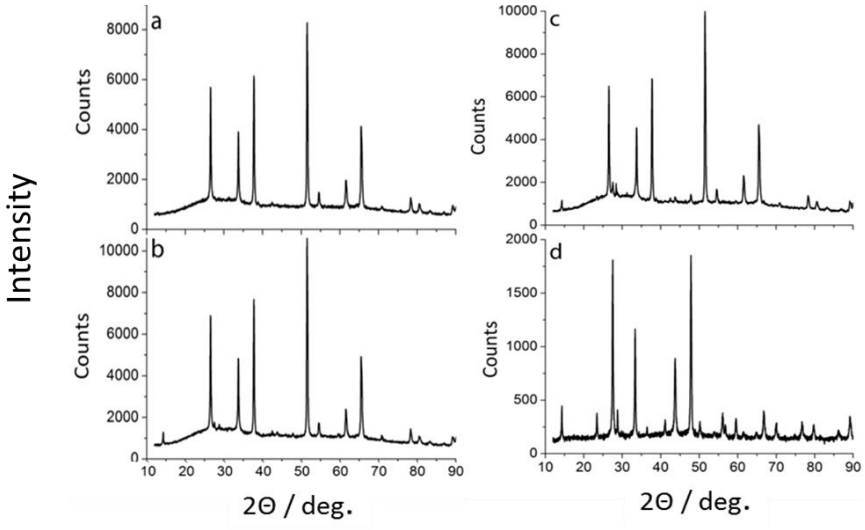

Figure 4.3.3 ***XRD*** *of FTO (a), FTO/In_2S_3 freshly prepared (b), FTO/In_2S_3 after + 1.0 V (vs. SHE) chronoamperometry during 360 s (c) and In_2S_3 as-synthesized (d).*

The crystallinity and stability of the In_2S_3 particles deposited on the FTO electrodes was tested by XRD for: an FTO electrode, FTO/In_2S_3 electrode before and after 1 V voltage (*vs.* SHE) was applied

during 360 s, and In_2S_3 before its addition to FTO. These XRD are shown in **Figure 4.3.3**. The peaks that characterize either FTO or In_2S_3 were still present in all cases, and new diffraction peaks did not appear after application of 1 V (*vs.* SHE) to FTO/In_2S_3 electrodes that could be attributed to the appearance of oxysulfides or any other possible oxidation product.

4.3.2 Photoelectrocatalytic O_2 production by FTO/In_2S_3/*Th*Lc electrode

Several strategies to immobilize the *Th*Lc on FTO/In_2S_3 electrodes were tested following the procedures described on **section 3.6.3.1.**

For covalent immobilization of *Th*Lc the semiconductor was functionalized with two different molecules: 4-ATP and 4-Dz. In_2S_3 particles modified with 4-ATP were characterized by FTIR. In **Figure 4.3.4A** are shown the FTIR spectra, in the range of 1400 – 1700 cm^{-1}, for In_2S_3 particles (a), and 4-ATP modified In_2S_3 particles (b). Characteristic bands from aromatics groups were present in the In_2S_3 modified with 4-ATP. The other functionalization method studied was the electrodeposition of 4-Dz on FTO/In_2S_3. The CVs for the electrodeposition of 4-Dz on FTO and FTO/In_2S_3 electrodes are shown in **Figure 4.3.4B**.

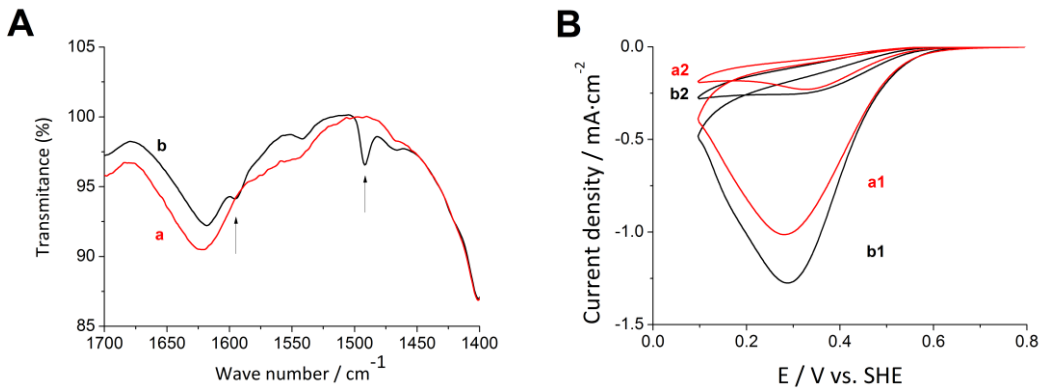

Figure 4.3.4 ***A) FTIR spectra*** *of In_2S_3 (a) and In_2S_3 modified with 4-ATP (b). Arrows indicate the vibrations from aromatic C-C bonds of 4-ATP.* ***B) CVs from 4-Dz deposition*** *on clean FTO (a) and FTO-In_2S_3 (b): first scan (1) and second scan (2). CVs recorded at 100 mV/s in 5 mL CH_3CN containing 2 mM 4-Dz and 100 mM Bu_4NBF_4.*

The electrochemical response of FTO, FTO/In_2S_3 and FTO/In_2S_3/*Th*Lc electrodes was followed by CV under dark and illumination conditions. The FTO/In_2S_3/*Th*Lc electrodes on which the laccase was physically adsorbed did not increase the electrochemical response provided by a FTO/In_2S_3 electrode under illumination, **Figure 4.3.5A**.

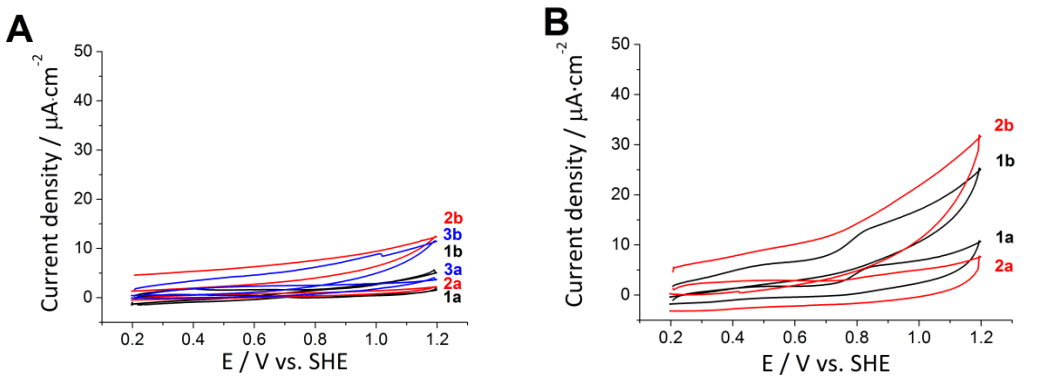

Figure 4.3.5 ***A) ThLc physical absorption immobilization.*** *CVs of a bare FTO (1), FTO/In_2S_3 (2) and a FTO/In_2S_3 with adsorbed ThLc (3) electrode under dark (a) and illumination (b) conditions.* ***B) ThLc covalent immobilization through 4-ATP monolayer.*** *CVs of a FTO/In_2S_3(4-ATP) (1) and a FTO/In_2S_3(4-ATP)/ThLc covalently immobilized (2) electrode under dark (a) and illumination (b) conditions. Recorded at 20 mV/s.*

The FTO/In_2S_3 functionalized electrodes were tested with *Th*Lc covalently bound to the aminoaryl group of the linker through an amide bond. In **Figure 4.3.5B** are shown the CVs under dark and illumination conditions from: (i) *Th*Lc bound through 4-ATP molecules attached to the In_2S_3, and (ii) control electrode of FTO/In_2S_3 functionalized with 4-ATP but lacking *Th*Lc. A current increase was detected when illuminating the electrodes containing laccase, although it was not considered significant since an increase due to the 4-ATP modification was also observed in the control electrode.

The CVs of *Th*Lc attached by forming amide bonds between its carboxylic residues and the electrodeposited amino phenyl groups on the semiconductor, under dark and illumination conditions, are shown in **Figure 4.3.6A.** A significant increase in the current is observed when irradiating the electrodes with *Th*Lc covalently bound by this strategy. At redox potentials higher than +0.8 V (*vs.* SHE), FTO/*Th*Lc (FTO modified with 4-Dz and covalently bound *Th*Lc) and FTO/In_2S_3 (modified with 4-Dz as control) gave a current increase when illuminating the electrodes that was much smaller than the FTO/In_2S_3/*Th*Lc ones, which increased more than 10-fold yielding 28 ± 5 µA/cm^2 at +1.0 V (*vs.* SHE).

Since the semiconductor surface in both modifications presented an amino aryl group facing the *Th*Lc that allows binding it through an amide bond, the difference between them in the measured photocurrents suggests that the interface between the In_2S_3 and the aromatic molecules was the limiting step. The 4-ATP is supposed to attach to the In_2S_3 through disulfide bridges, which can be quickly broken when illuminating due to the oxidation of the In_2S_3 surface, whereas 4-Dz was electrochemically deposited either on In_2S_3 or directly on FTO forming more stable bonds.[108,109] Since the In_2S_3 deposited on FTO were not covering the whole surface (Figure 4.3.2b,c), *Th*Lc may be also covalently bounded directly to FTO which well oriented the enzyme to the near In_2S_3 particles.

In order to confirm that the photocurrent measured on FTO/In_2S_3(4-Dz)/*Th*Lc electrode corresponded to O_2 evolution by the Laccase, an O_2 microsensor was placed at ~1.5 mm distance from the photoelectroactive surface. The sensor detected O_2 production by the FTO/In_2S_3/*Th*Lc electrode only when it was illuminated (**Figure 4.3.6A inset**). These results indicate that covalent attachment of *Th*Lc may have oriented adequately the enzyme on the semiconductor surface for DET to oxidize H_2O to O_2.[109] The detection of O_2 by the sensor started as the backwards scan of the CV was initiated, suggesting that O_2 production by the illuminated FTO/In_2S_3/*Th*Lc electrode took place at the higher potentials. The delay in the sensor signal was expected due to the diffusion time needed for the photobioelectrochemically produced O_2 to diffuse towards the sensor (**Figure 4.3.6B**).

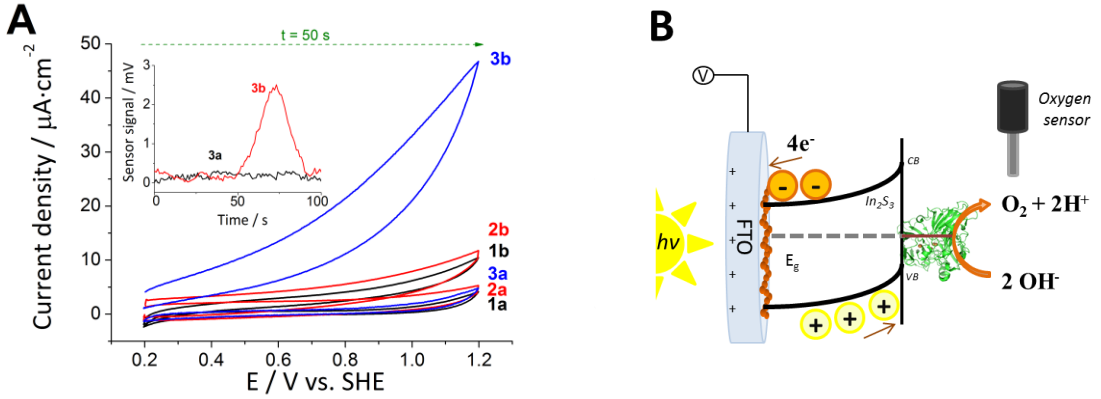

Figure 4.3.6 ***A) ThLc covalent immobilization through 4-Dz electrodeposited on In_2S_3*** *CVs under dark (a) and under illumination (b) of FTO/ThLc electrodes where ThLc is covalently bound to amino phenyl groups on the FTO (1), FTO/In_2S_3 (4-Dz) (2) and FTO/In_2S_3 (4-Dz)/ThLc covalently immobilized electrode (3). Inset: Potentiometric signal recorded by the O_2 microsensor while scanning 3a and 3b CVs. Recorded at 20 mV/s.* ***B) Scheme of photoeletrocatalytic production of O_2*** *monitored with the O_2 microsensor.*

The O_2 microsensor provided evidence of H_2O oxidation to O_2 catalyzed by a photoelectroenzymatic process, but there were many factors hindering the quantification of the O_2 produced: (i) the O_2 present in the solution was not homogeneous during the experiment timescale, as it was produced in the electrode surface and the solution was quiescent. (ii) not all the O_2 produced was diffused to or through the sensor and (iii) the O_2 in solution equilibrated with the gas phase.

These challenges were overcome by measuring transient O_2 signals during the chronoamperometries with a delay of approximately 30 s for the onset detection. An attempt to estimate the O_2 produced required a calibration able to correlate the charge measured by chronoamperometry (**Figure 4.3.7A**) with the integrated area of the sensor signal (**Figure 4.3.7B**). According to these factors a correlation was made between the O_2 produced on an equivalent clean

FTO surface at different overpotentials where H_2O oxidation takes place, with the O_2 detected by the sensor when located exactly at the same position with respect to the electrode as in the photoelectrochemical measurements. The O_2 produced on the FTO electrode was calculated from the charge converted to O_2 moles following the *Faraday´s Law*:

$$M = \frac{1}{F} \cdot \frac{Q}{n}$$

where *M* is mol of substance, *F* is the Faraday constant, *Q* is the charge and *n* is the number of equivalents/electrons involved on the reaction.

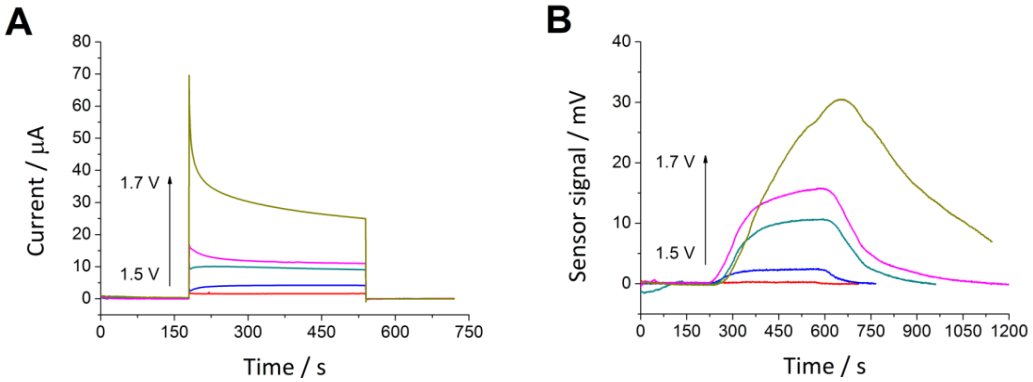

Figure 4.3.7 ***Charge and O_2 determination. A) Chronoamperogramms of FTO clean electrodes****. The initial potential for all experiments was +1.2 V (vs. SHE) during 170 s. Step potentials of +1.50 V, +1.55 V, +1.60 V, +1.65 V or +1.70 V (vs. SHE) were applied during 340 s before stepping back to the initial potential.* ***B) Signal measured by the O_2 microsensor*** *during the different step potential experiments.*

The chronoamperometries for O_2 evolution calibration on FTO ranged from +1.50 to +1.70 V (*vs.* SHE) and showed that an increase on the applied potential yielded a higher signal from the O_2 sensor. Moreover, it was checked that the charge measured for H_2O oxidation during the chronoamperometries was proportional to the integrated response of the O_2 sensor. However, incomplete H_2O oxidation to H_2O_2 is also possible when a potential ≥ 1 V (*vs*. SHE) is applied at an electrode. The extent of H_2O oxidation to the byproduct H_2O_2 by the FTO electrodes biased at different potentials was also analyzed. An aliquot of the resulting electrolyte was taken and HRP and ABTS were added to it for H_2O_2 determination, as described in **section 3.6.3.3**. The negligible ABTS oxidation detected spectrophotometrically at 414 nm implied an insignificant H_2O_2 formation at any applied potential, and consequently all the charge measured in Figure 4.3.7A was correlated to the O_2 detected in Figure 4.3.7B.

Since in all cases the absorbance values measured for H_2O_2 production were similar to or lower than that of the blank experiment (no potential applied) (**Figure 4.3.8A**), it could be assumed that the integrated charge at the FTO electrode during the chronoamperometry corresponded to O_2 production

exclusively; therefore, the Faradaic yield was negligible towards H_2O_2. Considering the Faraday constant and that 4 electrons are involved in H_2O oxidation to O_2, a linear correlation was obtained between the integrated O_2 signal at the sensor and the amount of O_2 produced at the FTO electrode (**Figure 4.3.8B**). From the calibration plot was obtained the equation:

$$O_2\ (nmol) = 0.00182 * Integrated\ sensor\ signal\ (mV{\cdot}s)$$

The equation was used to estimate the amount of O_2 produced during the photoelectrochemical experiments at the FTO electrodes modified with In_2S_3, *Th*Lc, and both of them.

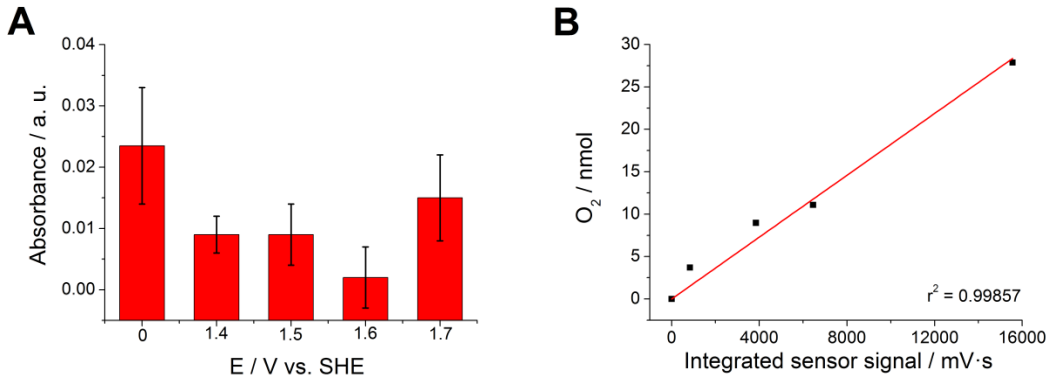

Figure 4.3.8 ***A) Enzymatic determination of H_2O_2*** *in the electrolyte solution after 20 min water oxidation chronoamperometries at different step potentials. The absorbance at 414 nm was measured after addition of HRP and ABTS.* ***B) Calibration plot for the determination of the O_2*** *produced at the FTO electrode from the integrated signal measured with the O_2 sensor.*

The calibration performed allowed measuring the O_2 photoproduced by a FTO/In_2S_3/*Th*Lc electrode under illumination. First, control experiments were done by performing chronoamperometry measurement during 5 min at +1.0 V (*vs.* SHE), under dark and illumination conditions in presence of the O_2 microsensor. A typical FTO/In_2S_3 electrode, without Laccase, provided a photocurrent increase due to illumination that yielded 0.262 mC charge over 150 s, although the O_2 sensor did not give any significant signal change during the experiment (**Figure 4.3.9A)**. When illuminating the FTO/In_2S_3/*Th*Lc electrode the photocurrent increase was higher, yielding 0.496 mC over nearly the same time period, while the O_2 detected was significant (**Figure 4.3.9B)**. These results supported the previous ones showing that covalent attachment of *Th*Lc on the semiconductor surface was needed to oxidize H_2O to O_2. However, the photocurrent registered for FTO/In_2S_3 without laccase suggested there were other processes occurring on the electrode.

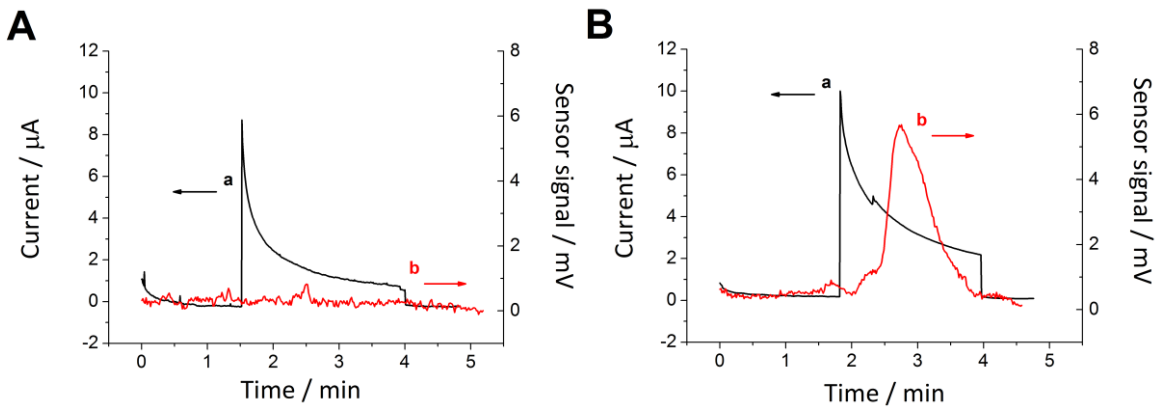

Figure 4.3.9 ***Detection of O_2 production. A)*** *Chronoamperometry recorded at +1.0 V (vs. SHE) on an FTO/In_2S_3 electrode represented in black (a), illuminating from 1.5 to 4 min, and O_2 signal measured by the microsensor in red (b).* ***B)*** *Chronoamperometry recorded at +1.0 V (vs. SHE) on an FTO/In_2S_3/ThLc electrode represented in black (a), illuminating from 1.8 to 4 min, and O_2 signal measured by the microsensor in red (b).*

In order to better estimate the amount of O_2 photoproduced by a FTO/In_2S_3/*Th*Lc electrode when illuminated, chronoamperometries at different bias potentials were performed. At the bias potential of +0.7 V (*vs.* SHE) there was no measurable O_2 signal, whereas in the case of the +0.8, +0.9 and +1.0 V (*vs.* SHE) potentials the amount of O_2 produced by the electrode could be estimated (**Table 4.3.1**). The current increase at higher overpotential provided a higher and more reproducible O_2 production. A faradaic yield of 45 ± 5% was obtained at +1.0 V (*vs.* SHE) from the ratio between the amount of O_2 produced and the charge measured at the electrode during the chronoamperommetry under light illumination.

Table 4.3.1 Charge and amount of O_2 produced by an illuminated FTO/In_2S_3/*Th*Lc electrode under different applied potentials during 6 min.

E / V (*vs. SHE*)	Charge / mC	O_2 / nmol	Faradaic yield / %
0.7	0.3 ± 0.1	0	0
0.8	0.7 ± 0.1	0.5 ± 0.1	30 ± 5
0.9	0.6 ± 0.2	0.44 ± 0.03	30 ± 10
1.0	0.8 ± 0.2	0.93 ± 0.04	45 ± 5

A control experiment was done with *Th*Lc covalently bound to the 4-Dz functionalized FTO (FTO/*Th*Lc), in absence of In_2S_3, to evaluate at which redox potential the enzyme was able to evolve O_2 without photochemical excitation. Without illuminating the FTO/*Th*Lc electrode, the O_2 production was not detected until a potential of +1.55 V (*vs.* SHE) was applied at the electrode (**Figure 4.3.10**),

which was the same potential required for measuring non-biocatalytic water oxidation directly at the bare FTO electrode (Figure 4.3.7). However, higher currents and O_2 detection on the sensor were measured in presence of the *Th*Lc.

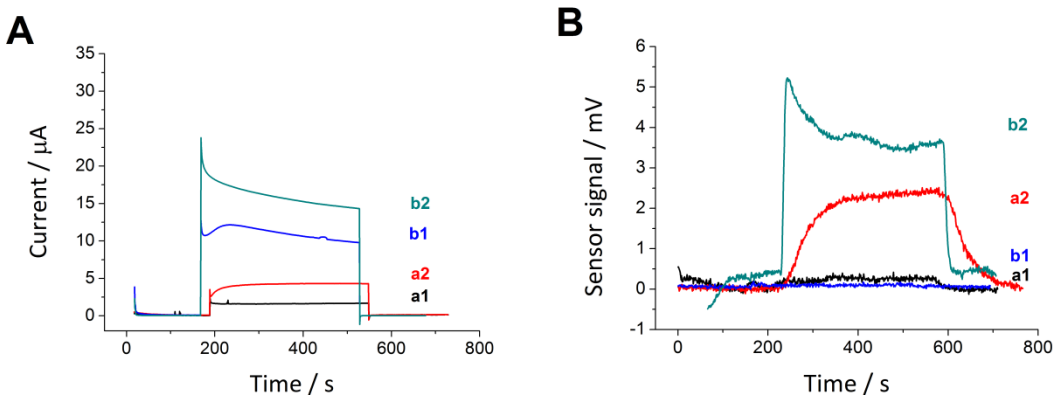

Figure 4.3.10 ***Charge and O_2 determination for bare FTO and FTO/ThLc. A) Chronoamperogramms*** *(without illumination) upon applying +1.5 V (1) or +1.55 V (2) step potentials for bare FTO (a) and FTO/ThLc (b) electrodes. The initial and final potential for all experiments was +1.2 V (vs. SHE). The step potential was applied during 360 s.* ***B) O_2 signals*** *measured by the microsensor during the chronoamperometric studies.*

4.3.3 *Th*Lc activity determination and stability

The amount of active laccase immobilized on the FTO/In_2S_3/*Th*Lc electrodes was estimated by the standard ABTS oxidation assay monitored by UV-VIS spectroscopy in the presence of O_2, as described in **section 3.6.3.3**, and shown in **Figure 4.3.11A**.[131] The calibration plot with different *Th*Lc concentrations in solution ranging from 2.3 ng/mL to 140 ng/mL, in **Figure 4.3.11B**, gave the equation:

$$Activity\ (\mu mol\ ABTS^{+\cdot}/min) = 0.0023 + 0.104 * ThLc\ (\mu g)$$

The equation was used to calculate the amount of active enzyme immobilized on the electrodes. The *Th*Lc remained active after its covalent immobilization on either sulfide-loaded or FTO electrodes (Figure 4.3.11AB, lines *a* and *b*).

The average amount of the active enzyme on 4 different FTO/In_2S_3/*Th*Lc electrodes was found to be 0.18 ± 0.08 µg. The stability of the laccase on the modified electrodes was tested. After being simultaneously exposed to a positive potential and illumination, its activity dropped drastically, losing 99 % of the initial value (Figure 4.3.11A, lines *d* and *e*). A sample from the electrolyte solution was measured to check if *Th*Lc leaked during the operation. Very small amount of active enzyme was detected in the solution (Figure 4.3.11A, line *c*). The *Th*Lc stability towards illumination was also measured by illuminating during 6 min in open circuit conditions a FTO/*Th*Lc electrode. The average amount of active enzyme after the illumination was 7.5 ± 0.1 ng (Figure 4.3.11A, line *f*), which is comparable to the activity measured on the electrodes after the photobioelectrochemical

experiments. These control experiments allowed attributing the laccase inactivation to the Xe lamp illumination.

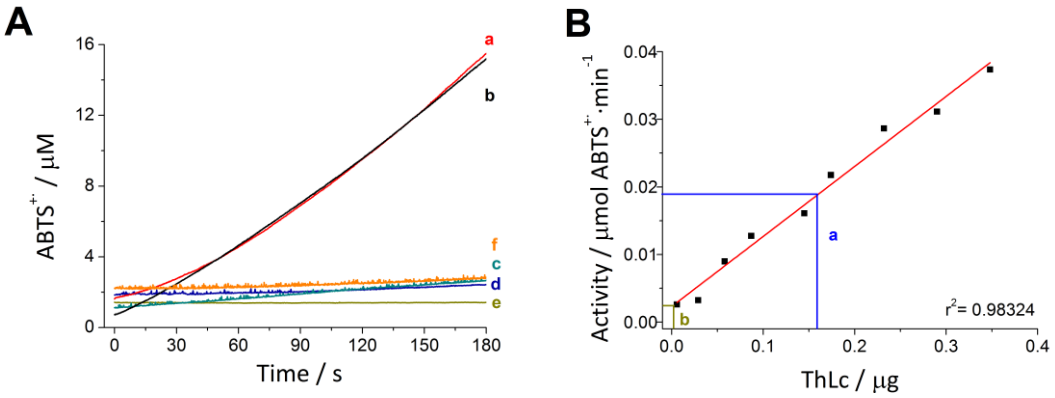

Figure 4.3.11 ***Determination of ThLc specific activity for O_2 reduction using ABTS as the electron donor. A) Kinetics of ABTS oxidation*** *by (a) Freshly prepared FTO/ThLc electrode, (b) freshly prepared FTO/In_2S_3/ThLc electrode, (c) sample of the solution from FTO/In_2S_3/ThLc electrode after 6 min of photochronoamperometry at +0.8 V (vs. SHE), (d) FTO/ThLc electrode after 6 min photochronoamperometry at +0.8 V (vs. SHE), (e) FTO/In_2S_3/ThLc electrode after 6 min photochronoamperometry at +0.8 V (vs. SHE) and (f) FTO/ThLc electrode illuminated during 6 min with no applied potential.* ***B) Calibration curve****. Lines (a) and (b) correspond to the interpolations of the amount of active enzyme immobilized on the FTO/In_2S_3/ThLc electrode before and after the photochronoamperometric experiments, respectively. $ABTS^{+\cdot}$ concentration was measured spectrophotometrically at λ = 414 nm in 100 mM phosphate buffer pH 4.4.*

4.3.4 Discussion

As already discussed in the hybrid system In_2S_3 – Hase, In_2S_3 is an example of n-type semiconductor able to absorb visible light and with the ability to transfer light-excited electrons to an enzyme at the expense of a sacrificial electron donor.[162] In_2S_3 may be also coupled to electrodes to promote oxidative reactions, as the excited electrons can be swiftly transferred to the positively polarized electrode before recombination.[87] Herein, the formation of hybrid inorganic/biochemical photoelectrocatalysts by attachment of an enzyme for H_2O oxidation to In_2S_3 semiconductor modified electrodes was the next step to develop in this thesis. Taking into account that the VB energy level of In_2S_3 is lower than the redox potential for H_2O oxidation,[75] the photogenerated hole is suitable to accept the electrons from H_2O molecules, if coupled with an adequate catalyst.

The use of copper complexes as electrochemical catalysts for H_2O oxidation has been proved,[88,164] as well as the use of copper-containing redox enzymes such as laccase.[58] Adsorption of a laccase to p-type silicon on a gold electrode has been reported for photoelectrochemical reduction of O_2.[165] According to a previous report, *Th*Lc has shown activity for the reverse reaction, *i.e.* water oxidation to O_2, at neutral pH when covalently attached to an electrode polarized at high potential.[58] Hence, immobilizing the laccase on the surface of the In_2S_3 modified electrode can take the advantage of the light energy to reduce the applied potential needed for H_2O electrooxidation.

The O_2 production by the FTO/In_2S_3/*Th*Lc system required a lower electric energy input thanks to the light assistance. The onset potential for the process was +0.8 V (*vs.* SHE) at pH 7.1, in which the hybrid photoelectrocatalyst was able to oxidize water to O_2 with 30 % faradaic efficiency. The faradaic yield of the FTO/In_2S_3/*Th*Lc device increased to 45%, when the electrode was polarized at +1.0 V (*vs.* SHE), which is comparable to the faradaic efficiencies reported for some inorganic photoelectrocatalysts for O_2 production.[166] When comparing the photocurrent measured at +1.0 V (*vs.* SHE) in the control FTO/In_2S_3 electrode without laccase, it is approximately half of that for the FTO/In_2S_3/*Th*Lc electrode (Figure 4.3.9). The measured photocurrents in absence of *Th*Lc suggest that the photocorrosion of the In_2S_3 is the main cause that decreases the faradaic yield of O_2 evolution. Monitoring of the XRD pattern of In_2S_3 before and after the photochemical water oxidation process gave no hint of indium traces of oxysulfides or oxides, but the technique is probably not sensitive enough to detect small changes in the semiconductor surface due to photocorrosion at the timescale of the experiments performed.

The specific activity of the biocatalyst after 6 min operation under illumination, either attached to the electrode or free in solution, was reduced by a factor of 99 %. This inactivation may be attributed (i) to the attack of the hydroxyl radicals formed from the photogenerated holes[146] to the copper cations

at the enzyme's active site, which blocks the enzyme and/or (ii) to the photodegradation of the enzyme under high power illumination. The second explanation is in agreement with our experimental result shown in Figure 4.3.11Af, where a freshly prepared electrode FTO/*Th*Lc lost any O_2 reducing/ABTS oxidizing catalytic activity after illumination, even if it was never connected to the electrochemical setup.

When the enzyme was covalently bound directly to an FTO electrode, O_2 production was negligible bellow the redox potential at which water is oxidized directly at the FTO (+1.55 V (*vs.* SHE)). The same laccase attached to porous graphite electrode did not produce O_2 below +1.2 V (*vs.* SHE) at the same pH,[58] thus the photoelectrochemical strategy allowed the reduction of the overpotential for H_2O electrooxidation by at least 0.4 V. The result obtained for FTO/*Th*Lc can be explained by the hindrance of establishing DET of the laccase at a less rough and conductive electrode than LDG.[58] Instead, the porous surface of the In_2S_3 favors the DET to the redox sites of the attached laccase molecules under light illumination, as has been previously described for the hydrogenase in **section 4.2**.[162] In the present case, covalent binding of the *Th*Lc to the functionalized semiconductor was required, possibly because the smaller size of the laccase molecules than the Hase ones prevents their retention in the In_2S_3 pores just by adsorption. Another possible explanation is that Hase was stabilized by S-S attracting interactions between the chalcogenide's surface and the distal cluster of the enzyme,[162] whereas in this work laccase lacks any surface motif to promote a strong and oriented adhesion by simple non-covalent adsorption.

The faradaic efficiency of In_2S_3-*Th*Lc photocatalyst, 45% at +1.0V (vs. SHE) is lower than other similar systems reported, such as by Reisner and co-workers using PSII immobilized within a Os-complex redox polymer on nanostructured ITO electrodes,[20] which lead high photocurrents up to 410 $\mu A/cm^2$ at +0.5 V (*vs.* SHE) with 85% faradaic efficiency. However, the photocurrents measured with PSII decreased two orders of magnitude when working in DET mode, i.e. in the absence of the redox polymer that shuttles electrons between the redox centers of PSII and the electrode.[167] Photocurrents up to 50 $\mu A/cm^2$ (at +1.0 V (*vs.* SHE)) in DET mode have been measured in this thesis with the FTO/In_2S_3-Laccase system. Considering the determined amount of active laccase immobilized on the photoanode, its TOF for O_2-production is on average 4.6 ± 0.1 s^{-1}, which equals that measured for PSII.[20] Indeed, PSII is able to evolve O_2 with the same TOF at 0.5 V lower potential, but it has to be taken into account that PSII is nature´s evolved catalyst for water oxidation, whereas the natural activity of laccases is the reverse reaction.

5. CONCLUSIONS

5. CONCLUSIONS

Artificial photosynthesis has been achieved by combining a light-harvesting element able to absorb visible light radiation with a redox enzyme for catalyzing either O_2 or H_2 production from water.

- The combination of PSI and *Dg*[NiFe] Hase by forming an hydrogel on a gold electrode surface allows H_2 photoproduction from water without using noble metals. However, PSI stability is a limiting step, losing 50% of its activity after 10 min of illumination.
- Cc-BPEI redox polymer provides a much better performance than MV-LPEI due to its more negative redox potential that guarantees a higher overpotential to mediate successfully the ET from PSI to Hase. Moreover, Cc-BPEI acts as O_2 scavenger while simultaneously reducing Hase for H_2 evolution. The onset potential of H_2 photoproduction with this polymer is +380 mV, which is 830 mV more positive than the redox potential of the MV redox mediator.
- PSI-Hase photoelectrocatalyst's TOF was 3 s^{-1} when Cc-BPEI was used, yielding a H_2 production of 83±4 pmol H_2/s. However, the TOF is probably underestimated since the calculated value was based on the molecular weight and amount of PSI, which was not pure but an enriched extract.
- In the In_2S_3 - Hase hybrid photosystem, the semiconductor was able to absorb in the visible light range spectra and provide electron flux to the *Dv*[NiFeSe] Hase for H_2 evolution from water. In_2S_3 characterization indicated that the average size of its pores, of 16.5 nm diameter, and the surface net charge at the range of pH 7-7.5 were suitable to host the Hase. Therefore, favoring the transfer of excited electrons from the semiconductor into the active site of the enzyme.
- The optimum experimental conditions for the formation of the In_2S_3-Hase hybrid photocatalyst are achieved for an incubation period of 6 hours. This leads to 89 % of the Hase being optimally attached to the semiconductor, proving the importance of the interfacing between the semiconductor particles and the enzymatic co-catalyst to favor the ET from the In_2S_3 CB to the active site of the Hase.
- The maximun TOF of the In_2S_3-Hase hybrid photocatalyst based on the amount of *Dv*[NiFeSe] Hase measured by mass-spectrometry was 986 s^{-1}, after 6 h incubation.

- *Trametes hirsuta* Laccase has been successfully used for the first time as catalyst for O_2 evolution in combination with In_2S_3 particles deposited on FTO transparent electrode to assemble a light-assisted photoelectrochemical anode.
- The faradaic yield of the FTO/In_2S_3/ThLc device was 30% when the electrode was polarized at 0.8 V (vs. SHE), and increased up to 45% when it was polarized at 1 V (vs. SHE). Hence, the photoelectrochemical strategy allows the reduction of the overpotential for H_2O electrooxidation by at least 0.4 V, compared to the 1.23 V (vs. SHE) thermodynamic potential for water splitting.
- In the In_2S_3-*Th*Lc hybrid photosystem photocurrents up to 50 µA/cm^2 (at 1 V *vs.* SHE) were measured in DET mode. Considering the determined amount of active laccase immobilized on the photoanode, its TOF for O_2 production was on average 4.6 ± 0.1 s^{-1}.

5. CONCLUSIONES

Se ha conseguido la fotosíntesis artificial mediante la combinación de absorbentes de luz visible con enzimas oxidoreductoras (redox) para catalizar, por un lado, la producción de O_2 y, por otro, la producción de H_2 a partir de agua.

- La combinación del PSI y la hidrogenasa (Hasa) *Dg*[NiFe] en un hidrogel sobre la superficie de un electrodo de oro permite la foto-producción de H_2 a partir de agua sin la necesidad de usar metales nobles. Sin embargo, la estabilidad del PSI es el factor limitante del proceso, perdiendo el 50% de su actividad a los 10 min de estar iluminado.
- Utilizando el polímero redox Cc-BPEI se consiguen mejores resultados que con MV-LPEI dado su potencial redox más negativo. Ésto garantiza la transferencia electrónica entre el PSI y la Hasa, protegiendo a la Hasa del O_2 presente, el cual puede ser reducido, y a la vez reduciendo a la Hasa para la evolución de H_2. El potencial de inicio de fotoproducción de H_2 con Cc-BPEI se observa a +380 mV, 830 mV más positivo que el potencial redox del mediador soluble MV.
- El TOF del fotoelectrocatalizador PSI-Hasa es 3 s^{-1}, para el hidrogel formado con Cc-BPEI, alcanzando una producción de 83±4 pmol H_2/s. Sin embargo, este valor de TOF está probablemente subestimado dado que el cálculo se ha realizado en base al peso molecular y cantidad depositada de extracto enriquecido de PSI; no se trata de una muestra pura.
- En el fotosistema híbrido In_2S_3 - Hasa, el semiconductor es capaz de absorber la luz visible y transferir el flujo de electrones excitados a la Hasa de *Dv*[NiFeSe] para la producción de H_2 a partir de agua. La caracterización del In_2S_3 ha evidenciado que el tamaño de poro, 16.5nm de diámetro, y su carga neta en el rango de pH 7-7.5, favorecen la inclusion de la Hasa en dichos poros.
- Las mejores condiciones para la formación del híbrido In_2S_3-Hase se consiguen a las 6 h de incubación. Tras dicha incubación, el 89 % de la Hasa se encuentra unida al semiconductor de forma óptima, permitiendo la transferencia electrónica entre la banda de conducción del semiconductor y el centro activo de la enzima.
- El TOF máximo calculado del fotocatalizador híbrido In_2S_3-Hase es 986 s^{-1}, basado en la cantidad *Dv*[NiFeSe] Hasa, medido por espectrometría de masas, después de 6 h de incubación.

- Se ha confirmado que la lacasa *Trametes hirsuta* puede ser utilizada como catalizador para la evolución de O_2 combinada con partículas de In_2S_3 depositadas en electrodos transparentes de FTO, obteniendo así un sistema fotoelectrocatalítico híbrido en el anodo.
- El rendimiento faradaico del sistema híbrido FTO/In_2S_3/ThLc es del 30% cuando el electrodo está polarizado a 0.8 V (*vs.* SHE), viéndose incrementado hasta el 45% cuando se polariza a 1 V (*vs*. SHE). Esta estrategia permite reducir el sobrepotencial de la electrooxidación del H_2O al menos en 0.4 V, comparándolo con los 1.23 V necesarios para la electrólisis del agua.
- El fotosistema híbrido In_2S_3-*Th*Lc produce fotocorrientes de hasta 50 µA/cm^2 (a 1 V *vs.* SHE) en modo de transferencia directa de electrones. El TOF del sistema para la producción de O_2 es 4.6 ± 0.1 s^{-1}, considerando la cantidad de lacasa inmovilizada en el electrodo.

6. REFERENCES

6. REFERENCES

(1) Fujishima, A.; Honda, K. (1971), Electrochemical Evidence for the Mechanism of the Primary Stage of Photosynthesis, *Bull. Chem. Soc. Japan*, 44, 1148-1150.

(2) Fujishima, A.; Honda, K. (1972), Electrochemical Photolysis of Water at a Semiconductor Electrode, *Nature*, 238, 37-38.

(3) Andreiadis, E. S.; Chavarot-Kerlidou, M.; Fontecave, M.; Artero, V. (2001), Artificial photosynthesis: from molecular catalysts for light-driven water splitting to photoelectrochemical cells, *Photochem. Photobiol*., 87, 946-964.

(4) Gust, D.; Moore, T. A., Moore, A. L. (2012), Realizing artificial photosynthesis, *Faraday discuss.*, 155, 9-26.

(5) Reisner, E. (2011), Solar hydrogen evolution with hydrogenases: From natural to hybrid systems, *Eur. J. Inorg. Chem*., 7, 1005-1016.

(6) House, R. L.; Iha, N. Y. M.; Coppo, R. L.; Alibabaei, L.; Sherman, B.D.; Kang, P.; Brennaman, M. K.; Hoertz, P. G.; Meyer, T. J.(2015), Artificial Photosynthesis: Where are we now? Where we can go?, *J. Photochem. Photobiol. C: Photochem*. Rev., 25, 32-45.

(7) Li, Z.; Luo, W.; Zhang, M.; Feng, J.; Zou, Z. (2013), Photoelectrochemical cells for solar hydrogen production: current state of promising photoelectrodes, methods to improve their properties, and outlook, *Energy Environ. Sci*., 6, 347-370.

(8) Khaselev, O.; Turner, J. (1998), A monolithic photovoltaic-photoelectrochemical device for hydrogen production via water splitting, *Science*, 280, 425-427.

(9) Park, H.; Holt, K. (2010), Recent advances in nanoelectrode architecture for photochemical hydrogen Production, *Energy Environ. Sci*., 3, 1028-1036.

(10) Caputo, C. A.; Wang, L.; Beranek, R.; Reisner, E. (2015), Carbon nitride-TiO_2 hybrid modified with hydrogenase for visible light driven hydrogen production, *Chem. Sci.,* 6, 5690−5694.

(11) Brown, K. A.; Wilker, M. B.; Boehm, M.; Dukovic, G.; King, P. W. (2012), Characterization of photochemical processes for H_2 production by CdS nanorod-[FeFe] hydrogenase complexes, *J. Am. Chem. Soc.*, 134, 5627−5636.

(12) a) Brown, K. A.; Dayal, S.; Ai, X.; Rumbles, G.; King, P. W. (2010), Controlled Assembly of Hydrogenase-CdTe Nanocrystal Hybrids for Solar Hydrogen Production, *J. Am. Chem. Soc.*, 132, 9672−9680. (b) Greene, B. L.; Joseph, C. A.; Maroney, M. J.; Dyer, R. B. (2012), Direct Evidence of Active-Site Reduction and Photodriven Catalysis in Sensitized Hydrogenase Assemblies, *J. Am. Chem*. *Soc*., 134, 11108−11111.

(13) Caputo, C. A.; Gross, M. A.; Lau, V. W.; Cavazza, C.; Lotsch, B. V.; Reisner, E. (2014), Photocatalytic hydrogen production using polymeric carbon nitride with a hydrogenase and a bioinspired synthetic Ni catalyst, *Angew. Chem., Int. Ed.*, 53, 11538−11542.

(14) Morozan, A; Bourgeteau, T.; Tondelier, D; Geffroy, B.; Jousselme, B; Artero, V. (2016), Noble metal-free hydrogen-evolving photocathodes based on small molecule organic semiconductors, *Nanotechnology*, 27, 355401-355408.

(15) Yamamoto, M.; Tanaka, K. (2016), Artificial Molecular Photosynthetic Systems: Towards Efficient Photoelectrochemical Water Oxidation, *ChemPlusChem*, 81, 1028-1044.

(16) Sprick, R. S.; Jiang, J.-X.; Bonillo, B.; Ren, S.; Ratvijitvech, T. Guiglion, P.; Zwijnenburg, M.A.; Adams, D. J.; Cooper, A. I. (2015), Tunable organic photocatalysts for visible-light-driven hydrogen evolution*, J. Am. Chem. Soc*., 137, 3265-3270.

(17) Amao, Y. (2011), Solar Fuel Production Based on the Artificial Photosynthesis System, *ChemCatChem*, 3, 458-474.

(18) Badura, A.; Esper, B.; Ataka, K.; Grunwald, C.; Woll, C.; Kuhlmann, J.; Heberle, J.; Rogner, M. (2006), Light-Driven Water Splitting for (Bio-)Hydrogen Production: Photosystem 2 as the Central Part of a Bioelectrochemical Device, *Photochem. Photobiol.*, 82, 1385-1390.

(19) Yehezkeli, O.; Tel-Vered, R.; Wasserman, J.; Trifonov, A.; Michaeli, D.; Nechushtai, R.; Willner, I. (2012), Integrated photosystem II-based photo-bioelectrochemical cells, *Nat. Commun*, 3, 742.

(20) Sokol, K.; Mersch, D.; Hartmann, V.; Zhang, J.; Nowaczyk, M.; Rogner, M.; Ruff, A.; Schuhmann, W.; Plumere, N.; Reisner, E. (2016), Rational wiring of photosystem II to hierarchical indium tin oxide electrodes using redox polymers, *Energy Environ. Sci*., 9, 3698-3709.

(21) Berg, J. M.; Tymoczko, J. L.; Stryer, L. (2002). Biochemistry, 5th edition. *New York: W H Freeman.*

(22) Vincent, K.A.; Parkin, A.; Amstrong, F. A. (2007), Investigating and exploiting the electrocatalytic properties of hydrogenases, *Chem. Rev*., 107, 4366-4413.

(23) King, P.W. (2013), Designing interfases of hydrogenase-nanomaterial hybrids for efficient solar conversion, *Biochim. Biophys. Acta*, 1827, 949-957.

(24) Lubitz, W.: Ogata, H.; Rüdiger, O.; Reijerse, E. (2014), Hydrogenases, *Chem. Rev*., 114, 4081-4148.

(25) Simmons, T. R.; Berggren, G.; Bacchi, M.; Fontecave, M., Artero, V. (2014), Mimicking hydrogenases: From biomimetics to artificial enzymes, *Coord. Chem. Rev*., 270-271, 127-150.

(26) Cracknell, J. A.; Vincent, K. A.; Armstrong, F. A. (2008), Enzymes as Working or Inspirational Electrocatalysts for Fuel Cells and Electrolysis, *Chem. Rev*., 108, 2439−2461.

(27) Fontecilla-Camps, J. C.; Volbeda, A.; Cavazza, C.; Nicolet, Y. (2007), Structure/function relationships of [NiFe]- and [FeFe]-hydrogenases, *Chem Rev*., 107, 4273-4303.

(28) De Lacey, A. L.; Hatchikian, E. C.; Volbeda, A.; Frey, M.; Fontecilla-Camps, J. C.; Fernandez, V. M. (1997), Infrared-spectroelectrochemical characterization of the [NiFe] hydrogenase of Desulfovibrio gigas, *J. Am. Chem. Soc*., 119, 7181-7189.

(29) Higuchi, Y., Ogata, H., Miki, K., Yasuoka, N., Yagi, T.(1999), Removal of the bridging ligand atom at the Ni-Fe active site of [NiFe] hydrogenase upon reduction with H_2, as revealed by X-ray structure analysis at 1.4 A resolution, *Structure Fold.Des*. 7,549-556.

(30) Shafaat, H. S.; Rüdiger, Olaf; Ogata, H.; Lubitz, W. (2013), [NiFe] hydrogenases: A common active site for hydrogen metabolism under diverse conditions, *Biochimica et Biophysica Acta*, 1827, 986–1002.

(31) Marques, M. C.; Coelho, R.; De Lacey, A. L.; Pereira, I. A.; Matias, P. M. (2010), The three-dimensional structure of [NiFeSe] hydrogenase from Desulfovibrio vulgaris Hildenborough: a hydrogenase without a bridging ligand in the active site in its oxidized, "as-isolated" state, *J. Mol. Biol*., 396, 893-907.

(32) Valente, F. M.; Oliveira, A.; Gnadt, N.; Pacheco, I.; Coelho, A.; Xavier, A.; Teixeira, M.; Soares, C.; Pereira, I. A. (2005), Hydrogenases in Desulfovibrio vulgaris Hildenborough: structural and physiologic characterization of the membrane-bound [NiFeSe] hydrogenase, *J. Biol. Inorg. Chem*., 10, 667-682.

(33) De Lacey, A. L.; Fernandez, V. M.; Rousset, M.; Cammack, R. (2007), Activation and inactivation of hydrogenase function and the catalytic cycle: spectroelectrochemical studies, *Chem. Rev.*, 107, 4304-4330.

(34) Montet, Y.; Amara, P.; Volbeda, A.; Vernede, X.; Hatchikian, E. C.; Field, M. J.; Frey, M.; Fontecilla-Camps, J. C. (1997), Gas access to the active site of Ni-Fe hydrogenases probed by X-ray crystallography and molecular dynamics*, Nat. Struct. Biol.*, 4, 523-526.

(35) Page, C. C.; Moser, C. C.; Chen, X.; Dutton, P. L. (1999), Natural engineering principles of electron tunneling in biological oxidation-reduction, *Nature*, 402, 47-52.

(36) Volbeda, A.; Charon, M.-H.; Piras, C.; Hatchikian, E. C.; Frey, M.; Fontecilla-Camps, J.C. (1995), Crystal structure of the nickel–iron hydrogenase from Desulfovibrio gigas, *Nature*, 373, 580 – 587.

(37) Rüdiger, O.; Abad, J. M.; Hatchikian, E. C.; Fernandez, V. M.; De Lacey, A. L. (2005), Oriented immobilization of Desulfovibrio gigas hydrogenase onto carbon electrodes by covalent bonds for non-mediated oxidation of H_2, *J. Am. Chem. Soc*., 127, 16008-16009.

(38) Volbeda, A.; Fontecilla-Camps, J. C.; Frey, M. (1996), Novel metal sites in protein structures, *Curr. Opin. Struct. Biol.*, 6, 804-812.

(39) Vincent, K. A.; Parkin, A.; Lenz, O.; Albracht, S. P. J.; Fontecilla-Camps, J. C.; Cammack, R.; Friedrich, B.; Armstrong, F. A. (2005), Electrochemical definitions of O_2 sensitivity and oxidative inactivation in hydrogenases, *J. Am. Chem. Soc*., 127, 18179-18189.

(40) Vincent, K. A.; Cracknell, J. A.; Lenz, O.; Zegber, I.; Friedrich, B.; Armstrong, F. A. (2005), Electrocatalytic hydrogen oxidation by an enzyme at high carbon monoxide or oxygen levels, *Proc. Natl Acad. Sci. USA*, 102, 16951-16954.

(41) Wulff, P.; Thomas, C.; Sargent, F.; Armstrong, F. A. (2016), How the oxygen tolerance of a [NiFe]-hydrogenase depends on quaternary structure, *J. Biol. Inorg. Chem*., 21, 121-134.

(42) Fritsch, J.; Lenz, O.; Friedrich, B. (2013), Structure, function and biosynthesis of O_2-tolerant hydrogenases, *Nature Reviews Microbiology*, 11, 106-114.

(43) Ciaccafava, A.; Hamon, C.; Infossi, P.; Marchi, V.; Giudici-Orticoni, M.-T.; Lojou, E. (2013), Light-induced reactivation of O_2-tolerant membrane-bound [Ni-Fe] hydrogenase from the hyperthermophilic bacterium *Aquifex aeolicus* under turnover conditions, *Phys.Chem.Chem.Phys*, 15, 16463-16467.

(44) Gutiérrez-Sánchez, C.; Rüdiger, O.; Fernández, V. M.; De Lacey, A. L.; Marques, M.; Pereira, I. A. C. (2010), Interaction of the active site of the Ni-Fe-Se hydrogenase from Desulfovibrio vulgaris Hildenborough with carbon monoxide and oxygen inhibitors, *J Biol Inorg Chem* 15, 1285–1292.

(45) Parkin, A.; Goldet, G.; Cavazza, C.; Fontecilla-Camps, J. C.; Armstrong, F. A. (2008), The difference a Se makes? Oxygen-tolerant hydrogen production by the [NiFeSe]-hydrogenase from Desulfomicrobium baculatum, *J. Am. Chem. Soc*., 130, 13410-13416.

(46) Yaropolov, A. I.; Skorobogat'ko, O. V.; Vartanov, S. S.; Varfolomeyev, S. D. (1994), Laccase-Properties, catalytic mechanism, and applicability, *Appl. Biochem. Biotechnol*., 49, 257-280.

(47) Solomon, E. I.; Sundaram, U. M.; Machonkin, T. E. (1996), Multicooper Oxidases and Oxygenases, *Chem. Rev.,* 96, 2563-2606.

(48) Givaudan, A.; Effosse, A.; Faure, D.; Potier, P.; Boulliant, M. L.; Bally, R. (1993), Polyphenol oxidase in Azospirillum lipoferum isolated from rice rhizosphere: Evidence for laccase activity in non-motile strains of Azospirillum lipoferum, *FEMS Microbiol. Lett*., 108, 205-210.

(49) Barrett, F. M.; Andersen, S. O. (1981), Phenoloxidases in larval cuticle of the blowfly, Calliphora vicina*, Insect Biochemistry*, 11, 17-23.

(50) Blaich, R.; Esser, K. (1975), Function of enzymes in wood destroying fungi. II. Multiple forms of laccase in white rot fungi, *Arch. Microbiol*., 103, 271-277.

(51) Eggert, C.; Temp, U.; Dean, J. F.; Eriksson, K. E. (1995), Laccase-mediated formation of the phenoxazinone derivate cinnabarinic acid, *FEBS Lett*., 376, 202-206.

(52) Galhaup, C.; Haltrich, D. (2001), Enhanced formation of laccase activity by the white-rot fungus *Trametes pubescens* in the presence of copper, *Appl. Microbiol. Biotechnol*., 56, 225-232.

(53) Morozova, O. V.; Shumakovich, G.P.; Gorbacheva, M. A.; Shleev, S. V.; Yaropolov, A. I. (2007), "Blue" laccases, *Biochemistry (Moskow)*, 72, 1136-1150.

(54) Solomon, E. I.; Augustine, A. J.; Yoon, J. (2008), O_2 Reduction to H_2O by the Multicopper Oxidases, *Dalton Trans*., 3921-3932.

(55) Tsujimura, S.; Kamitaka, Y.; Kano, K. (2007) Diffusion-Controlled Oxygen Reduction on Multi-Copper Oxidase-Adsorbed Carbon Aerogel Electrodes without Mediator, *Fuel Cells*, 7, 463-469.

(56) Blanford, C. F.; Foster, C. E.; Heath, R. S.; Armstrong, F. A. (2008) Efficient electrocatalytic oxygen reduction by the 'blue' copper oxidase, laccase, directly attached to chemically modified carbons, *Faraday Discuss*., 140, 319-335.

(57) Pita, M.; Mate, D. M.; Gonzalez-Perez, D.; Shleev, S.; Fernandez, V. M.; Alcalde, M.; De Lacey, A. L. (2014), Bioelectrochemical Oxidation of Water, *J. Am. Chem. Soc.*, 136, 5892-5895.

(58) Shleev, S.; Andoralov, V.; Pankatrov, D.; Falk, M.; Aleksejeva, O.; Blum, S. (2016), Oxygen Electroreduction versus Bioelectroreduction: Direct Electron Transfer Approach, *Electroanalysis*, 28, 2270-2287.

(59) Shleev, S.; Pita, M.; Yaropolov, A. I.; Ruzgas, T.; Gorton, L. (2006), Direct heterogeneous electron transfer reactions of *Trametes hirsuta* laccase at bare and thiol-modified gold electrodes, *Electroanalysis*, 18, 1901-1908.

(60) Di Bari, C.; Goni-Urtiaga, A.; Pita, M.; Shleev, S.; Toscano, M. D.; Sainz, R.; De Lacey, A. L. (2016), Fabrication of high surface area graphene electrodes with high performance towards enzymatic oxygen reduction, *Electrochim. Acta*, 191, 500-509.

(61) Vaz-Dominguez, C.; Campuzano, S.; Rüdiger, O; Pita, M.; Gorbacheva, M.; Shleev, S.; Fernandez, V. M.; De Lacey, A. L. (2008), Laccase electrode for direct electrocatalytic reduction of O_2 to H_2O with high-operational stability and resistance to chloride inhibition, *Biosens. Bioelectron*., 24, 531-537.

(62) Shleev, S. V.; Morozova, O. V.; Nikitina, O. V.; Gorshina, E. S.; Rusinova, T. V.; Serezhenkov, V. A., Burbaev, D. S:, Gazaryan, I. G.; Yaropolov, A. I. (2004), Comparison of physico-chemical characteristics of four laccases from different basidiomycetes, *Biochimie*, 86, 693-703.

(63) Barber, J.; Tran, P. D. (2013), From natural to artificial photosynthesis., *J. R. Soc. Interface*, 10, 20120984.

(64) Neamen, D. A. (2003), Semiconductor physics and devices: basic principles, *McGraw-Hill*.

(65) Babu, V. S. (2010), Solid State Devices and Technology, 3rd Edition. *Peason*.

(66) Gueymard, C. (2004), The suns total and spectral irradiance for solar energy applications and solar radiation models, *Solar Energy*, 423–453.

(67) Gibson, J. H. (2000). UVB Radiation: Definition and Characteristics. In UV-B Monitoring and Research Program.

Retrieved from http://uvb.nrel.colostate.edu/UVB/publications/uvb_primer.pdf.

(68) Li, X.; Yu, J.; Low, J.; Fang, Y.; Xiao, J.; Chen, X. J. (2015), Engineering heterogeneous semiconductors for solar water splitting, *Mater. Chem. A*, 3, 2485-2534.

(69) Lewis, N. S.; Nocera, D. G. (2006), Powering the planet: Chemical challenges in solar energy utilization, *Proc. Natl. Acad. Sci. U.S.A.,* 103, 15729-15735.

(70) Lewis, N. S. (2016), Research opportunities to advance solar energy utilization, *Science*, 351, 353-362.

(71) Babu, V. J.; Vempati, S.; Uyar, T.; Ramkrishna, S. (2015), Review of one-dimensional and two-dimensional nanostructured materials for hydrogen generation, *Phys. Chem. Chem. Phys.* , 17, 2960-2986.

(72) Kubacka, A.; Fernández-García, M.; Colón, G. (2012), Advanced Nanoarchitectures for Solar Photocatalytic Applications, *Chem. Rev.*, 112, 1555-1614.

(73) Sivula, K.; Van de Krol, R. (2016), Semiconducting materials for photoelectrochemical energy conversion, *Nat. Rev. Materials*, 1, 15010.

(74) Fondriest Environmental, Inc. “Solar Radiation and Photosynethically Active Radiation.” Fundamentals of Environmental Measurements. 21 Mar. 2014.

(75) Xu, Y.; Schoonen, M. A. A. (2000), The absolute energy positions of conduction and valence bands of selected semiconducting minerals, *Am. Mineralogist*, 85, 543-556.

(76) Sparkes, J.J. (1966), Junction transistors, *The Commonwealth and International Library.*

(77) Cardon, F; Gomes, W. P. (1978), On the determination of the flat-band potential of a semiconductor in contact with a metal or an electrolyte from the Mott-Schottky plot, *J. Phys. D: Appl. Phys*., 11, 63-67.

(78) Uosaki, K.; Kita, H. (1983), Effects of the Helmholtz Layer Capacitance on the Potential Distribution at Semiconductor/Electrolyte Interface and the Linearity of the Mott-Schottky Plot, *J. Electrochem. Soc*., 130, 895-897.

(79) Bakke, J. R.; Pickrahn, K. L.; Brennan, T. P.; Bent, S. F. (2011), Nanoengineering and Interfacial Engineering of Photovoltaics by Atomic Layer Deposition, *Nanoscale*, 3, 3482−3508.

(80) Mughal, M. A.; Engelken, R.; Sharma, R. (2015), Progress in indium (III) sulfide (In_2S_3) buffer layer deposition techniques for CIS, CIGS, and CdTe-based thin film solar cells, *Sol. Energy*, 120, 131−146.

(81) Hariskos, D.; Spiering, S.; Powalla, M. (2005), Buffer layers in Cu(In,Ga)Se_2 solar cells and modules, *Thin Solid Films*, 480−481, 99−109.

(82) Spiering, S.; Hariskos, D.; Powalla, M.; Naghavi, N.; Lincot, D. (2003), CD-free Cu(In,Ga)Se_2 thin-film solar modules with In_2S_3 buffer layer by ALCVD, *Thin Solid Films*, 431-432, 359−363.

(83) Jiang, F.; Gunawan; Harada, T.; Kuang, Y.; Minegishi, T.; Domen, K.; Ikeda, S. (2015), Pt/In_2S_3/CdS/Cu_2ZnSnS_4 Thin Film as an Efficient and Stable Photocathode for Water Reduction under Sunlight Radiation, *J. Am. Chem. Soc*., 137, 13691−13697.

(84) Reich, F.; Richter, T. (1863), Vorläufige Notiz über ein neues Metall, *J. Prakt. Chem*., 89, 441–448.

(85) Chai, B.; Peng, T.; Zeng, P.; Mao, J. (2011), Synthesis of Floriated In_2S_3 Decorated With TiO_2 Nanoparticles for Photocatalytic Hydrogen Production Under Visible Light, *J. Mater. Chem*., 21, 14587-14593.

(86) Becker, R. S.; Zheng, T.; Elton, J.; Saeki, M. (1986), Synthesis and photoelectrochemistry of In_2S_3, *Sol. Energ. Mat*., 13, 97-107.

(87) Tapia, C.; Berglund, S. P.; Friedrich, D.: Dittrich, T.; Bogdanoff, P.; Liu, Y.; Levcenko, S.; Unold, T.; Conesa, J. C.; De Lacey, A. L.; Pita, M.; Fiechter, S. (2016), Synthesis and Characterization of V-Doped β-In_2S_3 Thin Films on FTO Substrates, *J. Phys. Chem. C*., 120, 289753-28761.

(88) An, L.; Zhou, P.; Yin, J.; Chen, F.; Liu, H.; Du, Y.; Xi, P. (2015), Phase Transformation Fabrication of a Cu_2S Nanoplate as an Efficient Catalyst for Water Oxidation with Glycine, *Inorg. Chem.*, 54, 3281-3289.

(89) Balzani, V. (2001), Electron transfer in chemistry, *WILEY-YCH Verlag GmbH & Co*.

(90) Bartlett, P. N. (2008), Bioelectrochemistry. Fundamentals, Experimental Tehniques and Applications, *John Wiley & Sons Ltd*.

(91) Kuznetsov, A. M.; Ulstrup, J. (1999), Electron transfer in chemistry and biology. An introduction to the theory, *John Wiley & Sons Ltd*.

(92) Bard, A. J.; Faulkner, L. R. (2001), Electrochemical methods: fundamentals and applications, 2nd ed., *Wiley*.

(93) Pita, M; De Lacey, A. L. (2012) "Métodos Electroanalíticos." Faraldos, M; Goberna, C. "Técnicas de Análisis y Caracterización de Materiales", 2nd Ed., *Publicaciones del CSIC, Madrid, España*.

(94) Helmholtz, H. (1853), In Annalen der Physik, 165, 211-233.

(95) Marcus, R. A.; Sutin, N. (1985), Electron transfers in chemistry and biology, *Biocim. Biophys. Acta, Rev. Bioenergy*, 811, 265-322.

(96) Marcus, R. A. (1993), Electron transfer reactions in chemistry: Theory and Experiment (Nobel Lecture)*, Angew. Chem. Int. Ed. in English*, 32, 1111-1121.

(97) Bond, A. M. (1994), Chemical and Electrochemical Approaches to the Investigations of Redox Reactions of Simple Electron Transfer Metaloproteins, *Inorg. Chim. Acta*, 226, 293-340.

(98) Jeuken, L. J. C. (2003), Conformational reorganization interfacial protein electron transfer, *Biochim. Biophys. Acta, Bioenerg*. 1604, 67-76.

(99) Léger, C.; Bertrand, P. (2008), Direct Electrochemistry of Redox Enzymes as a Tool for Mechanistic Studies, *Chem. Rev*., 108, 2379-2438.

(100) Ferapontova, E.E.; Shleev, S; Ruzgas, T.; Stoica, L.; Christenson, A.; Tkac, J.; Yaropolov, A. I.; Gorton, L. (2005), Perspectives in Bioanalysis, *Elsevier*, 1, 517-598.

(101) Ghazi, I.; Gómez De Segura, A.; Fernández-Arrojo, L.; Alcalde, M.; Yates, M.; Rojas-Cervantes, M. L., Plou, F. J.; Ballesteros, A. (2005), Immobilization of fructosyltransferase from Aspergillus aculeatus on epoxy-activated Sepabeads EC for the synthesis of fructo-oligosaccharides, *J. Mol. Catal. B: Enzym*., 35, 19-27.

(102) Grazú, V.; López-Gallego, F.; Montes, T.; Abian, O.; González, R.; Hermoso, J. A.; García, J. L.; Mateo, C.; Guisán, J. M. (2010), Promotion of multipoint covalent immobilization through different regions of genetically modified penicillin G acylase from E. coli, *Process Biochem*. 45, 390-398.

(103) Gooding, J. J.; Mearns, F.; Yang, W.; Liu, J. (2003), Self-assembled monolayers into the 21st century: Recent advances and applications, *Electroanalysis*, 15, 81-96.

(104) Ihs, A.; Liebberg, B. (1994), Infrared stud of ethyl and octyl xanthate ions adsorbed on metallic and sulfidized copper and silver surfaces, *Langmuir*, 10, 734-740.

(105) Shimazu, K.; Yagi, I.; Sato, Y.; Uosaki, K. (1994), Electrochemical quartz crystal microbalance studies of self-assembled monolayers of 11-ferrocenyl-1-undecanethiol: Structure-dependent ion-pairing and solvent uptake, *J. Electroanal. Chem.*, 372, 117-124.

(106) Laibinis, P. E.; Whitesides, G. M. (1992), ω-Terminated alkanethiolate monolayers on surfaces of cooper, silver, and gold have similar wettabilities, *J. Am. Chem. Soc*., 114, 1990-1995.

(107) Stratmann, M. (1990), Chemically modified metal surfaces – A new class of composite materials, *Adv. Mater*., 2, 191-195.

(108) Delamar, M.; Hitmi, R.; Pinson, J.; Savéant, J. M. (1992), Covalent modification of carbon surfaces by grafting of functionalized aryl radicals produced from electrochemical reduction of diazonium salts, *J. Am. Chem. Soc*., 114, 5883-5884.

(109) Allongue, P.; Delamar, M.; Desbat, B.; Fagebaume, O.; Hitmi, R.; Pinson, J.; Savéant, J. M. (1997), Covalent modification of carbon surfaces by aryl radicals generated from the electrochemical reduction of diazonium salts, *J. Am. Chem. Soc*., 119, 201-207.

(110) Heller, A. (2006), Electron-conducting redox hydrogels: design, characteristics and synthesis, *Current Opinion in Chemical Biology*, 10, 664-672.

(111) Aoki, A.; Heller, A. (1993), Electron Diffusion Coefficients in Hydrogels Formed of Cross-Linked Redox Polymers, *J. Phys. Chem*., 97, 11014-11019.

(112) Efrati, A.; Lu, C.; Michaeli, D.; Nechushtai, S.; Alsoub, S.; Schuhmann, W.; Willner, I. (2016), Assembly of photo-bioelectrochemical cells using photosystem I-functionalized electrodes, *Nat. Energy*, 1, 15021.

(113) Badura, A.; Guschin, D.; Kothe, T.; Kopezak, M. J.; Schuhmann, W.; Rögner, M. (2011), Photocurrent generation by photosystem 1 integrated in crosslinked redox hydrogels, *Energy Environ. Sci*., 4, 2435-2440.

(114) Kothe, T.; Plumeré, N.; Badura, A.; Nowaczyk, M. M.; Guschin, D. A.; Rögner, M.; Schuhmann, W. (2013), Combination of A Photosystem 1-Based Photocathode and a Photosystem 2-Based Photoanode to a Z-Scheme Mimic for Biophotovoltaic Applications, *Angew. Chem. Int. Ed*., 52, 14233-14236.

(115) Zhao, F.; Conzuelo, F.; Hartmann, V.; Li, H.; Nowaczyk, M.; Plumere, N.; Rögner, M.; Schuhmann, W. (2015), Light Induced H_2 Evolution from a Biophotocathode Based on Photosystem 1 − Pt Nanoparticles Complexes Integrated in Solvated Redox Polymers Films, *J. Phys. Chem. B*, 119, 13726-13731.

(116) Barriere, F; Ferry, Y; Rochefort, D.; Leech, D. (2004), Targetting redox polymers as mediators for laccase oxygen reduction in a membrane-less biofuel cell, *Electrochemistry Communications*, 6, 237–241.

(117) Tasca, F.; Timur, S.; Ludwig, R.; Haltrich, D.; Volc, J.; Antiochia, R.; Gorton, L. (2007), Amperometric Biosensors for Detection of Sugars Based on the Electrical Wiring of Different Pyranose Oxidases and Pyranose Dehydrogenases with Osmium Redox Polymer on Graphite Electrodes, *Electroanalysis*, 19, 294-302.

(118) Albertsson, P.-A.; Andreasson, E.; Svensson, P. (1990), The domain organization of the plant thylakoid membrane, *FEBS Letters*, 273, 36-40.

(119) Danielsson, R.; Albertsson, P.-A. (2009), Fragmentation and separation analysis of the photosynthetic membrane from spinach, *Biochimica et Biophysica Acta*, 1787, 25–36.

(120) Arnon, D. I. (1948), Localization of Polyphenoloxidase in the Chloroplasts of Beta Vulgaris, *Nature*, 162, 341-342.

(121) Cammack, R.; Fernandez, V. M.; Hatchikian, E. C. (1994), Nickel-iron hydrogenase, *Methods Enzymol*., 243, 43-68.

(122) Marques, M. C.; Tapia, C.; Gutiérrez-Sanz, O.; Ramos, A. R.; Keller, K. L.; Wall, J. D.; De Lacey, A. L.; Matias, P. M.; Pereira, I. A. C. (2017), The direct role of selenocysteine in [NiFeSe] hydrogenase maturation and catalysis, *Nat. Chem. Bio*., 13, 544-550.

(123) Najafpour, M.; Ghobadi, M.; Larkum, A.; Shen, J.; Allahkhverdiev, S. (2015), The biological wateroxidizing complex at the nano–bio interface, *Trends Plant Sci.*, 20, 559-568.

(124) Bradford, M.M. (1976), A Rapid and Sensitive Method for the Quantitation of Microgram Quantities of Protein Utilizing the Principle of Protein-Dye Binding, *Anal. Biochem*., 72, 248−254.

(125) Lucena, R.; Aguilera, I.; Palacios, P.; Wahnón, P.; Conesa, J. C. (2008), Synthesis and Spectral Properties of Nanocrystalline V-Substituted In_2S_3, a Novel Material for More Efficient Use of Solar Radiation, *Chem. Mater.*, 20, 5125−5127.

(126) Zafar, M. N.; Tasca, F.; Boland, S.; Kujawa, M.; Patel, I.; Peterbauer, C. K.; Leech, D.; Gorton, L. (2010), Wiring of pyranose dehydrogenase with osmium polymers of different redox potentials, *Bioelectrochemistry*, 80, 38-42.

(127) Meredith, M. T.; Kao, D. Y.; Hickey, D.; Schmidtke, D. W.; Glatzhofer, D. T. (2011), High Current Density Ferrocene-Modified Linear Poly(ethylenimine) Bioanodes and Their Use in Biofuel Cells, *J. Electrochem. Soc.*, 158, B166-B174.

(128) Tapia, C.; Milton, R. D.; Pankratova, G.; Minteer, S. D.; Åkerlund, H.-E.; Leech, D.; De Lacey, A. L.; Pita, M.; Gorton, L. (2017), Wiring of Photosystem I and Hydrogenase on an Electrode for Photoelectrochemical H_2 Production by using Redox Polymers for Relatively Positive Onset Potential, *ChemElectroChem,* 4, 90 – 95.

(129) (a) Vignais, P. M.; Cournac, L.; Hatchikian, E. C.; Elsen, S.; Serebryakova, S.; , Zorin, N.; Dimon, B. (2002), Continuous monitoring of the activation and activity of [NiFe]-hydrogenases by membrane-inlet mass spectrometry, *International Journal of Hydrogen Energy*, 27, 1441-1448. (b) Jouanneau, Y.; Kelley, B. C.; Berlier, Y.; Lespinat, P. A.; Vignais, P. M (1980),Continuous Monitoring, by Mass Spectrometry, of H_2 Production and Recycling in *Rhodopseudomonas capsulata , J. Bacteriol.,* 143, 628-636.

(130) Gupta, G.; Rajendran, V.; Atanassov, P. (2004), Bioelectrocatalysis of oxygen reduction reaction by laccase on gold electrode, *Electroanalysis*, 16, 1182-1185.

(131) Pita, M.; Shleev, S.; Ruzgas, T.; Fernandez, V. M.; Yaropolov, A. I.; Gorton, L. (2006), Direct Heterogeneous Electron Transfer Reactions of Fungal Laccases at Bare and Thiol-Modified Gold Electrodes, *Electrochem. Commun*., 8, 747–753.

(132) Timura, S; Yigzawa, Y.; Gorton, L. (2006), Electrical wiring of pyranose oxidase with osmium redox polymers, *Sensors and Actuators B,* 113, 684–691.

(133) Kavanagh, P.; Leech, D. (2006), Redox Polymer and Probe DNA Tethered to Gold Electrodes for Enzyme-Amplified Amperometric Detection of DNA Hybridization, *Anal. Chem.*, 78, 2710-2716.

(134) Coman, V.; Gustavsson, T.; Finkelsteinas, A.; von Wachenfeldt, C.; Hägerhäll, C.; Gorton, L. (2009), Electrical Wiring of Live, Metabolically Enhanced Bacillus subtilis Cells with Flexible Osmium-Redox Polymers, *J. Am. Chem. Soc*., 131, 16171–16176.

(135) Timura, S.; Haghighia, B.; Tkaca, J.; Pazarlıoğlub, N.; Telefoncu, A.; Gorton, L. (2007), Electrical wiring of Pseudomonas putida and Pseudomonas fluorescens with osmium redox polymers, *Bioelectrochemistry,* 71, 38–45.

(136) Hamidi, H.; Hasan, K.; Emek, S. C.; Dilgin, Y.; Åkerlund, H.-E.; Albertsson, P.-Å.; Leech, D.; Gorton, L. (2015) Photocurrent Generation from Thylakoid Membranes on Osmium-Redox-Polymer-Modified Electrodes, *ChemSusChem*, 8,990 –993.

(137) Badura, A.; Guschin, D.; Esper, B.; Kothe, T.; Neugebauer, S.; Schuhmann, W.; Rögner, M. (2008), Photo-Induced Electron Transfer Between Photosystem 2 via Cross-linked Redox Hydrogels, *Electroanalysis 20*, 10, 1043 – 1047.

(138) Plumeré, N.; Rüdiger, O.; Oughli, A. A.; Williams, R.; Vivekananthan, J.; Pöller, S.; Schuhmann, W.; Lubitz, W. (2014), A redox hydrogel protects hydrogenase from high-potential deactivation and oxygen damage, *Nat. Chem.*, 6, 822-827.

(139) De Lacey, A. L.; Moiroux, J.; Bourdillon, C. (2000), Simple formal kinetics for the reversible uptake of molecular hydrogen by [Ni-Fe] hydrogenase from Desulfovibrio gigas, *Eur. J. Biochem*., 267, 6560-6570.

(140) Eng, L. H.; Elmgren, M.; Komlos, P.; Nordling, M.; Lindquist, S.; Neujahr, H. Y. (1994), Viologen-Based Redox Polymer for Contacting the Low-Potential Redox Enzyme Hydrogenase at an Electrode Surface, *J. Phys. Chem.*, 98, 7068-7072.

(141) Gizzie, E. A.; LeBlanc, G.; Jennings, G. K.; Cliffel, D. E. (2015) Electrochemical Preparation of Photosystem I−Polyaniline Composite Films for Biohybrid Solar Energy Conversion, *ACS Appl. Mater. Interfaces*, 7, 9328−9335.

(142) Reisner, E.; Fontecilla-Camps, J.C.; Armstrong, F.A. (2009), Catalytic electrochemistry of a [NiFeSe]-hydrogenase on TiO_2 and demonstration of its suitability for visible-light driven H_2 production, *Chem Commun.,* 5, 550-552.

(143) De Lacey, A. L.; Gutiérrez-Sánchez, C.; Fernández, V. M.; Pacheco, I.; Pereira, I. A. C. (2008), FTIR spectroelectrochemical characterization of the Ni–Fe–Se hydrogenase from *Desulfovibrio vulgaris* Hildenborough, *J. Biol. Inorg. Chem*., 13, 1315–1320.

(144) Gutierrez-Sanchez, C.; Olea, D.; Marques, M.; Fernandez, V. M.; Pereira, I. A. C.; Velez, M.; De Lacey, A. L. (2011), Oriented Immobilization of a Membrane-Bound Hydrogenase onto an Electrode for Direct Electron Transfer, *Langmuir*, 27, 6449–6457.

(145) Lucena, R.; Conesa, J. C.; Aguilera, I.; Palacios, P.; Wahnón, P. (2014), V-substituted In_2S_3: an intermediate band material with photocatalytic activity in the whole visible light range, *J. Mater. Chem. A,* 2, 8236−8245.

(146) Lucena, R.; Fresno, F.; Conesa, J. C. (2012), Spectral response and stability of In_2S_3 as Visible Light-active Photocatalyst, *Catal. Commun.,* 20, 1−5.

(147) Kambas, K.; Anagnostopoulos, A.; Ves, S.; Ploss, B.; Spyridelis, J. (1985), Optical Absorption Edge Investigation of $CdIn_2S_4$ and β-In_2S_3 Compounds, *J. Phys. Status Solidi B*, 127, 201−208.

(148) Bryant, M. A.; Crooks, R. M. (1993), Determination of surface pKa values of surface-confined molecules derivatized with pH-sensitive pendant groups, *Langmuir*, 9, 385−387.

(149) Smith, C. P.; White, H. S. (1993), Voltammetry of molecular films containing acid/base groups, *Langmuir*, 9, 1−3.

(150) Marques, M.; Coelho, R.; Pereira, I. A. C.; Matias, P. M. (2013), Redox state-dependent changes in the crystal structure of [NiFeSe] hydrogenase from Desulfovibrio vulgaris Hildenborough*, International journal of hydrogen energy,* 38, 8664-8682.

(151) Gutiérrez-Sanz, O.; Tapia, C.; Marques, M.; Zacarias, S.; Vélez, M.; Pereira, I. A. C.; De Lacey, A. L. (2015) Induction of a Proton Gradient across a Gold-Supported Biomimetic Membrane by Electroenzymatic H_2 Oxidation, *Angew. Chem. Int. Ed.*, 54, 2684 –2687.

(152) Jones, A. K.; Lamle, S. E.; Pershad, H. R.; Vincent, K. A.; Albracht, S. P.; Armstrong, F. A. (2003), Enzyme electrokinetics: electrochemical studies of the anaerobic interconversions between active and inactive states of Allochromatium vinosum [NiFe]-hydrogenase, *J. Am. Chem. Soc*., 125, 8505-8514.

(153) Gutierrez-Sanchez, C. (2012), Estrategias de inmovilización de metaloenzimas redox de forma orientada y estable sobre electrodos nanoestructurados, *Tesis Doctoral*.

(154) Zhang, K.; Guo, L. (2013), Metal sulphide semiconductors for photocatalytic hydrogen production, *Catal. Sci. Technol*., 3, 1672−1690.

(155) Grande, H. J.; Van Berkel-Arts, A.; Bregh, J.; Van Dijk, K.;Veeger, C. (1983), Kinetic properties of hydrogenase isolated from Desulfovibrio vulgaris (Hildenborough), *Eur. J. Biochem*., 131, 81−88.

(156) De Lacey, A. L.; Detcheverry, M.; Moiroux, J.; Bourdillon, C. (2000), Construction of multicomponent catalytic films based on avidin-biotin technology for the electroenzymatic oxidation of molecular hydrogen, *Biotechnol. Bioeng*., 68, 1−10.

(157) Reisner, E.; Powell, D. J.; Cavazza, C.; Fontecilla-Camps, J. C.; Armstrong, F. A. (2009), Visible Light-Driven H_2 Production by Hydrogenases Attached to Dye-Sensitized TiO_2 Nanoparticles, *J. Am. Chem. Soc.*, 131, 18457−18466.

(158) Herrasti, P.; Fatas, E.; Herrero, J.; Ortega, J. (1990), Determination of the flat band potential for In_2S_3/electrolyte interfaces, *Electrohimica Acta,* 35, 345-349.

(159) Bachmeier, A.; Armstrong, F. (2015), Solar-driven proton and carbon dioxide reduction to fuels—lessons from metalloenzymes, *Curr. Opin. Chem. Biol.*, 25, 141−151.

(160) Hexter, S. V.; Esterle, T. F.; Armstrong, F. A. (2014), A unified model for surface electrocatalysis based on observations with enzymes, *Phys. Chem. Chem. Phys*., 16, 11822−11833.

(161) Smith, W. A. Photoelectrochemical Cell Design, Efficiency, Definitions, Standards, and Protocols. Giménez, S.; Bisquert, J. (Eds.) Photoelectrochemical Solar Fuel Production, From Basic Principles to Advanced Devices. (2016) *Springer*.

(162) Tapia, C.; Zacarias, S.; Pereira, I. A. C.; Conesa, J. C.; Pita, M.; De Lacey, A. L. (2016) In Situ Determination of Photobioproduction of H_2 by In_2S_3-[NiFeSe] Hydrogenase from Desulfovibrio vulgaris Hildenborough Using Only Visible Light, *ACS Catalysis*, 6, 5691-5698.

(163) Plyakov, K. M.; Federova, T. V.; Stepanova, E. V.; Cherkashin, E. A.; Kurzeev, S. A.; Strokopytov, B. V., Lamzin, V. S.; Koroleva, O. V. (2009), Structure of native laccase from Trametes hirsuta at 1.8 A resolution, *Acta Crystallogr*., 65, 611-617.

(164) Chen, Z.; Meyer, T. (2013), Copper(II) Catalysis of Water Oxidation, *Angew. Chem. Int. Ed.*, 52, 700-703.

(165) Skorupska, K.; Lewerenz, H. J.; Berzal, P. U.; Rutkowska, I.A.; Kulesza, P. J. (2012), A semiconductor–enzyme photoelectrode for oxygen reduction by direct transfer of photo-generated electrons to laccase, *J. Mater. Chem.*, 22, 15267-15274.

(166) Alibabaei, L.; Sherman, B.; Norris, M.; Brennaman, M.; Meyer, T. (2015), Visible photoelectrochemical water splitting into H_2 and O_2 in a dye-sensitized photoelectrosynthesis cell, *Proc. Natl. Acad. Sci. USA*, 112, 5899-5902.

(167) Kato, M.; Cardona, T.; Rutherford, A.; Reisner, E. (2013), Covalent Immobilization of Oriented Photosystem II on a Nanostructured Electrode for Solar Water Oxidation, *J. Am. Chem. Soc.*, 135, 10610-10613.

7. PUBLICATIONS

Enzymatic Electrodes

DOI: 10.1002/anie.201411182

Induction of a Proton Gradient across a Gold-Supported Biomimetic Membrane by Electroenzymatic H_2 Oxidation**

*Óscar Gutiérrez-Sanz, Cristina Tapia, Marta C. Marques, Sonia Zacarias, Marisela Vélez, Inês A. C. Pereira, and Antonio L. De Lacey**

Dedicated to Professor V. M. Fernandez on the occasion of his 70th birthday

Abstract: *Energy-transduction mechanisms in living organisms, such as photosynthesis and respiration, store light and chemical energy in the form of an electrochemical gradient created across a lipid bilayer. Herein we show that the proton concentration at an electrode/phospholipid-bilayer interface can be controlled and monitored electrochemically by immobilizing a membrane-bound hydrogenase. Thus, the energy derived from the electroenzymatic oxidation of H_2 can be used to generate a proton gradient across the supported biomimetic membrane.*

In many cases, human society has progressed technologically by observing nature and copying its strategies, which have developed during millions of years of evolution. In the last two decades, the specificity and high turnover of enzymes under mild conditions has inspired the development of new catalysts.[1] Furthermore, many industrial processes use biocatalytic routes based on enzyme activity.[2] In a similar way, the field of bionanoelectronics has emerged for interfacing biological systems with artificial electronic structures with the aim of establishing communication between them in both directions.[3] The combination of biology, electrochemistry, and nanotechnology provides potential alternative and innovative solutions to the challenges in various fields (i.e. medicine, analytical chemistry, alternative energies, materials development).

Energy-transduction mechanisms in living organisms, such as photosynthesis and respiration, store light and chemical energy in the form of an electrochemical gradient created across a lipid bilayer, as described by the chemiosmotic theory proposed by Mitchell and Moyle.[4] Model membranes can be stably formed over conductor surfaces for the study of biological systems and potential biotechnological applications.[5] Adequate tailoring of the conductor surface and biomimetic membrane formation enables the incorporation of membrane-bound enzymes that maintain their functionality.[6]

Herein we show that a modified surface, in which a hydrogenase is immobilized between a phospholipid bilayer and a gold electrode, permits the storage of energy produced by electrochemically driven H_2 consumption in a proton gradient across the supported membrane; this proton gradient can be monitored electrochemically. For this purpose we used two strategies developed in our laboratory: a) the oriented and functional immobilization of the membrane-bound NiFeSe hydrogenase from *Desulfovibrio vulgaris* Hildenborough (*Dv*-SeHase) onto a gold electrode with a phospholipid bilayer (PhBL) on top[7] and b) monitoring of the proton concentration at a phospholipid-bilayer/electrode interface by an immobilized redox probe.[8]

The structural and catalytic characteristics of the *Dv*-SeHase make this enzyme ideal for our purpose. First, this hydrogenase has a lipid tail in the opposite region to the distal iron–sulfur cluster ([4Fe4S]),[9] which is the redox site for electron transfer with the electrode. The distal [4Fe4S] cluster is surrounded by negatively charged amino acids that enable enzyme orientation by electrostatic interactions with the partially protonated self-assembled monolayer (SAM) of 4-aminothiophenol (4-ATP) on the electrode, followed by covalent binding,[10] and the lipid tail enables the formation of a biomimetic bilayer on top.[7] Figure 1a is a schematic representation of the configuration of this biomimetic construction. Second, like hydrogenases, *Dv*-SeHase catalyzes reversibly the oxidation of molecular hydrogen to protons. In particular, NiFeSe hydrogenases have been shown to tolerate the presence of O_2 (a common inhibitor of many hydrogenases) during H_2-production activity when immobilized on electrodes or semiconductors.[11]

Figure 2 shows the chronoamperometric measurement of the H_2-production activity of the Au/4-ATP/*Dv*-SeHase/PhBL electrode. A stable cathodic current was measured at −340 mV owing to direct electron transfer to the enzyme and its proton-reduction activity.[10] Upon the addition of O_2 (20 μM), an immediate increase in the negative current was observed as a result of the direct reduction of O_2 at the electrode;[11a] however, after 5–6 min, the initial catalytic current level of H_2 production was recovered owing to the linear diffusion limitation of oxygen transport towards the electrode and to equilibration of the solution with the N_2 atmosphere. The subsequent addition of CO (20 μM; also

[*] Ó. Gutiérrez-Sanz, C. Tapia, Dr. M. Vélez, Dr. A. L. De Lacey
Instituto de Catáisis y Petroleoquímica, CSIC
c/ Marie Curie 2, 28049 Madrid (Spain)
E-mail: alopez@icp.csic.es

M. C. Marques, S. Zacarias, Dr. I. A. C. Pereira
Instituto de Tecnologia Quimica e Biologica
Universidade Nova de Lisboa
Apartado 127, 2781-901 Oeiras (Portugal)

[**] This research was funded by the Spanish MINECO (project CTQ2012-32448) and by the Fundação para a Ciência e a Tecnologia (project PTDC/BBB-BEP/0934/2012). O.G.-S. thanks MINECO for an FPI grant.

Supporting information for this article is available on the WWW under http://dx.doi.org/10.1002/anie.201411182.

ACS Catalysis

Research Article

pubs.acs.org/acscatalysis

In Situ Determination of Photobioproduction of H_2 by In_2S_3-[NiFeSe] Hydrogenase from *Desulfovibrio vulgaris* Hildenborough Using Only Visible Light

Cristina Tapia,[†] Sonia Zacarias,[‡] Inês A. C. Pereira,[‡] Jose C. Conesa,[†] Marcos Pita,*[,†] and Antonio L. De Lacey*[,†]

[†]Instituto de Catálisis y Petroleoquímica, CSIC, c/Marie Curie 2, 28049 Madrid, Spain

[‡]Instituto de Tecnologia Quimica e Biologica, Universidade Nova de Lisboa, Apartado 127, 2781-901 Oeiras, Portugal

Supporting Information

ABSTRACT: An interesting strategy for photocatalytic production of hydrogen from water and sunlight is the formation of a hybrid photocatalyst that combines an inorganic semiconductor able to absorb in the visible light spectral range with an enzymatic catalyst for reducing protons. In this work we study how to optimize the interfacing of In_2S_3 particles with the soluble form of [NiFeSe] hydrogenase from *Desulfovibrio vulgaris* Hildenborough by means of its initial H_2 photoproduction rate. The kinetics of the photocatalytic process was studied by membrane-inlet mass spectrometry, in order to optimize the interaction between both components of the hybrid photocatalyst. Membrane-inlet mass spectrometry allows measuring in the same experiment, for comparison, the rate of H_2 production by the photocatalyst hybrid directly in the aqueous solution in real time and the result of a standard assay of the hydrogenase activity. An incubation period of 6 h with mild stirring of hydrogenase with In_2S_3 particles was necessary for optimal interaction of the enzyme molecules with the porous surface of the semiconductor. A turnover frequency of the NiFeSe hydrogenase (TOF_{Hase}) for H_2 photobioproduction of 986 s^{-1} was measured under the optimized conditions. This means that the immobilized hydrogenase has a photocatalytic efficiency for H_2 generation which is 94% of that obtained in the standard specific activity test of H_2 production using reduced methyl viologen as an electron donor.

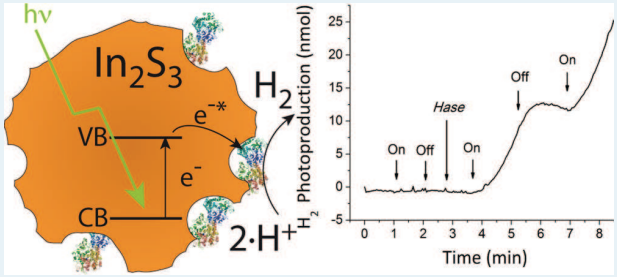

KEYWORDS: *hydrogenase, In_2S_3, biocatalysis, photocatalysis, visible light, hydrogen*

INTRODUCTION

Hydrogen is considered a clean energy vector, although nowadays most hydrogen is still produced from fossil fuels or by water electrolysis using noble metals as electrocatalysts.[1] Therefore, efficient photocatalytic production of hydrogen from water and sunlight is currently a major goal of research toward a sustainable energy generation.[2] An interesting strategy for this purpose is the formation of a hybrid photocatalyst that combines an inorganic semiconductor able to absorb in the visible light spectral range with a non-noble-metal inorganic[3] or enzymatic[4] catalyst for reducing protons. Many metal sulfide semiconductors have attracted much attention due to their band gap in the energy range of visible light radiation and their conduction band energy level situated above that required for reducing protons.[5] Some of them, specially CdS, have shown excellent properties for photocatalytic production of hydrogen under visible light in aqueous solution using a cocatalyst and a sacrificial compound for hole replenishment.[6] In_2S_3 is another semiconductor frequently used as a buffer layer in photovoltaic solar cells[7] or water-splitting photochemical cells[8] because of its interesting electron-handling properties. It has also other potential applications such as visible-light driven photodegradation of organic dyes.[9] In_2S_3 is also of interest in photocatalytic production of hydrogen due to its similar band gap energy ($E_g \approx 2-2.3$ eV) in comparison to that of CdS, conduction band potential of −0.8 V vs RHE, and lower toxicity.[5] In_2S_3 is easily synthesized by a solvothermal reaction, with no further modification being needed.[10]

In the present work we study a hybrid system based on an In_2S_3 semiconductor and an enzymatic cocatalyst for proton reduction in aqueous solution. Hydrogenases are redox metalloproteins that efficiently catalyze H_2 production and oxidation under mild conditions.[11] Hydrogenases are classified according to the metal content of their redox centers. The main groups of hydrogenases are the [NiFe] and the [FeFe] hydrogenases, which have a bimetallic complex coordinated by thiolates, CO, and CN^- ligands as catalytic sites for H_2 oxidation/production and have an electron transfer pathway formed by iron−sulfur clusters that connect the active site with the enzyme surface.[12] Hydrogenases have shown an excellent

Received: May 30, 2016
Revised: July 19, 2016
Published: July 22, 2016

DOI: 10.1021/acscatal.6b01512
ACS Catal. 2016, 6, 5691−5698

THE JOURNAL OF PHYSICAL CHEMISTRY C

Article

pubs.acs.org/JPCC

Synthesis and Characterization of V-Doped β-In_2S_3 Thin Films on FTO Substrates

Cristina Tapia,[†] Sean P. Berglund,[‡] Dennis Friedrich,[‡] Thomas Dittrich,[#] Peter Bogdanoff,[‡] Yang Liu,[§,∥] Sergiu Levcenko,[⊥] Thomas Unold,[⊥] José Carlos Conesa,[†] Antonio L. De Lacey,[†] Marcos Pita,*[,†] and Sebastian Fiechter*[,‡]

[†]Instituto de Catalisis y Petroleoquimica, CSIC, Calle de Marie Curie, 2, L10, 28049 Madrid, Spain

[‡]Institute for Solar Fuels and [#]Institute for Silicon Photovoltaics, Helmholtz-Zentrum Berlin für Materialien und Energie GmbH, Kekuléstr. 5, D-12489 Berlin, Germany

[§]Nanooptical Concepts for PV and [⊥]Dept. Structure and Dynamics of Energy Materials, Helmholtz-Zentrum Berlin für Materialien und Energie GmbH, Hahn-Meitner-Platz 1, 14109 Berlin, Germany

[∥]Institut für Chemie, Freie Universität Berlin, Fabeckstrasse 34-36, 14195 Berlin, Germany

Supporting Information

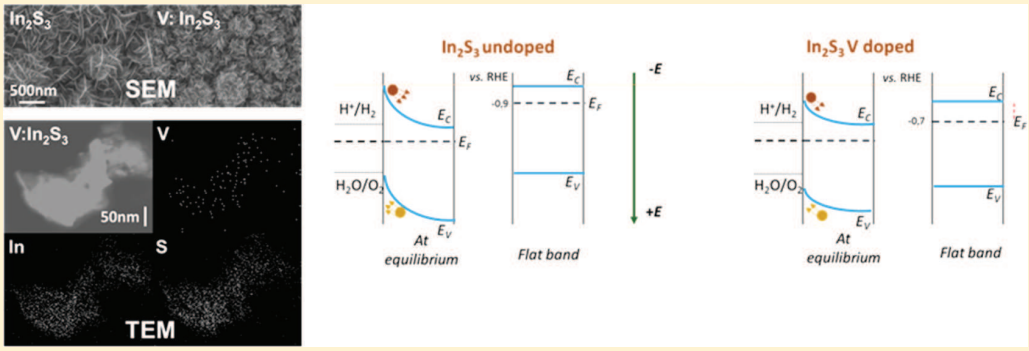

ABSTRACT: Intermediate band semiconductors have raised interest as materials to both enhance photovoltaics' efficiency and promote photocatalytic activity driven by visible light. The present work shows the synthesis of In_2S_3 doped with four different ratios of V using the ILGAR technique. This nebulize-spray based technique allows the deposition of $In_2(V)S_3$ thin layers controlling the layer thickness and providing high reliability on sample preparation. The samples have been characterized by X-ray diffraction, electron microscopy, profilometry, UV−vis spectroscopy, inductively coupled plasma mass spectrometry, X-ray photoemission spectroscopy, surface photovoltage spectroscopy, time-resolved microwave conductivity, photoelectrochemical, photoluminescence measurements, and electrochemical impedance spectroscopy. An optimum of 1.4% V content yielded the highest enhancement of photocurrent density compared to undoped In_2S_3. The results suggest that the inclusion of V in the In_2S_3 at 1.4% yields a high amount of in-gap levels within the crystalline structure that causes a Fermi energy level shift, which also induces the shift of the level of both valence and conduction bands.

INTRODUCTION

Harvesting energy from the sunlight has been a matter of research for both its direct conversion to electricity (via photovoltaic solar cells) and its photochemical possibilities (i.e., photocatalytic processes). One strategy that can be used to boost the energy collected in the photoabsorption process is the addition of dopants to semiconductor materials. Dopants cause several effects on the hosting materials. The most typical effect is influencing the energy band structure of the hosting semiconductor, broadly known for TiO_2 or ZnO.[1−3]In some specific cases the dopant alters the energy level structure of the pure material and causes the appearance of an intermediate band in its structure. Intermediate band semiconductors became popular a few decades ago[2,3] although they were first described in 1960.[4] Such intermediate band allows the successful excitation of electrons from the valence band (VB) to the conduction band (CB) in two steps with photons of energy lower than the fundamental band gap of the host material. The first step requires a photon with enough energy to excite a valence electron to the intermediate level while the second step requires another photon with energy able to excite the electron again to the CB. In theory this feature allows solar cell efficiencies above 60%.[5,6]

Received: September 22, 2016
Revised: November 23, 2016
Published: November 23, 2016

DOI: 10.1021/acs.jpcc.6b09601
J. Phys. Chem. C 2016, 120, 28753−28761

ARTICLE
PUBLISHED ONLINE: 20 MARCH 2017 | DOI: 10.1038/NCHEMBIO.2335
nature chemical biology

The direct role of selenocysteine in [NiFeSe] hydrogenase maturation and catalysis

Marta C Marques[1], Cristina Tapia[2], Oscar Gutiérrez-Sanz[2], Ana Raquel Ramos[1], Kimberly L Keller[3,4,6], Judy D Wall[3,4], Antonio L De Lacey[2], Pedro M Matias[1,5]* & Inês A C Pereira[1]*

Hydrogenases are highly active enzymes for hydrogen production and oxidation. [NiFeSe] hydrogenases, in which selenocysteine is a ligand to the active site Ni, have high catalytic activity and a bias for H_2 production. In contrast to [NiFe] hydrogenases, they display reduced H_2 inhibition and are rapidly reactivated after contact with oxygen. Here we report an expression system for production of recombinant [NiFeSe] hydrogenase from *Desulfovibrio vulgaris* Hildenborough and study of a selenocysteine-to-cysteine variant (Sec489Cys) in which, for the first time, a [NiFeSe] hydrogenase was converted to a [NiFe] type. This modification led to severely reduced Ni incorporation, revealing the direct involvement of this residue in the maturation process. The Ni-depleted protein could be partly reconstituted to generate an enzyme showing much lower activity and inactive states characteristic of [NiFe] hydrogenases. The Ni-Sec489Cys variant shows that selenium has a crucial role in protection against oxidative damage and the high catalytic activities of the [NiFeSe] hydrogenases.

Hydrogenases catalyze the simplest of chemical reactions—the reversible conversion of protons and electrons to hydrogen. These metalloenzymes have attracted immense interest because they are extremely active catalysts for these reactions and can be applied in fuel cells, electrocatalytic or photocatalytic devices and serve as models for synthetic catalysts[1–4]. Of particular interest are systems aiming at artificial photosynthesis for solar-based H_2 production from water splitting, forming the basis for a carbon-free, hydrogen-fueled economy[5,6]. In terms of enzyme-based systems, [FeFe] hydrogenases are an obvious choice for this application, as they have the highest H_2 production activities[7,8], but these enzymes are irreversibly inactivated by even trace amounts of O_2, which limits their use in H_2 evolution devices. In contrast, [NiFe] hydrogenases can be reductively reactivated after exposure to O_2, but the standard enzymes form inactive Ni(III) species (Ni-A and Ni-B), of which Ni-A reactivates only very slowly[9]. A group of [NiFe] hydrogenases are O_2 tolerant[10], producing only the rapidly reactivated Ni-B species upon contact with O_2, but these enzymes are not suited for H_2 production owing to a very strong bias toward H_2 oxidation and pronounced H_2 inhibition of H^+ reduction[3].

The subfamily of [NiFeSe] hydrogenases[11], which have a selenocysteine as a direct ligand to the active site Ni (**Fig. 1a**,**b**), are the enzymes that display the most interesting properties for H_2 evolution applications[12]. They have a fast rate and catalytic bias toward H_2 production, in contrast to standard [NiFe] hydrogenases[13–15], and show much less product inhibition by H_2 (refs. 15–17). In addition, they do not form the inactive Ni(III) species characteristic of [NiFe] hydrogenases and are reactivated quickly at low potentials[16,18–21], being capable of H_2 production in the presence of small amounts of O_2 (refs. 15,16). These properties have been exploited in biocatalytic applications of [NiFeSe] hydrogenases for photo- and electrochemical H_2 production[14,17,22–26] and also for electrochemical ATP synthesis[27]. Furthermore, the superiority of [NiFeSe] hydrogenases has also been revealed *in vivo*, as these enzymes are preferentially expressed when selenium is available[28,29]. For example, in *D. vulgaris* Hildenborough the [FeFe] and [NiFe] hydrogenases are downregulated in the presence of selenium, indicating a physiological preference for the [NiFeSe] hydrogenase[29].

However, the incorporation of selenocysteine requires a complex dedicated machinery and has a very high energetic cost. Given also that sulfur is a much more abundant element than selenium, there must a strong biological advantage for using selenocysteine over cysteine[30,31]. Selenoproteins are mostly oxidoreductases in which selenocysteine is involved in the catalytic reaction. Despite numerous studies, there is still no consensus about why selenocysteine is used in selenoenzymes. The most studied group is that involved in thiol-disulfide exchange reactions, and possible factors discussed include selenocysteine's lower pK_a compared to cysteine, its increased nucleophilicity, increased electrophilicity, higher polarizability and hypervalency, better leaving group ability or a combination of all these, as selenocysteine performs multiple roles during the catalytic cycle[31,32]. However, several cysteine homologs of selenocysteine-containing enzymes can catalyze their enzymatic reactions with high catalytic efficiency, raising questions about the real necessity for selenium[32,33]. Another important argument for the superiority of selenocysteine is its ability to resist irreversible oxidative inactivation[31,33,34]. In fact, although selenium is more easily oxidized than sulfur, the resulting selenium oxides are much more electrophilic and unstable than their sulfur analogs and therefore easier to reduce back to the parent state. Thus, oxidation of the selenocysteine residue to the corresponding selenenic or seleninic acids is readily reversible, whereas reduction of a sulfenic acid is more difficult, and that of a sulfinic acid virtually impossible[34,35]. This property apparently enables selenoenzymes to better resist irreversible oxidative inactivation compared to their cysteine counterparts[34].

Here we report the first recombinant expression system for a [NiFeSe] hydrogenase allowing the production of engineered forms of the enzyme. We generated a protein variant in which the selenocysteine residue was replaced by cysteine, converting the [NiFeSe] enzyme into a [NiFe] hydrogenase and thus enabling us to

[1]Instituto de Tecnologia Química e Biológica António Xavier, Universidade Nova de Lisboa, Oeiras, Portugal. [2]Instituto de Catálisis y Petroleoquímica (CSIC), Madrid, Spain. [3]Biochemistry Department, University of Missouri, Columbia, Missouri, USA. [4]Ecosystems and Networks Integrated with Genes and Molecular Assemblies (ENIGMA), Berkeley, California, USA. [5]Instituto de Biologia Experimental e Tecnológica (iBET), Oeiras, Portugal. [6]Present address: Biology Department, William Woods University, Fulton, Missouri, USA. *e-mail: ipereira@itqb.unl.pt or matias@itqb.unl.pt

ChemPubSoc Europe

DOI: 10.1002/celc.201600506

CHEMELECTROCHEM Articles

Wiring of Photosystem I and Hydrogenase on an Electrode for Photoelectrochemical H_2 Production by using Redox Polymers for Relatively Positive Onset Potential

Cristina Tapia,*[a] Ross D. Milton,[b, d] Galina Pankratova,[c] Shelley D. Minteer,[b] Hans-Erik Åkerlund,[c] Dónal Leech,[d] Antonio L. De Lacey,[a] Marcos Pita,*[a] and Lo Gorton[c]

Photosystem I (PSI) is combined with *Desulfovibrio gigas* hydrogenase for the bioelectrocatalytic photosynthesis of hydrogen at an electrode surface. The activity of these two biocatalysts is linked by two redox polymers; a redox polymer with a relatively positive potential (loaded with an Os complex) is able to reduce PSI and thus facilitates the production of photoexcited electrons, whereas redox polymers of relatively low potential are able to transfer electrons to the hydrogenase. Two negative-potential redox polymers are tested, with either a viologen pendant (4-methyl-4′-bromopropylviologen functionalized linear polyethylenimine) or a cobaltocene pendant (cobaltocene-functionalized branched polyethylenimine, Cc-BPEI). Both are able to protect hydrogenase from O_2 inactivation, but only the use of Cc-BPEI yields significant photocurrents for H^+ reduction, likely due to its lower redox potential. The photocurrents obtained are found to be proportional to the quantity of H_2 produced, reaching a maximum of $-30\ \mu A\,cm^{-2}$ for the system incorporating Cc-BPEI and showing a relatively positive onset potential at $+0.38$ V versus SHE.

1. Introduction

Artificial photosynthesis is currently a major topic of research towards sustainable energy generation from water and sunlight. A major artificial photosynthetic process is water splitting with the aim of producing hydrogen as a fuel while avoiding formation of CO or CO_2 as side product. Current synthetic methods for H_2 start from hydrocarbons and produce oxidized carbon byproducts and waste.[1] Therefore, natural photosynthesis is a continuous source of inspiration for developing efficient photocatalytic devices.[2–4]

In particular, photoelectrochemical systems are of great interest for studying the production of H_2 from protons, because in this case the electrons surge from a polarized electrode. The electrode also allows 1) control of the reaction driving force by tuning the applied potential, 2) determining the reaction kinetics from the produced current, and 3) immobilization of both the photosensitive compound and the hydrogen-producing catalyst.[5,6] Moreover, the H_2-producing photocathode can then be combined with an oxygen-evolving anode to form a photoelectrochemical cell that supplies the cathode with electrons extracted from water oxidation at the anode.[7,8] Different inorganic semiconductors, photosensitive organometallic complexes, noble metals, and biomimetic catalysts have been incorporated in photoelectrochemical systems for H_2 production.[6,9,10] An interesting alternative is the use of natural light harvesters and catalysts. In photosynthetic organisms a large protein complex, known as photosystem I (PSI), is capable of absorbing visible light by exciting low-energy electrons to high-energy ones. The fast transfer of excited electrons to a redox protein (ferredoxin) prevents charge recombination. Oxidized ferredoxin is then regenerated by the subsequent reduction of redox enzymes that catalyze the reduction of $NADP^+$ (ferredoxin $NADP^+$ reductase) or H_2 production (hydrogenase).[11]

Several studies targeting the connection of PSI to electrodes for photocurrent generation, based on direct electron transfer (DET) or mediated electron transfer (MET), have been published.[12–14] In many cases PSI is integrated in cross-linked redox hydrogels.[15–17] A particularly interesting study involved the co-immobilization of PSI and Pt nanoparticles on an Os-complex redox polymer over an electrode for light-induced H_2 evolution. The redox polymer delivered the low-energy electrons from the electrode to PSI, while the Pt nanoparticles collected the photoexcited electrons from PSI for reducing protons to H_2.[18] A further step towards a completely photobioelectrochemical system, thus avoiding the use of noble-metal-based catalysts, is to connect PSI to a hydrogenase (Hase). Many studies on optimizing the wiring of PSI to Hases have

[a] C. Tapia, Dr. A. L. De Lacey, Dr. M. Pita
Instituto de Catalisis y Petroleoquimica, CSIC
C/ Marie Curie 2, L10, 28049, Madrid (Spain)
E-mail: cristina.tapia@csic.es
marcospita@icp.csic.es

[b] Dr. R. D. Milton, Prof. S. D. Minteer
Department of Chemistry, University of Utah
315 S 1400 E Rm 2020, Salt Lake City, Utah (USA)

[c] G. Pankratova, Prof. H.-E. Åkerlund, Prof. L. Gorton
Department of Biochemistry and Structural Biology, Lund University
P.O.Box 124, 22100, Lund (Sweden)

[d] Dr. R. D. Milton, Prof. D. Leech
School of Chemistry, National University of Ireland Galway
University Road, Galway (Ireland)

Supporting Information for this article can be found under: http://dx.doi.org/10.1002/celc.201600506.

ACS Catalysis

Research Article

pubs.acs.org/acscatalysis

Laccase-Catalyzed Bioelectrochemical Oxidation of Water Assisted with Visible Light

Cristina Tapia,[†] Sergey Shleev,[‡] José Carlos Conesa,[†] Antonio L. De Lacey,*[,†] and Marcos Pita*[,†]

[†]Instituto de Catálisis y Petroleoquímica, CSIC, C/Marie Curie, 2, L10 28049 Madrid, Spain

[‡]Biomedical Sciences, Faculty of Health and Society, Malmo University, SE-0205 06 Malmo, Sweden

Supporting Information

ABSTRACT: Here we present the modification of fluorinated tin oxide electrodes with In_2S_3, an n-type semiconductor chalcogenide that absorbs visible light ($\lambda \leq 600$ nm), and its further use as an active scaffold for laccase-catalyzed oxidation of water. Illumination of an FTO-In_2S_3-laccase electrode yields O_2 production at much lower applied potential in comparison to the previous example using the same laccase, where only electric energy was applied. The present system allows a diversification of the energy applied to accomplish the water splitting, taking a portion of it from the sun. This work is the first example where an enzyme other than PSII has been used in combination with visible light to biocatalyze O_2 evolution.

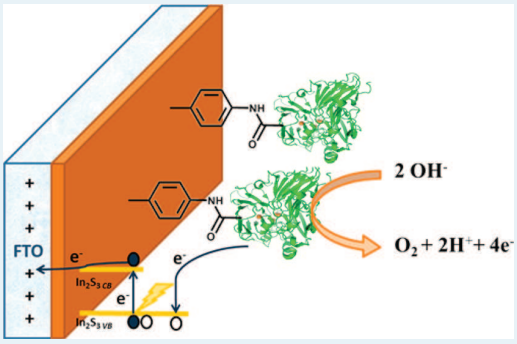

KEYWORDS: *photocatalysis, biocatalysis, laccase, water splitting, oxygen, visible light*

INTRODUCTION

Solar and wind energies, which play an increasingly important role in sustainable development, suffer from an intermittency problem which demands some sort of storage. One way to solve it is to capture CO_2 or decompose water through processes such as

$$nCO_2 + mH_2O \rightarrow C_nH_{2m}O_p + (n + (m - p)/2)O_2 \quad (1)$$

or

$$H_2O \rightarrow H_2 + 1/2\ O_2 \quad (2)$$

This allows storing energy as fuel. In the case of solar energy these processes are usually named solar fuel generation or artificial photosynthesis and were revealed as possible for the first time by work by Fujishima and Honda in the early 1970s,[1,2] showing that water could be split into H_2 and O_2 using a TiO_2 photoelectrode. Because of the importance and potential of the concept, many reviews[3−7] have been devoted to this subject. Photoelectrochemistry has advantages against pure photocatalysis, since it facilitates the fuel and O_2 production in separate compartments (thus avoiding their recombination) and also against photovoltaics + electrolysis, as it may diminish the energy losses due to the smaller number of interfaces that charge carriers must go through. Furthermore, electrochemistry and photoelectrochemistry of semiconductors had already been deeply studied,[8−11] building a sound scientific basis to understand and develop that technology. The study of photocatalysis by oxides had begun much earlier[12] and provides additional knowledge of the surface chemistry involved.

The production of solar fuels needs a compound able to capture solar light and separate the photogenerated positive (holes) and negative (electron) charges so that chemistry can be made from them. In addition, the resulting redox levels must have potential enough to produce the desired chemistry. For water splitting the potential difference must be higher than 1.23 V (E_0 for O_2 evolution at pH 0), implying that those energy levels should be separated by a significant extra energy to overcome the energy losses; in addition, the excited electrons should appear at energy higher than the H_2 evolution redox potential and the holes at energies lower than the O_2 evolution redox potential. Many light absorbers, i.e. molecular entities or polymers, have been proposed and reviewed.[5,13−15] Here we focus on semiconducting light absorbers with band gap energy $E_g \geq 1.7$ eV. TiO_2 (rutile or anatase) is the best-known photocatalyst and photoelectrode; it is stable, affordable, and highly photoactive. However its large band gap (E_g = 3.0−3.2 eV) limits TiO_2 to UV light, disregarding ≥95% of the solar spectrum. Huge efforts have been driven toward other materials able to use efficiently visible light. These include TiO_2 doped with cations (Cr, V, Fe) or anions (N or S), oxides such as $BiVO_4$, Cu_2O, WO_3, and Fe_2O_3, nitrides or oxinitrides such as Ta_3N_5, TaON, the perovskites $LaTiO_2N$ and $LaNbON_2$, and two-dimensional g-C_3N_4, and sulfides such as $CuGaS_2$, CdS, In_2S_3, $ZnIn_2S_4$, SnS_2, and MoS_2, although the mentioned sulfides and some of the nitrides are prone to photooxidation

Received: May 12, 2017
Revised: June 1, 2017
Published: June 12, 2017

DOI: 10.1021/acscatal.7b01556
ACS Catal. 2017, 7, 4881−4889

Cristina Tapia García was born in 1986 in Barcelona, Spain. She finished her studies in Biotechnology degree in 2009, at Autonomous University of Barcelona. She received her MSc. in Applied Chemistry in 2015 from the Faculty of Science at Autonomous University of Madrid, Spain. During her MSc. and PhD studies she worked with semiconductors, hydrogenase and laccase enzymes under the supervision of Dr. Marcos Pita and Dr. Antonio Lopez de Lacey at the Bioelectrocatalysis laboratory, in the Institute of Catalysis and Petrochemistry from the Spanish Research Council (CSIC) in Madrid. The focus of her thesis is the development of hybrid systems for hydrogen and oxygen photoproduction from water.